AN INVESTIGATION ON THE ELECTRICAL CHARACTERISTICS OF ANTIMONY TRISULPHIDE FILMS AND CERTAIN METAL - SEMICONDUCTOR (Sb_2S_3) CONTACTS

M. K. RADHAKRISHNAN

THESIS SUBMITTED IN
PARTIAL FULFILMENT OF THE REQUIREMENTS
FOR THE DEGREE OF
DOCTOR OF PHILOSOPHY

SOLID STATE PHYSICS LABORATORY
DEPARTMENT OF PHYSICS
UNIVERSITY OF COCHIN

1981

CERTIFICATE

Certified that the work reported in the present thesis is based on the bona fide work done by M.K. Radhakrishnan, research scholar, under my guidance in the Department of Physics, University of Cochin, and has not been included in any other thesis submitted previously for the award of any degree.

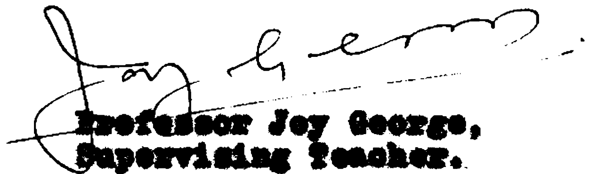

Cochin-22
February 25, 1981

Professor Joy George,
Supervising Teacher.

DECLARATION

Certified that the work presented in this thesis is based on the original work done by me under the guidance of Professor Joy George in the Department of Physics, University of Cochin, and has not been included in any other thesis submitted previously for the award of any degree.

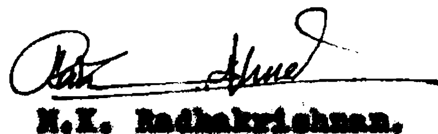

Cochin-22
February 25, 1981

M.K. Radhakrishnan.

SYNOPSIS

AN INVESTIGATION ON THE ELECTRICAL CHARACTERISTICS OF ANTIMONY TRISULPHIDE FILMS AND CERTAIN METAL–SEMICONDUCTOR (Sb_2S_3) CONTACTS

The thesis consists of the study of the electrical properties of antimony trisulphide films and the electrical behaviour of different metal contacts to antimony trisulphide films. Since the thermal evaporation of the compound antimony trisulphide as such may result in nonstoichiometric compound films, Sb_2S_3 films in the present work were mostly prepared by the three temperature method, keeping the substrate at different temperatures ranging from 303K to 423K and evaporating antimony and sulphur simultaneously from separate sources. The evaporations were carried out at a pressure less than 1 x 10^{-5} torr.

The electrical conductivity of the films prepared at different substrate temperatures have been measured in the temperature range 303K to 373K and the activation energies in each case evaluated. For films prepared at substrate temperatures between 323K and 373K, the activation energy values were found to be

nearly the same indicating the stoichiometric uniformity in these films. As such, for the entire study, the antimony trisulphide films were prepared keeping the substrates at a temperature 345 ± 2K. This substrate temperature is in agreement with the substrate temperatures theoretically predicted by Vincett et al [1] for compound semiconductor films. Sb_2S_3 films were also prepared, by the flash evaporation of the compound antimony trisulphide, on substrates kept at 345 ± 2K. In all these cases, the Sb_2S_3 films were found to be p-type.

The current-voltage characteristics of antimony trisulphide films sandwiched between metal electrodes were investigated using different metal films as top electrodes. Antimony film was used as the bottom electrode in all the cases.

With antimony, indium and tin as top electrodes the current-voltage characteristics showed a $I \propto V^2/d^3$ dependence indicating the conduction mechanism in the film system to be space charge limited (SCL). From the observed trap-filled-limit voltage, and the cross-over voltage from Ohm's law to square law region, the

trap density and the trap energy level in the film systems have been calculated. The activation energy analysis has been carried out, from the temperature dependence of the Ohm's law region and SCL conduction region, using the Roberts-Schmidlin model [2], and the Sb_2S_3 films have been found to be non-extrinsic. An energy band structure showing the dominant electron and hole levels has been proposed.

The dielectric properties of antimony tri-sulphide films have been measured in the frequency range 100 Hz to 20 KHz and in the temperature range 303 to 373K. The variation of capacitance, dielectric constant and tan δ with frequency and temperature have been studied.

The electrical behaviour of different metal contacts to Sb_2S_3 films, have been investigated on films prepared by the three temperature method by analysing the current-voltage characteristics of the Sb-Sb_2S_3-metal systems. Aluminium makes a rectifying contact to Sb_2S_3 and the conduction mechanism has been found to be of the Poole-Frenkel type. The experimentally determined values of Poole-Frenkel factor (β_{PF})

for different film thicknesses are in agreement with the theoretically calculated value. Tin and indium make ohmic contacts with antimony trisulphide. Bismuth provides an ohmic injecting type contact and the Sb-Sb_2S_3-Bi system showed a current controlled negative resistance behaviour which is explained on the basis of a double injection model. Silver contacts showed very poor stability even at low fields.

An attempt has also been made to evaluate certain semiconductor-insulator combinations for fabricating a MIS thin film transistor using Sb_2S_3 as the semiconductor.

References

1. P.S. Vincett, W.A. Barlow and G.G. Roberts, J. Appl. Phys., 48, 3800 (1977).
2. F.W. Schmidlin and G.G. Roberts, Phys. Rev., B9, 1578 (1974).

CONTENTS

		Page
SYNOPSIS	.. ..	i
INTRODUCTION	.. ..	1
CHAPTER ONE	TRANSPORT PHENOMENA IN SEMICONDUCTORS ..	7
1.1	Transport in Bulk Semiconductors ..	7
1.2	Conduction in Semiconductor Films..	19
1.3	High Field Conduction ..	25
1.4	Conduction in Disordered Compound Semiconductor Films ..	31
CHAPTER TWO	CONTACT PHENOMENA IN THIN FILMS ..	35
2.1	Ohmic Contacts ..	35
2.2	Schottky and Bardeen Barrier ..	39
2.3	Blocking and Neutral Contact ..	42
2.4	Metal-Semiconductor Interface Reactions ..	43
CHAPTER THREE	CURRENT INJECTION IN SEMICONDUCTOR FILMS	45
3.1	General Features ..	45
3.2	Steady State One Carrier SCL Currents ..	48
3.3	Two Carrier Injection Problem ..	56
3.4	Activation Energy Analysis ..	60
CHAPTER FOUR	DIELECTRIC PROPERTIES OF THIN FILMS ..	66
4.1	Dielectric Losses ..	66
4.2	Dielectric Polarization ..	69
4.3	Permittivity ..	71
4.4	Temperature Coefficient of Capacitance and Permittivity..	73

Page

CHAPTER FIVE	METHODS OF THIN FILM PREPARATION	..	76
	A. Chemical Methods		
5.1	Chemical Vapour Deposition	..	76
5.2	Electrodeposition	..	78
5.3	Other Methods	..	80
	B. Physical Methods		
5.4	Sputtering	..	81
5.5	Evaporation	..	83
CHAPTER SIX	GROWTH AND STRUCTURE OF THIN FILMS	..	91
6.1	Film Nucleation	..	91
6.2	Stages of Growth	..	96
6.3	Factors Affecting the Growth of Films	..	97
6.4	Structure of Films	..	98
CHAPTER SEVEN	EXPERIMENTAL DETAILS	..	100
7.1	Vacuum Coating Unit	..	100
7.2	Film Deposition	..	104
7.3	Structure Fabrication	..	112
7.4	Film Thickness Measurement	..	115
7.5	Electrical Measurements	..	117
7.6	Thin Film Transistor	..	121
CHAPTER EIGHT	RESULTS AND DISCUSSION	..	125
8.1	Conductivity Studies	..	126
8.2	Metal-Semiconductor Contacts	..	130
8.3	SCL Conduction and Dominant Level Analysis	..	141
8.4	Dielectric Studies	..	151
8.5	Thin Film Transistor	..	156
CONCLUSION	..	..	160
REFERENCES	..	..	163
ACKNOWLEDGEMENTS			

INTRODUCTION

The scientific and technological impact of thin films in the modern world is so great that without which the whole communication network around the globe stands still. The innovations of thin film physics rewarded, in the form of microminiaturization of components and devices, the electronics industry. The development of various methods to prepare thin solid films of elements and binary and ternary systems in controlled composition and rate, enhanced the study of the physical properties of metals and semiconductors, during the last few years. Such an achievement paved the way for suggesting new compounds in place of commonly used elemental semiconductors, silicon and germanium, in solid state technology.

Thin solid films are extensively used in a variety of satellite programmes. During the mid sixties, Weimer et al [1,2] produced thin film microelectronic circuits having thousands of active and passive elements. Large area circuits such as television image sensors [3] on glass substrates have

been developed using thin films. The numerous studies in this field have initiated the development of thin film transistors, diodes, magnetic bubble and ferroelectric memories, infrared detectors, photovoltaic solar cells, capacitors and solid state imaging and display systems. The ability to deposit active and passive components on insulating substrates using compound semiconductors offers much scope for applications in large scale integration. Various film combinations are under investigation [4-6] for increasing the efficiency of solar energy converters.

The stability, reliability and efficiency of the microelectronic circuits using thin film devices depend mostly on the electrical properties of the semiconductor film and the interface reactions at the metal-semiconductor contacts. Several compound semiconductors are now commonly in use with silicon and germanium in fabricating thin film devices. The vacuum evaporation of the compound may result in the production of non-stoichiometric films. The departures from the stoichiometry affect the electronic and photoelectric properties of the films, as reported by Mostovskii et al [7] in the case of certain group V chalcogenides.

In the vacuum deposition, since the difference in the partial vapour pressures of the elements of the compound complicates the problem of maintaining the proper stoichiometric ratio of the films, two methods are employed to prepare compound films. One is a single step process such as flash evaporation of the compound [8] and its synthesis on a hot substrate. The second method employs the evaporation of the constituents from separate sources at a chosen rate to meet the condition of stoichiometry of the condensed compound layer [9-11].

To investigate the electrical properties of the semiconductor films, proper electrical contacts are to be made to the films. While using different metal films as electrodes, the nature of the contact, ohmic, blocking or rectifying, depends on the work function of the metal and the semiconductor [12]. Low work function metals are reported to make ohmic contacts [13] to the semiconductor. However, the metal-semiconductor contact has a good bearing in determining the type of electronic conduction in the semiconductor film.

The electrical properties of thin films of several III-V group compound semiconductors such as

GaAs [14-16] and InSb [17-19] and II-VI compound semiconductors such as CdS [20-22] and CdSe [23,24] have been extensively explored for use in device applications. Among the V-VI compounds, sulphides of arsenic and antimony are being used in optical imaging. The properties of arsenic trisulphide films have been investigated to study the photo-decomposition and oxidation reactions [25-27] and the electrical conduction mechanisms [28] in the film system. Forgue et al [29] studied the photoconducting properties of antimony trisulphide to fit it for use as a television pick up tube target material. Properties of single crystals of Sb_2S_3, such as, dielectric properties at microwave frequencies [30], switching effect [31] and electrical and magnetic properties [32] have been studied earlier. The optical properties of antimony sulphide films [33,34] and the charge carrier transport [35] and the photoelectric behaviour [36] are reported in the literature. However, in all the reported studies, the films were prepared by the thermal evaporation of the compound Sb_2S_3, which may cause some departures in the stoichiometry of the film formed.

In the present investigation, antimony trisulphide films have been prepared by two methods, the coevaporation of antimony and sulphur and the flash evaporation of Sb_2S_3 powder. The coevaporation of antimony and sulphur has been carried out from two separate sources, keeping the substrate at different temperatures ranging from 303K to 423K. The electrical conductivity of these films have been measured at various temperatures and the activation energies have been evaluated. The current-voltage characteristics of the Sb_2S_3 films have been reported in this study, using metal electrodes of antimony, indium, tin, bismuth, aluminium and silver. Also the nature of the contact made by each metal to the semiconductor has been investigated in detail, and the different conduction mechanisms have been proposed. The dielectric properties of antimony trisulphide films in a wide frequency range at various temperatures have also been presented in this study. An attempt has also been made in the present study to evaluate the suitability of this semiconductor film for the fabrication of thin film transistor.

A part of these investigations have been published in the form of the following papers.

1. Electrical Conduction in Coevaporated Antimony Trisulphide Films

   Solid State Commun., **33**, 987 (1980).

2. Electrical Behaviour of Metal Contacts to Sb_2S_3 Films

Int. J. Electron., 49, 397 (1980).

3. Space Charge Limited Conduction in Antimony Trisulphide Films

J. Phys. D: Appl. Phys.,

(accepted for publication).

CHAPTER ONE

TRANSPORT PHENOMENA IN SEMICONDUCTORS

1.1. Transport in Bulk Semiconductors

A semiconductor, strictly speaking, is an insulator, and is characterized by the electrical conductivity which increases with temperature, contrary to that of normal metals. Distinction between metal and semiconductor is qualitative, however, between the semiconductor and the insulator it is only a quantitative one depending upon the magnitude of the energy gap separating the valence and the conduction band edges [37]. In a semiconductor, the gap is sufficiently small so that the thermal excitation can promote electrons to the conduction band and can contribute to electronic conduction [38,39], while the thermal excitation of carriers across the gap is negligible in the insulator.

1.1.1. Energy Band Structure

(i) Intrinsic case

In the band structure of an ideal semiconductor, the energy gap separates the uppermost allowed energy level in the valence band and the lowest energy state in

the conduction band. At absolute zero, the valence band is completely filled and the conduction band is empty. As the temperature is increased, there is a finite probability that an electron in the valence band may gain sufficient energy from the lattice and make a transition into an allowed state in the conduction band.

The density of electrons, n, and holes, p, at thermal equilibrium in an intrinsic semiconductor [40] is

$$n = N_c \exp -(E_c - E_F)/kT \tag{1.1}$$

and

$$p = N_v \exp -(E_F - E_v)/kT \tag{1.2}$$

where N_c and N_v are the density of states in the conduction band and valence band respectively, E_c and E_v are the corresponding energy levels of the bottom of the conduction band and top of the valence band and E_F is the Fermi level.

$$N_c = 2(2\pi m_n^* kT/h^2)^{3/2} \tag{1.3}$$

and

$$N_v = 2(2\pi m_p^* kT/h^2)^{3/2} \tag{1.4}$$

where m_n^* and m_p^* are the effective electron and hole

masses respectively. The Fermi energy is determined by the condition of electrical neutrality, $n = p$. Then the intrinsic carrier concentration

$$n_i = (np)^{\frac{1}{2}}$$

$$= (N_c N_v)^{\frac{1}{2}} \exp(-E_g/2kT) \qquad (1.5)$$

where E_g is the band gap equal to $E_c - E_v$.

From equation (1.5), using (1.3) and (1.4) it can be deduced that

$$np = AT^3 \exp(-E_g/kT) \qquad (1.6)$$

where $A = 4 \left(\frac{2\pi k}{h^2}\right)^3 (m_n^* m_p^*)^{3/2}$.

Experimental values of log (np/T^3) plotted against $1/T$ gives a straight line [41], and is the intrinsic energy gap of the semiconductor. If the effective masses in the two bands are not equal, the Fermi energy will change with temperature and shift in the direction of the band which has the lower effective mass.

When electron-lattice interaction is taken into account, the energy gap is equal to the optical

threshold energy of the material [42]. According to Bardeen and Shockley [43], the dependence of energy gap on the lattice dilation can be deduced from the mobilities of electrons and holes.

(ii) Extrinsic case

If an impurity atom is introduced in the lattice of the semiconductor, the semiconductor behaves as n-type or p-type depending upon the nature of the impurity, donor or acceptor type. A donor impurity brings with it an extra electron which cannot be the part of the valence bond structure. This extra electron uses wave functions in the conduction band and its effective mass will be different from that of the electron in the crystal. In the presence of the impurity the extra electron behaves much similar to a free electron in the presence of a positive charge [44-47].

Considering a semiconductor containing N_D donors and N_A acceptors with localised levels at E_D and E_A in the forbidden gap (figure 1.1), the electrical neutrality demands

$$n + N_A^- = p + N_D^+ \qquad (1.7)$$

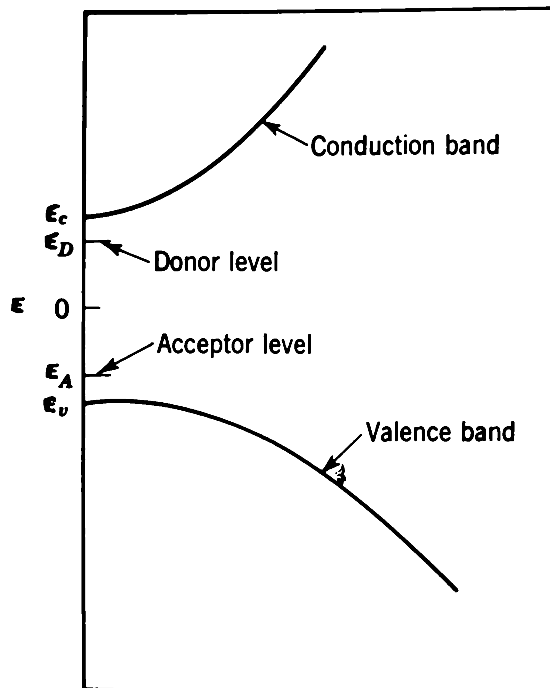

Figure 1.1. Energy band structure of an ideal semiconductor.

where N_A^- and N_D^+ are the number of ionised acceptors and donors respectively. The Fermi energy, which gives the electron distribution, is determined by the condition of electrical neutrality.

In the case of an n-type semiconductor

$$n = p - N_A + (N_D - N_A)$$

i.e., $$n = p + (N_D - N_A) - N_D f_D \qquad (1.8)$$

where f_D is the Fermi-Dirac distribution function. Using (1.1) and taking $n > p$ (n-type),

$$\frac{n(n + N_A)}{N_D - N_A - n} = \frac{N_c}{g_D} \exp -(E_c - E_D)/kT \qquad (1.9)$$

where g_D is the degeneracy factor and $E_c - E_D$ gives the ionization energy of the donors. At high temperatures, the right hand side of the equation (1.9) is larger than N_D, the intrinsic concentration n_i becomes large compared to $N_D - N_A$, and the semiconductor becomes intrinsic with $n \sim p$. At very low temperature, the R.H.S. of (1.9) becomes very small and

$$n = \frac{N_D - N_A}{N_A} \frac{N_c}{g_D} \exp -(E_c - E_D)/kT \qquad (1.10)$$

For a p-type semiconductor, $p > n$, and the concentration of holes is

$$p = n + (N_A - N_D) - N_A f_A \qquad (1.11)$$

Taking the Fermi-Dirac distribution function, the analogous case for (1.9) becomes

$$\frac{p(p + N_D)}{N_A - N_D - p} = \frac{N_V}{g_A} \exp -(E_A - E_V)/kT \qquad (1.12)$$

This gives a carrier concentration at low temperatures as

$$p = \frac{N_A - N_D}{N_D} \frac{N_V}{g_A} \exp - (E_A - E_V)/kT \qquad (1.13)$$

The impurity ionisation energy can be experimentally determined from this temperature dependence of conduction electron/hole concentration.

1.1.2. Conduction Phenomena

(i) Scattering

The motion of electrons or holes under the influence of applied electric or magnetic fields or temperature gradients is termed as transport phenomena.

The motion of carriers would be uninhibited by the lattice if the crystal is perfectly periodic. However, departures from a perfectly periodic structure produce scattering of the moving charges [48]. These departures can be thermal vibrations of lattice ions or atoms, lattice defects, both ionised and neutral impurities, and other charge carriers. The various scattering processes can often be characterised by a relaxation time. The relaxation time represents the average time required for a disturbance in the equilibrium electron distribution to die out by the randomising action of the scattering [49]. The scattering is isotropic when, after a single scattering process, the charge carrier emerges with a random velocity, having lost all memory of its previous motion. The relaxation time in this case is identical with the mean free time between collisions.

The effect of lattice scattering due to thermal vibrations have been treated by Seitz [50] and shown that the relaxation time τ is proportional to density of the crystal and inversely proportional to the square of the interaction parameter. The interaction parameter is related to the variation of

the energy gap with lattice dilation. The characteristics of this scattering process is that the mean free path is inversely proportional to the temperature and is independent of the energy of the carrier. The relaxation time in the case of scattering due to impurities is dependent on the concentration of ionised [51] and neutral impurities [52,53]. For semiconductors with large conductivity, the screening of charged centres by the conduction carriers becomes predominant [54]. The interaction of carriers with one another may affect the distribution of the drift momentum among carriers of different velocities and this in turn will influence the average relaxation time.

(ii) Current flow due to drift

An applied electric field accelerates the motion of charge carriers in the direction of the field. Considering a hole transport, the velocity, v_τ, due to a field F is

$$v_\tau = v_o + \left(\frac{e}{m_p^*}\right) F\tau \qquad (1.14)$$

where v_o is the initial velocity component in the direction of the field, and m_p^* is the effective hole mass. Taking the initial velocity distribution to be

isotropic, the average value of v_o is zero.

i.e., $$v_\tau = \left(\frac{e}{m_p^*}\right) F\tau \tag{1.15}$$

The average drift velocity v_d is

$$v_d = \left(\frac{e}{m_p^*}\right) F\tau = \mu_p F \tag{1.16}$$

where μ_p is the hole mobility.

$$\mu_p = \left(\frac{e}{m_p^*}\right) \tau \tag{1.17}$$

The hole current density, J_p, caused by the average drift velocity, v_d, is

$$J_p = e\, v_d p$$

where p is the hole density.

i.e., $$J_p = e\mu_p p F \quad = \sigma_p F \tag{1.18}$$

Therefore, the hole conductivity, σ_p, is

$$\sigma_p = e\mu_p p \tag{1.19}$$

Similarly, the electron conductivity is

$$\sigma_n = e\mu_n n \quad (1.20)$$

where μ_n is the electron mobility and n is the electron density.

Considering both the hole and electron current in a semiconductor, the total current density, J, is

$$J = J_p + J_n$$

i.e.,
$$J = (e\mu_p p + e\mu_n n) \quad (1.21)$$

and the conductivity, σ, is

$$\sigma = e\mu_p p + e\mu_n n \quad (1.22)$$

(iii) Current flow due to diffusion

If there is no applied field, and a gradient in the carrier concentration is present, then the current flow by diffusion occurs. Considering the hole transport, the diffusion current density, J_p, is

$$J_p = -eD_p \text{ grad } p. \quad (1.23)$$

where D_p is the hole diffusion constant and grad p is the concentration gradient.

For electrons, the current density, J_n, is

$$J_n = eD_n \text{ grad } n \qquad (1.24)$$

If there are both drift and diffusion, then the total current density for holes and electrons are given by

$$J_p = e\mu_p pF - eD_p \text{ grad } p \qquad (1.25)$$

$$J_n = e\mu_n nF + eD_n \text{ grad } n \qquad (1.26)$$

In an inhomogeneous semiconductor, the electron and hole densities are position dependent and hence in the calculations of diffusion current densities the values of n and p to be taken are not the equilibrium values.

(iv) Temperature dependence

The number of charge carriers in a semiconductor is generally a sensitive function of temperature and purity. The temperature variation of the conductivity, σ , is determined primarily by

the number of charge carriers. As the temperature is increased the number of these thermally excited intrinsic carriers increases exponentially. At high temperatures, the lattice scattering by acoustic phonons plays the dominant role and the mobility decreases with increasing temperature as $T^{-3/2}$ [37]. The conductivity, σ, is

$$\sigma = \frac{1}{\rho} = \frac{ne^2\tau}{m^*} \qquad (1.27)$$

Comparing this with equation (1.22) gives

$$\mu = \frac{e\tau}{m^*} \qquad (1.28)$$

Taking equation (1.5), (1.27) and (1.28) gives

$$\sigma \propto \exp\left(-E_g/2kT\right) \qquad (1.29)$$

in the intrinsic region. Hence a plot of log σ versus $1/T$ should be a straight line from the slope of which the energy gap of the semiconductor, can be determined.

This gap is approximately equal to the energy gap determined by the optical absorption measurements [33]. At high temperatures (above 500K)

the diffusion is very rapid [56] and the concentration of carriers are determined largely by the stoichiometric deviations rather than by the thermal excitation across the forbidden gap.

The mobility of carriers varies exponentially with temperature [57-60] in the case of scattering by the optical and vibrational modes of the lattice. The electron and hole mobility ratios are generally assumed to be independent of temperature. However, it is seen that the ratio actually increases with increasing temperature [61].

1.2. Conduction in Semiconductor Films

The electrical properties of semiconductor films are profoundly influenced by minute structural and chemical imperfections. Conversely, the electrical measurements can be used to characterise with great sensitivity the defect structure of thin films. In the studies of electrical conduction, the influence of surface scattering, defects associated with film growth, diffusion, dislocations, etc. [62], have to be considered.

1.2.1. Mobility

The carrier mobility of a vacuum deposited polycrystalline film will have contributions from

scattering of conducting carriers by thermal lattice vibrations, ionised impurities, dislocations and unspecified surface phenomena [63,64]. Hence the carrier mobility can be expressed as

$$\frac{1}{\mu} = \frac{1}{\mu_L} + \frac{1}{\mu_I} + \frac{1}{\mu_d} + \frac{1}{\mu_x} \qquad (1.30)$$

where the suffices L, I and d represent the lattice, impurity and dislocation scattering and the term μ_x is to represent all deviations observed in the value of μ from the sum of the first three terms.

The average relaxation time, τ_F, for carriers in thin films is given by

$$\frac{1}{\tau_F} = \frac{1}{\tau_s} + \frac{1}{\tau_B} \qquad (1.31)$$

where τ_s represents the average collision time due to surface scattering and τ_B due to bulk scattering. The surface scattering term can be written as [65]

$$\tau_s = \gamma \, \tau_B \qquad (1.32)$$

where $\gamma = d/l$, d is the thickness of the film and l is the mean free path.

In analogy to (1.28), the average carrier mobility, μ_F, in the film can be written as

$$\mu_F = \frac{e\,\tau_F}{m^*} \qquad (1.33)$$

Using equations (1.31) and (1.32),

$$\mu_F = \frac{\mu_B}{1+1/\gamma} \qquad (1.34)$$

where μ_B is the bulk mobility.

Introducing the scattering coefficient, p, which is the probability that a carrier is specularly reflected, as in the case of metal films [66], i.e., only a fraction (1 - p) of carriers will be scattered diffusively, the term $1/\tau_s$ in equation (1.31) will change to $(1 - p)/\tau_s$.

Hence μ_F is

$$\mu_F = \frac{\mu_B}{1+(1-p)/\gamma} \qquad (1.35)$$

The mobility values in films appear to be small which is an indication of localisation [67,68] of carriers. If the mean free path is of the order of, or less than, the lattice spacing then the charge carrier is not moving in extended states.

1.2.2. Quantum Size Effects

When the thickness of the film is comparable with or smaller than the mean free path and the effective deBroglie wavelength of carriers, an oscillatory behaviour in the transport properties [69-71] as a function of thickness is observed. This is because, the transverse component of quasi-momentum is quantised due to the finite thickness of the film and the electron states assume quasi discrete energy values in the thin film. This discreteness will be predominant only if the spacing between the sub bands is larger than the broadening of the sub band due to thermal scattering. This quantisation will result in the separation of the bottom of the conduction band and the top of the valence band by a value which is the spacing between the sub bands. Studies of Davey et al [72] on evaporated polycrystalline germanium films show the presence of size effects.

1.2.3. Anisotropy Effects

The energy surface is commonly considered as spherical. However, for an ellipsoidal energy surface, it is found that the conductivity and effective mobility decreases to a finite limiting value, even for specular

reflection, for very thin films [65,73]. The transport parameters in a semiconductor film, for the ellipsoidal energy surface vary with the orientation of the normal to the film with respect to crystallographic axes [74].

1.2.4. Activation Energy

The temperature dependence of conductivity of the films gives the activation energy values. For crystalline films well defined energies are obtained while for non-crystalline films the plots will not be exactly linear and no well defined activation energies will be obtained. The activation energy, ΔE, from the temperature dependence of conductivity is

$$\Delta E = - \frac{d \ln \sigma}{d(1/kT)}$$

i.e.,
$$\Delta E = - \frac{1}{\sigma} \frac{d\sigma}{d(1/kT)} \tag{1.36}$$

The conductivity, σ, according to the Kubo-Greenwood formula [68] is

$$\sigma = - \int \sigma(E) \frac{\partial f}{\partial E} \, dE \tag{1.37}$$

where f is the Fermi-Dirac function and the physical significance of $\sigma(E)$ is that it is the conductivity of

carriers at energy E. Using equation (1.37), the activation energy can be written as

$$\Delta E = \frac{1}{\sigma}\left[\int \frac{\partial f}{\partial E}\,\frac{\partial \sigma(E)}{\partial(1/kT)}\,dE + \int \sigma(E)\,\frac{\partial(\partial f/\partial E)}{\partial(1/kT)}\,dE\right] \tag{1.38}$$

From this equation it can be seen that there are two specific cases for the activation energy.

The first case is, when

$$\frac{\partial \sigma(E)}{\partial(1/kT)} = 0,\ \text{i.e.},\ (E - E_F) > kT,$$

Then

$$\Delta E = \frac{1}{\sigma}\ \sigma(E)\ \ E - E_F\ \ \frac{f}{E}\ \ dE \tag{1.39}$$

This denotes a conductivity averaged energy. So the activation energy measured experimentally as the gradient of the conductivity curve represents the average energy of carriers with respect to the Fermi energy. Hence, if the carriers can only move at the bottom and top of the bands, as in the case of crystalline semiconductors, the activation energy is constant. In other words, a well defined activation energy indicates the band-like properties of the material.

As a second case, if $(E - E_F) < kT$,

$$\Delta E = -\frac{k}{\sigma}\int \sigma(E)\,\frac{\partial f}{\partial E}\,T\,dE = kT \qquad (1.40)$$

The average energy of carriers in such a system is the thermal energy and the Fermi function is constant.

1.3. High Field Conduction

1.3.1. General

The effect of high electric fields on the electronic conduction in solids was carried out for the first time [75,76] in connection with the dielectric breakdown in insulators. In homogeneous semiconductors, at high fields, Schokley [77] reported that the mobility of carriers decreases with increasing fields. This decrease in mobility is due to the increase in energy and speed of the carriers [78] by the applied field. The current in a semiconductor is ohmic upto the field for which the electron drift velocity equals the sound velocity and above this increases slowly with increasing field [79]. This non ohmic behaviour is due to the generation of acoustic flux by the carriers which takes place when the drift velocity exceeds the sound velocity [80]. Not all the conductivity changes observed in the high fields are due to changes in

mobility. Due to impact ionization of shallow-level impurities by hot carriers, changes in conductivity have been observed in germanium [81-83], silicon [84], InP [85] and InSb [86,87].

1.3.2. Electrode-limited Process

The electrical conduction through a semiconductor is highly dependent on the potential barrier at the metal-semiconductor interface. The potential step changes as a result of the image force [88]. The metal surface becomes polarised due to the escape of an electron and this in turn exerts an attractive force on the electron. The potential energy of the electron due to the image force is

$$\phi_{im} = - \frac{e^2}{16\pi \varepsilon \varepsilon_0 x} \qquad (1.41)$$

where ε is the high frequency dielectric constant and x is the distance of electron from the electrode surface. This image force effects, play an important role in the conduction process when the current is electrode-limited [89].

According to Schottky [88], the image force is limited to a distance, x_0, of the electron from the electrode surface. Under the application of the

electric field, the interaction of the field with the image force at the interface lowers the potential barrier. Such a potential barrier for Schottky emission [90] is shown in figure 1.2. The barrier is lowered by $\Delta\phi_S$, (dotted line in the figure 1.2) and the potential energy of the barrier, under the influence of the field with respect to the Fermi level of the electrode, is less than ϕ_o by $\Delta\phi_S$. This difference in the barrier height, $\Delta\phi_S$, is

$$\Delta\phi_S = \left(\frac{e^3}{4\pi\epsilon\epsilon_o}\right)^{\frac{1}{2}} F^{\frac{1}{2}}$$

i.e., $\Delta\phi_S = \beta_S F^{\frac{1}{2}}$ (1.42)

where $\beta_S = (e^3/4\pi\epsilon\epsilon_o)^{\frac{1}{2}}$ is the Schottky factor. The electrode limited current density in this barrier lowering case, obeys the Richardson-Schottky law.

$$J = AT^2 \exp\left(-\frac{\phi_o - \Delta\phi}{kT}\right) \qquad (1.43)$$

i.e., $J = AT^2 \exp(-\phi_o/kT) \exp\left(\frac{\beta_S F^{\frac{1}{2}}}{kT}\right)$

(1.44)

where $A = \frac{4\pi em(kT)^2}{h^2}$. When the electron mean free path is of the order of the insulator thickness this

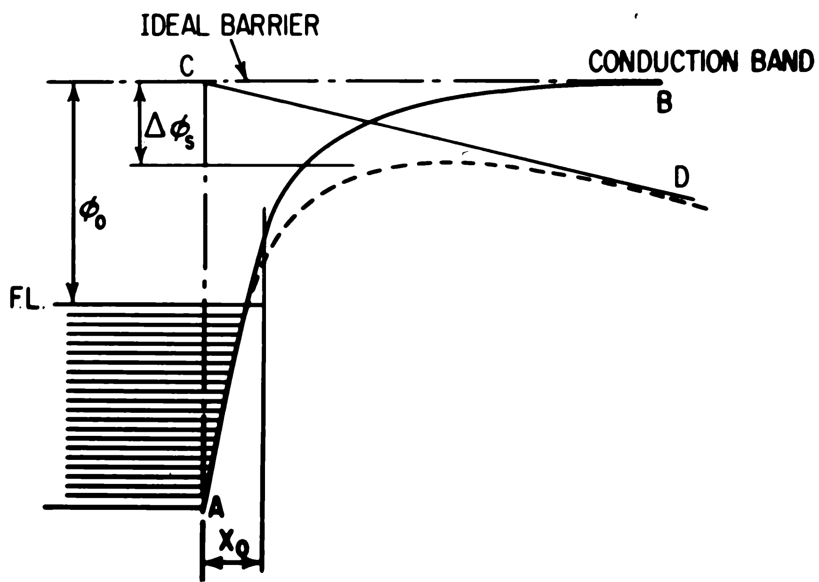

Figure 1.2. Schottky effect.

equation holds [91], taking into account the effective mass of the electron for the calculation of the constant A [92].

However, log I Vs. $F^{\frac{1}{2}}$ relationship does not necessarily imply a Schottky effect as reported by Mead [93] in ZnO films. At low temperature field emission can be the dominating conduction process. The electrode limited conduction process change from Schottky to field emission mechanism [94,95] as the temperature of the sample is lowered. If the mobility of carriers is too low, it will control the total current and the effect of diffusion may modify the Schottky barriers [96,97] at the metal-semiconductor interface.

1.3.3. Bulk limited Process

An applied electric field lowers the coulombic potential barrier, similar to the lowering of the interfacial barrier in the Schottky effect. This lowering of the potential obeys Poole's law [98,99], and is called the Poole-Frenkel effect [100,101], as shown in figure 1.3. The Poole-Frenkel lowering of a coulombic barrier, $\Delta\phi_{PF}$, will be twice that due to Schottky effect, because the potential

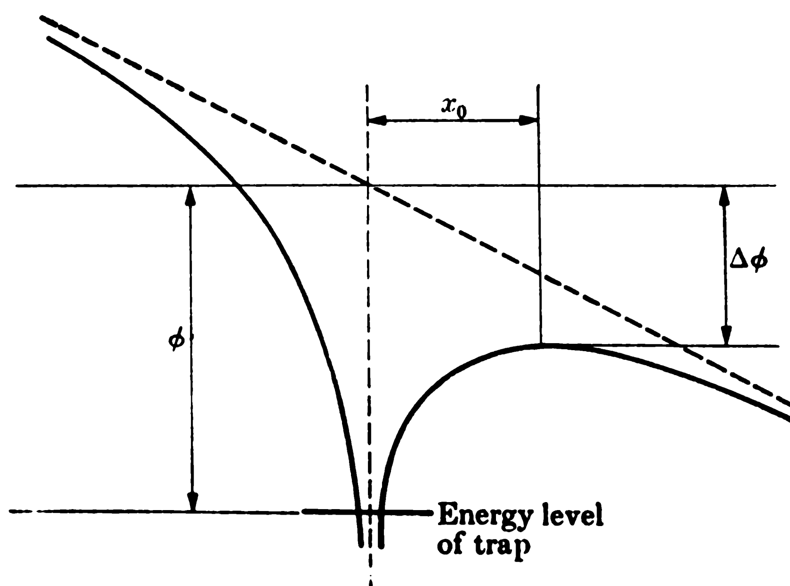

Figure 1.3. Poole-Frenkel effect.

energy of an electron at the coulombic field is $-e^2/4\pi\varepsilon\varepsilon_0 x$, which is four times that due to image force (equation 1.41)

$$\Delta\phi_{PF} = \left(\frac{e^3}{\pi\varepsilon\,\varepsilon_0}\right)^{\frac{1}{2}} F^{\frac{1}{2}}$$

$$\Delta\phi_{PF} = \beta_{PF} F^{\frac{1}{2}} \tag{1.45}$$

where $\beta_{PF} = \left(\frac{e^3}{\pi\varepsilon\varepsilon_0}\right)^{\frac{1}{2}}$ is the Poole-Frenkel factor. The value of $\Delta\phi_{PF} = 2\,\Delta\phi_s$. According to Frenkel [100,101], the current density in this case is given by

$$J = J_0 \exp\left(\frac{\beta_{PF} F^{\frac{1}{2}}}{2kT}\right) \tag{1.46}$$

where J_0 is the low field current density. Considering the shallow traps in the materials, the high field current density [102] due to this bulk limited conduction is

$$J = J_0 \exp\left(\frac{\beta_{PF} F^{\frac{1}{2}}}{kT}\right) \tag{1.47}$$

However, this Poole-Frenkel equation applies only for the field emission in the direction of the field [103,104]. In the reverse direction, if the field being lowered, a hypothetical reverse peak is

suggested by Hill [105]. Hartman et al [106] proposed a modification to the Poole-Frenkel law, considering the temperature dependence of the current. According to Jonscher and Ansari [107], the temperature dependent term in the exponent cannot be taken for a proper distinction between Poole-Frenkel and Richardson-Schottky mechanisms.

1.3.4. Electrode limited to Bulk limited

If the trap level in a semiconductor/insulator is deeper than the Fermi level, even if the donor density is high, the conductivity in the material will be low, and under these conditions it is possible to observe an electrode to bulk limited transition in the conduction process [108]. At low voltages, the conduction process will be electrode limited.

At higher voltages, either field emission of electrons from the cathode to the conduction band can occur if the barrier at the Fermi level is very thin, or as the voltage exceeds 3/2 of the energy gap impact ionization can occur. The net effect of both these will be a rapid decrease in the contact resistance.

The electrode limited process predominates at the lower field, and in that case the contact resistance will be higher than the bulk resistance. As the field

increases, the contact resistance decreases and at a particular applied voltage the contact resistance and the bulk resistance become equal. Thereafter, there will be no effect for the contact resistance and the conduction will be bulk limited.

1.4. Conduction in Disordered Compound Semiconductor Films

1.4.1. General

The features of the energy distribution of the density of electronic states of crystalline semiconductors are the sharp structure in the valence and conduction bands, and the abrupt terminations at the valence band maximum and conduction band minimum. The states are extended within the band and the features of the band structure are the consequences of the perfect short range and long range orders of the crystal. In a disordered or amorphous semiconductor, the long range order is destroyed and the short range order—the interatomic distance and the valence angle—is only slightly perturbed [55,109,110]. The concept of the band model with density of states can be applicable to these non crystalline semiconductors [111] also.

1.4.2. Band Models

Different models have been proposed for the density of states of amorphous semiconductors and according to Anderson [112], the states become localised near the top and bottom of the band.

(i) CFO model

According to a model proposed by Cohen, Fritzsche and Ovshinsky [113] (CFO model), the localised states in the band tails are assumed to extend across the gap in a structureless distribution (figure 1.4). The sharpness of the conduction and valence band edges are destroyed by the gradual decrease in the localised states. The overlapping of the tails of the conduction and valence band leads to the positioning of the Fermi level near the middle of the band. This CFO model was proposed to explain the electrical properties of multicomponent chalcogenide glasses.

(ii) Davis-Mott model

Another model proposed by Davis and Mott [114,115] illustrates that the tails of the localised states are narrow and extend only to a few tenths of an electron volt in the forbidden gap and a band of

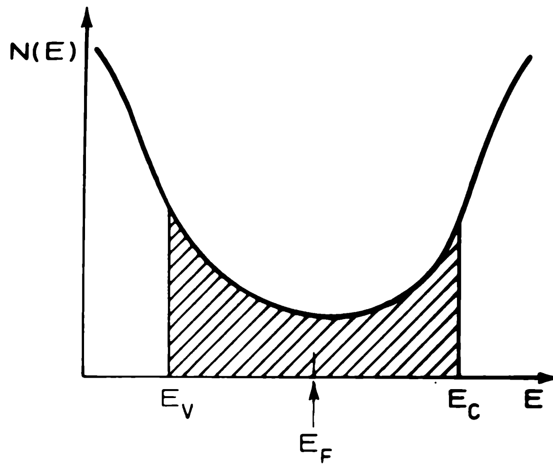

Figure 1.4. CFO model.

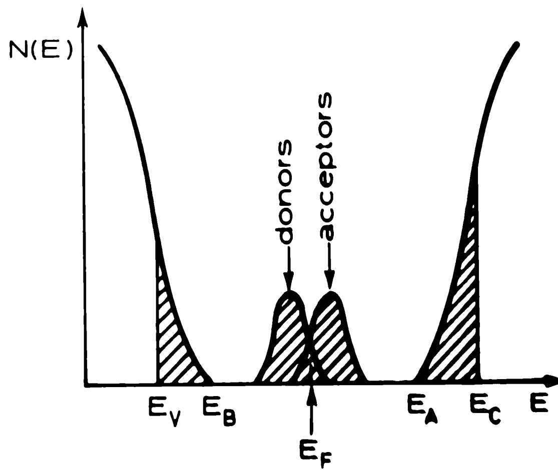

Figure 1.5. Davis-Mott model.

compensated levels exists near the middle of the gap (figure 1.5). This new band is due to the defects in the material and may split into a donor and acceptor band which will pin the Fermi level. A continuous drop of the mobility [116] occurs in the extended states and at the transition from extended to localised states producing a mobility edge.

The above models suggest that in amorphous semiconductors the density of states does not decrease monotonically into the gap, but shows many well defined peaks [117]. The Fermi level in such a system can be determined by the charge distribution in the gap states.

1.4.3. Conductivity

The electrical conduction in an amorphous semiconductor is closely related to the energy distribution of the density of states. Three conduction processes, predominating at different temperature regions, can be explained using the Davis-Mott model. At very low temperatures conduction can occur by the thermally assisted tunnelling between states at the Fermi level. At high temperatures charge carriers

are excited into the localised states of band tails. These carriers in localised states take part in conduction by hopping [118,119]. Carriers are excited across the mobility edge into the extended states at very high temperatures and conduction occurs in extended states above the mobility edge [120].

The charge carriers in some amorphous semiconductors may enter a self trapped state (small-polaron) due to the polarisation of the surrounding atomic lattice as suggested by Emin [121]. Emin et al [122] have explained the temperature dependence of conductivity by the small polaron hopping.

Experimental results obtained for various tetrahedral amorphous semiconductor films like germanium [123], silicon [118], and lone pair semiconductor films line As_2Se_3 [124] and cross linked ternary systems like As-Te-Ge [125] agree with the conductivity proposed using the band models.

CHAPTER TWO

CONTACT PHENOMENA IN THIN FILMS

Metal-semiconductor contacts are very important in the semiconductor device technology. The electrical properties of the semiconductor films are governed by the combined effect of bulk and contacts. The difference in the electrostatic potential that develops across the interface between a semiconductor and a metal plays an important role in conduction. There are different types of metal-semiconductor contacts depending upon the potential difference at the interface.

2.1. Ohmic Contacts

An ohmic contact at the metal-semiconductor interface must offer a minimum resistance to the current flow in both directions over a wide temperature range. These contacts can be electrically characterized by their specific contact resistance, R_c [126]. This contact resistance, which is smaller for the larger contact area, should be smaller or comparable to the series resistance of the semiconductor material adjacent

to the contact, for an ohmic contact. This series resistance can be taken as the spreading resistance, R_s, [127] which is given by

$$R_s = \frac{\rho_s}{2\pi r} \tan^{-1} \left(\frac{2d}{r}\right) \tag{2.1}$$

where r is the effective contact radius and d is the thickness of the film.

For $d \gg r$,

$$R_s \sim \frac{\rho_s}{4r} \tag{2.2}$$

and for $d \ll r$,

$$R_s \sim \frac{\rho_s d}{\pi r^2} \tag{2.3}$$

The experimental measurements give the value $R_{c,s}$ which is the sum of both R_c and R_s. According to Fang et al [128], the shape of the metal contact, periphery and wafer thickness play important role in controlling the contact resistance.

2.1.1. Formation of the Contact

On most of the semiconductors, the formation of the contact is by the alloying of the metal on the

surface of the semiconductor [129], in which a thin film alloy is formed in the molten form at the interface. Recrystallisation from the melt results in a good ohmic contact at the semiconductor-conductor interface. Such contacts are reported on n-GaAs using Ag-In-Ge [127,130] and Au-Ge [131,132] and on p-InP using Be-Au [133].

Another ohmic contact metallisation scheme is the sintering process (i.e.,solid-state interdiffusion) [134]. The ohmic behaviour results from a combination of the doping action and fast indiffusion of the metal atoms into the semiconductor. A change in the covalent bonding present in semiconductors to metallic bonding occurs through the interface which diffuse over several inter atomic distances, resulting in a semiconductor-conductor interface which is not abrupt on an atomic scale.

2.1.2. Types of the Contact

As the interface offers low resistance to the current flow, the metal contact can inject sufficient carriers to the semiconductor. There are different types of injecting contacts.

(i) Non degenerate case

An electron injecting non-degenerate contact is shown in figure 2.1(a). Injection takes place from n^+ region to the left of the interface over the n^+- n or n^+-intrinsic junction. This contact is not effective at low temperatures where carrier freeze out takes place.

(ii) Degenerate case

The difference between this contact and the non-degenerate one is that the n^+ region is degenerate in this case (Figure 2.1(b)). Hence carrier freeze-out cannot take place in this region and this contact can be used at low temperatures.

(iii) Tunneling contact

At low voltages this contact (Figure 2.1(c)) acts as a blocking contact. The potential barrier is so thin that the application of a small voltage promotes the tunneling of electrons from the metal to the semiconductor. Beyond this voltage the contact acts as an injecting contact.

(iv) Light generated reservoir contact

A reservoir of electrons can be created at the interface, by illuminating the surface with an

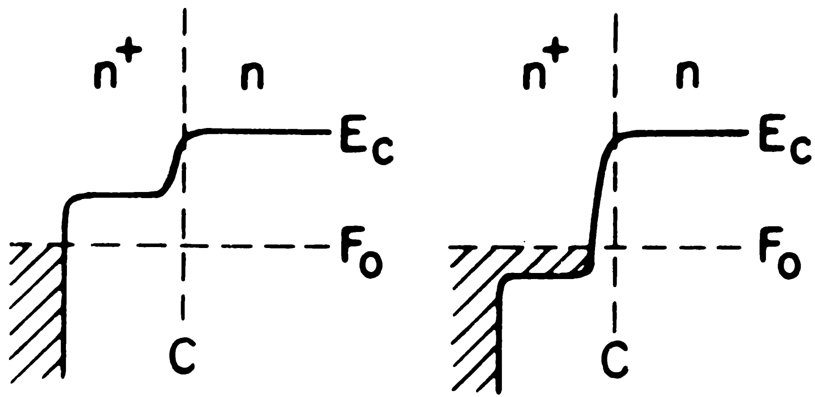

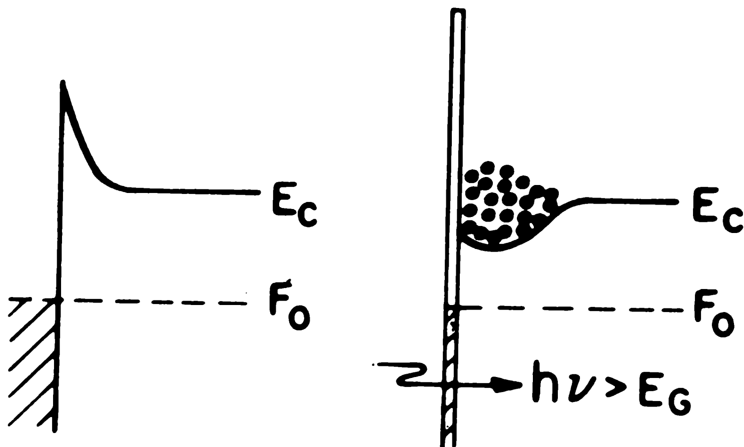

Figure 2.1. Schematic energy band contacts for electron injection. (a) Nondegenerate contact, (b) Degenerate contact, (c) Tunnelling contact, (d) Light generated reservoir contact.

intense beam of light of frequency ν such that $h\nu > E_g$. (Figure 2.1(d)). By this process a reservoir of holes can also be produced in the valence band simultaneously. The electrical contact in this case can be provided by a transparent conducting film.

2.2. Schottky and Bardeen Barrier

Metal-semiconductor interface which offers low resistance to current flow in one direction and high resistance in the opposite direction is commonly called a Schottky barrier and has wide use in integrated circuit technology as fast switch or for protecting circuit elements from high voltage transients. The potential barrier or barrier height, ϕ_B, between the Fermi level in the metal and the majority carrier band edge of the semiconductor, at the interface is most important in a metal-semiconductor contact. Such a barrier height ϕ_B between a metal and a p-type semiconductor is shown in figure 2.2. The potential barrier between the interior of the semiconductor and the interface is called the band bending ψ_s. The barrier height is determined by the density of interface states. The interface states are potential wells containing energy levels in the semiconductor band gap

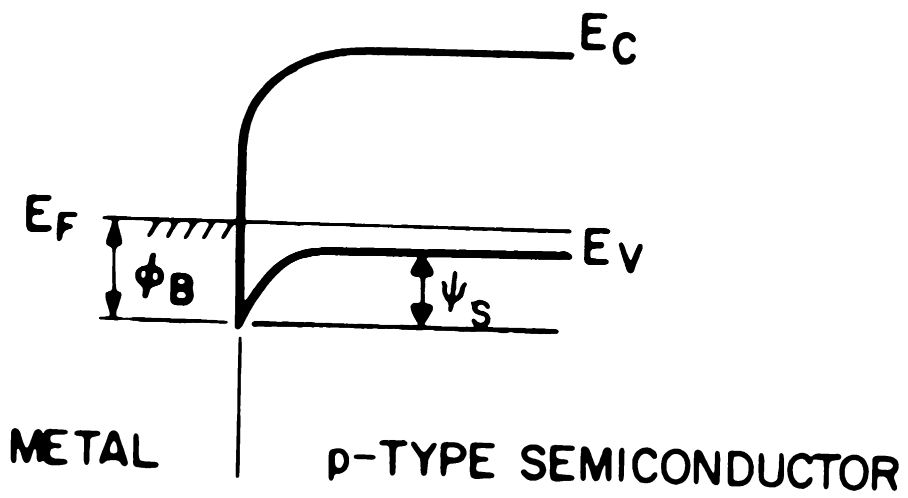

Figure 2.2. Band bending diagram of a metal-semiconductor contact.

located at the metal-semiconductor interface [126]. These interface states are highly predominant in modifying the barrier height in covalent semiconductors [135-137]. Considering the influence of interface states, rectifying barriers can be classified into four types [138], even though all of them are generally called by the name Schottky barriers.

2.2.1. True Schottky Barrier

In a true Schottky barrier, the barrier height ϕ_B is nearly proportional to the work function difference between metal and the semiconductor. At the metal-semiconductor interface the metal is physisorbed on the semiconductor surface. The contact between a metal and an ionic semiconductor is an example of a true Schottky barrier contact.

2.2.2. Bardeen Barrier

The barrier height is nearly independent of the work function difference between the metal and the semiconductor in a Bardeen barrier contact [12] and is determined largely by the interface states. In this case, the nonmetal is a highly polarisable semiconductor and the metal does not react with it

to form a bulk compound and hence the metal is weakly bonded to the semiconductor. Metal-covalent semiconductor contacts, such as Au-Si contact, are Bardeen barrier contacts.

2.2.3. Modified Bardeen Barrier

A highly polarised semiconductor makes a contact with metal resulting in the formation of one or more bulk compounds at the interface. This contact is characterised by a strong chemical reaction between the metal and the semiconductor. In this type, the interface is between an intermetallic compound and the semiconductor. However, the barrier height is still influenced by the interface states and hence this contact is called a modified Bardeen barrier. But the density of the interface states have been reduced because of the chemical bond between the intermetallic compound and the semiconductor. Both the Bardeen barrier and modified Bardeen barrier contacts are widely used in integrated circuits and microwave devices such as IMPATT diodes and GaAs FETs.

2.2.4. Oxide Layer Contact

In an oxide layer contact an intervening oxide layer is produced deliberately or otherwise

between the metal and semiconductor. This type of contact has two interfaces, one between the metal and the oxide and the other between the oxide and the semiconductor. The interface between the oxide and the semiconductor is more important because any charged traps at or near the oxide-semiconductor interface will affect the barrier height. The interface between the metal and the oxide layer will have virtually no effect on the electrical properties of the contact. This oxide barrier contact is important in reliability studies and have uses in solar cell applications.

2.3. Blocking and Neutral Contact

2.3.1. Blocking Contact

A metal-insulator contact is said to be blocking when the current flow through the interface is practically zero, regardless of the applied field. On the application of the field a depletion region is created at the interface and as a result an electrostatic interaction between oppositely charged regions occurs and a local field is produced within the surface of the insulator. This causes the bending of the bottom of the conduction band. The depth of the

depletion layer at the interface is dependent on the density of donors in the insulator.

2.3.2. Neutral Contact

If there is no reservoir of charge at the contact, the contact is called neutral contact. This means, the conduction band is flat right upto the interface and no band bending is present.

2.4. Metal-Semiconductor Interface Reactions

Any good contact between a metal and a semiconductor requires a limited and uniform reaction at the contact interface [139]. The movement of metal and semiconductor atoms across the metal-semiconductor interface has great significance in determining the electronic properties of compound semiconductors [140,141]. For interfaces exhibiting strong chemical reaction [142,143], significant inter-diffusion can take place which may affect the Schottky barrier features [144,145]. Since the interface chemical reactions greatly modify the metal-semiconductor junctions, detailed investigation of the interface atomic microstructures is necessary to determine the

exact electronic properties of the interface [146]. In a reactive interface, the physical properties of the interface are related to the interfacial layer which is manifested through the correlation between Schottky barrier height and eutectic temperature of the compound formation at the interface [147]. Also, it is observed that the interdiffusion effects can alter the Schottky barrier properties of relatively unreactive metal-semiconductor interfaces [148-152].

Several analytical techniques such as soft X-ray photo-emission spectroscopy [153], glancing incidence X-ray diffraction, Rutherford back scattering, transmission electron microscopy etc. are used to study the interface reactions at the metal-semiconductor interfaces.

CHAPTER THREE

CURRENT INJECTION IN SEMICONDUCTOR FILMS

3.1. General Features

Current injection in insulators and semiconductors provides a valuable technique for obtaining information about the defect states in these materials such as their density and energy location in the forbidden gap. Mott and Gurney [154] made the important observation that it should be possible to obtain injection of electrons from a suitable contact into an insulator in a manner analogous to the electron injection from a thermionic cathode into vacuum. However, the detailed studies by Rose [155,156] showed that the trapping of injected carriers at localised trapping centres reduces the injected current. For a detailed analysis of the current injection, the conditions for injection and the energy band basis for injection are to be considered.

3.1.1. Conditions for Current Injection

If the applied field is large enough and the metal makes an ohmic contact to the semiconductor, the injection of carriers into the bulk of semiconductor takes place. The carrier concentration near the contact therefore increases due to the flow of current. As a result, a space charge cloud of charge carriers will be formed in the vicinity of the contacts. Mutual repulsion between the individual carriers limits the total injected charge and the resulting current is said to be space charge limited (SCL). For the flow of the injected carriers two major requirements have to be satisfied. First one is that the electrodes must furnish ohmic contacts to the solid. Secondly, the semiconductor should be relatively free from trapping centres, since these trapping centres can reduce the magnitude of the current and modify the current-voltage characteristics.

3.1.2. Energy Band Basis for Injection

The interface dipole energy barrier at a metal-semiconductor contact can be substantially smaller than the corresponding work function barrier at a metal-vacuum contact. As a result, there may

be sufficient number of electrons available at the contact even at room temperature [157] for injection into the bulk of the semiconductor. Electron flow in the conduction band is dominated by the frequent collisions with phonons, chemical impurities and structural imperfections. The important effect will be produced by the localised traps associated with impurities and structural imperfections [158] energetically located in the forbidden gap. Such trapping states, E_{tn1} and E_{tn2} for electrons in case of electron injection into conduction band and E_{tp1} and E_{tp2} for holes in the case of hole injection into valence band, are schematically shown in figures 3.1(a) and 3.1(b) respectively. Hence a study of the current-voltage characteristics of a semiconductor system can undoubtedly give informations regarding the density and energy distribution of defect states in the system [159,160]. Theoretical investigations [158,161-165] of different simple models provided a clear picture of trapping effects in solids.

3.1.3. Technological Applications

Space charge limited conduction in semiconductors has wide technological applications.

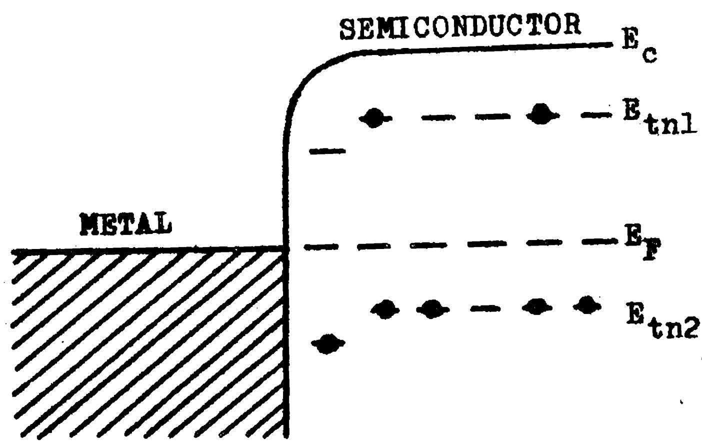

(a)

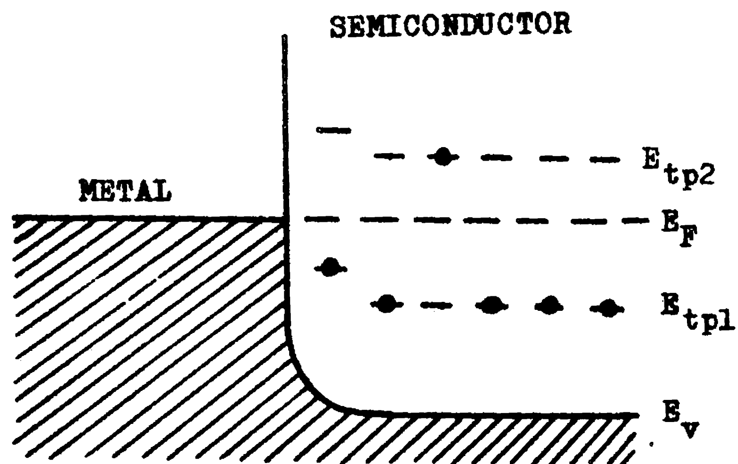

(b)

Figure 3.1. Schematic energy band diagram of metal-semiconductor contact. (a) ohmic for electron injection, including electron trapping states; (b) ohmic for hole injection, including hole trapping states.

SCL injection diodes using CdS single crystals [166-168] and evaporated films [169], thin film field effect transistors using CdS [170,171] and CdSe [172] were found very useful in device applications. Injection electroluminescence in wide-band gap materials [173] and organic solids [174] paved a new branch of study. Coherent light emission or laser action was achieved due to injection electroluminescence [175] in semiconductors such as GaAs and GaAs-GaP alloys.

3.2. Steady State One Carrier SCL Currents

3.2.1. Trap Free Case

In the case of perfect insulator, free of traps with a negligible concentration of free carriers in thermal equilibrium, all the injected electrons remain free in the conduction band and will contribute to space charge. The current density, J, in that case may be written as

$$J = \bar{\rho} v \tag{3.1}$$

where $\bar{\rho}$ is the average injected free charge concentration and v is the average drift velocity of the electron

$$J = Q/t \tag{3.2}$$

where Q is the total injected free charge and t is the transit time of a free electron between the electrodes. In determining the current density, the contribution of diffusion current can be neglected since it is predominant only at the immediate neighbourhood of the contacts. The total charge injected, Q, can be written in terms of the dielectric constant, ε, of the material and the electrode spacing, d, which is the thickness of the film.

$$Q \simeq (\varepsilon/d)\, V \qquad (3.3)$$

where V is the applied voltage. The transit time $t = d/v$, and combining equations (3.2) and (3.3)

$$J \simeq \varepsilon v V/d^2 \qquad (3.4)$$

The electron drift velocity is proportional to the applied field.

$$\text{i.e., } v = \mu(V/d) \qquad (3.5)$$

where μ is the free electron drift mobility and V/d denotes the applied field.

Therefore,

$$J = \varepsilon\, \mu\, (V^2/d^3) \qquad (3.6)$$

The current density obeys a trap free square law in this case.

If there are thermal free carriers present having a concentration n_o, then at low fields the current voltage behaviour holds Ohm's law.

$$J = e n_o \mu (V/d) \tag{3.7}$$

As the field is increased, the injected free electron concentration, n_i, becomes comparable to that of thermally generated concentration, n_o. Thus a cross over from Ohm's law (3.7) to a trap free square law (3.6) takes place, which is the onset of space charge limited current injection [176]. The cross over voltage, V_x, is characterised by

$$V_x \simeq e n_o d^2/\epsilon \tag{3.8}$$

Further, the injected excess electrons will dominate the thermally generated electrons.

3.2.2. Semiconductor with Traps

The presence of electron traps in the semiconductor will generally result in a greatly reduced current at lower injection levels, since these traps

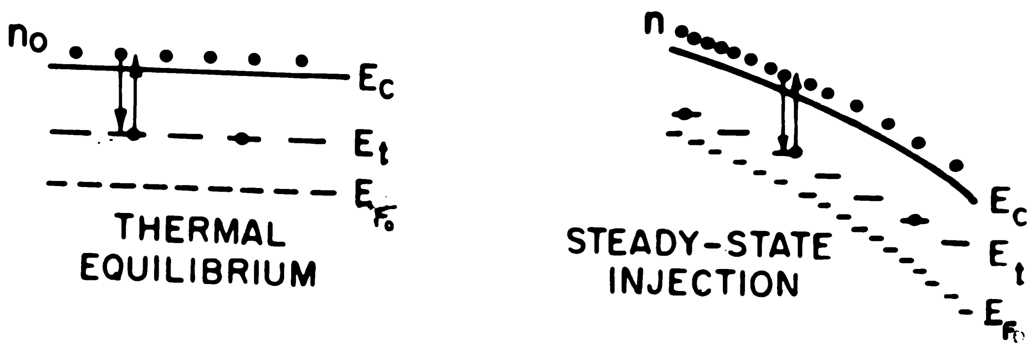

Figure 3.2. Thermal equilibrium characterised by thermodynamic Fermi level E_{F_o} and steady state injection characterised by quasi Fermi level E_F.

will capture and immobilise most of the injected carriers. In determining the current density, a relationship between free and trapped carriers in thermal equilibrium is to be taken into account. This relationship can be expressed via the thermodynamic Fermi level E_{F_o}. For non degenerate semiconductors, the thermal equilibrium free electron concentration is given by

$$n_o = N_c \exp[(E_{F_o} - E_c)/kT] \qquad (3.9)$$

where N_c is the effective density of states in the conduction band and E_c is the energy of the bottom edge of the conduction band. Figure 3.2(a) and 3.2(b) show the thermal equilibrium characterised by the thermodynamic Fermi level E_{F_o} and the steady state injection characterised by the quasi-Fermi level, E_F, respectively, with electron traps at level E_t. The concentration $n_{t,o}$ of filled electron traps is given by the Fermi-Dirac expression

$$n_{t,o} = \frac{N_t}{1+(1/g)\exp[(E_t-E_{F_o})/kT]}$$

$$\text{i.e., } n_{t,o} = \frac{N_t}{1+(1/g)(N/n_o)} \qquad (3.10)$$

where $N = N_c \exp[(E_t - E_c)/kT]$ (3.11)

and N_t is the density of traps and g, the degeneracy factor for the traps.

However, under the application of a field, a balance between free and trapped electrons is reached only with the free electron concentration n, achieved under injection, instead of thermal equilibrium concentration n_o. The corresponding Fermi level E_F is called the quasi-Fermi level or electron steady state Fermi level [177] and is related to n.

$$n = n_i + n_o = N_c \exp[(E_F - E_c)/kT] \quad (3.12)$$

where n_i is the average excess injected free electron concentration. The trapped electron concentration n_t is then given by

$$n_t = \frac{N_t}{1+(1/g)\exp[(E_t - E_F)/kT]}$$

i.e.,

$$n_t = \frac{N_t}{1+(1/g)(N/n)} \quad (3.13)$$

Now, this quasi Fermi level and the quasi-thermal equilibrium condition can be used to discuss different trap models.

(i) Shallow traps

An electron trap E_t is said to be shallow if E_F lies well below E_t. That means $(E_t - E_F)/kT > 1$, or the trap states are at energy E_{tm1} in figure 3.1(a). Then,

$$\theta = \frac{n}{n_t} = \frac{\bar{\rho}}{\bar{\rho}_t} = \frac{n}{gN_t} = \frac{N_c}{gN_t}\exp\left(\frac{E_t - E_c}{kT}\right) \tag{3.14}$$

where θ is a constant independent of the injection level, and $\bar{\rho}_t$ is the average injected trapped charge concentration.

If $\theta \ll 1$, the shallow trap density N_t will affect the SCL injection current. Hence the total injected free charge will be

$$Q \simeq \bar{\rho}_t d \simeq \bar{\rho} d/\theta \simeq \epsilon V/d \tag{3.15}$$

Combining equations (3.1), (3.5) and (3.15) gives the current density

$$J \simeq \theta \epsilon \mu V^2/d^3 \tag{3.16}$$

However, the analytically derived results give the exact value for the current density in the shallow

trap case [160] as

$$J = \frac{9}{8} \theta \varepsilon \mu V^2/d^3 \qquad (3.17)$$

The crossover voltage, V_x, from Ohm's law to shallow trap square law differs from that for trap free case by a factor $1/\theta$.

i.e., $$V_x \simeq \frac{e n_0 d^2}{\theta \varepsilon} \qquad (3.18)$$

(ii) Deep traps

An electron trap E_t is said to be deep if E_F lies above E_t, which means the trap states are at energy E_{tn2} in figure 3.1(a), i.e., $(E_F - E_t)/kT > 1$. At thermal equilibrium, the concentration of traps not occupied by electrons is

$$P_{t,0} = N_t - n_{t,0} \simeq \frac{N_t}{g} \exp\left(\frac{E_t - E_F}{kT}\right) \qquad (3.19)$$

As the injected free electron concentration, n_i, becomes comparable to n_0, the quasi-Fermi level E_F will move up. This motion is sufficient to fill the deep traps. In this case the cross over voltage V_x for the onset of SCL current injection, coincides with the trap filled limit voltage, V_{TFL}, required to fill

the set of deep traps.

$$V_{TFL} \simeq \frac{e p_{t,0} d^2}{\epsilon} \qquad (3.20)$$

The trap filled limit voltage V_{TFL} measures that fraction of the total concentration of traps which is empty in thermal equilibrium [160]. Also, V_{TFL} is independent of mobility, even under high field, so long as impact ionisation do not take place.

3.2.3. Lampert's Triangle

The current-voltage characteristics for a system with a single set of trap density, located below and above the Fermi level, on a log-log scale is as shown in figure 3.3. Curve I corresponds to the Fermi level lying above E_t, i.e., deep traps, and curve II corresponds to Fermi level lying below E_t, i.e., shallow traps. The entire family is contained in a "triangle" called Lampert's triangle. The triangle is bounded by Ohm's law, trap free square law and the trap filled limit law (TFL law) regions. Independent of the position of the trap level, the current-voltage plot cannot lie above the trap free square law or below the Ohm's law or right of the TFL law, i.e., the characteristic must lie inside the triangle [157].

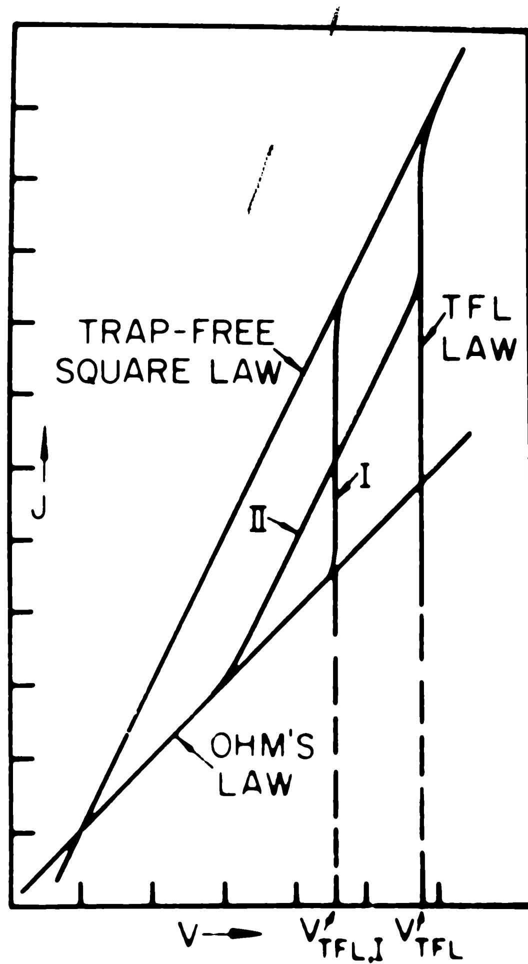

Figure 3.3. Lampert's triangle.

3.2.4. Energy Distribution of Traps

It is not exact to define a set of traps at a particular energy level E_t. This may be true for single crystals of high chemical and structural purity. However, for amorphous semiconductors and evaporated thin films of poorly defined crystallinity discrete energy levels of traps have to be assumed, even though they are of high chemical purity. In such cases a broad smearing out of trap level have to be considered and the set of traps can be represented by a Gaussian distribution [156]. A simple representation of many different set of traps is the exponential distribution

$$\mathcal{N}_t(E) = \mathcal{N}_o \exp\left(\frac{E - E_c}{kT_t}\right)$$

$$= \mathcal{N}_n \exp\left(\frac{E - E_F}{kT_t}\right)$$

When $\mathcal{N}_n = \mathcal{N}_0 \exp\left(\frac{E_F - E_c}{kT_t}\right)$ with T_t, the temperature parameter characterising the trap distribution.

3.3. Two Carrier Injection Problem

3.3.1. Double Injection

If one electrode is ohmic to electrons and the other ohmic to holes, space charge limited currents of both electrons and holes can flow into the

semiconductor. Since the injected electrons and holes can largely neutralise each other, the number of injected carriers can greatly exceed the injected space charge. Therefore double injection current will generally be larger than single carrier injection under the same conditions of voltage bias.

For the two carrier SCL conduction, the dielectric relaxation time will be greater than the transit times for both electrons and holes [162]. A feature which is important in the double injection problem is the recombination. Electrons and holes can recombine through localised centres and these recombination centres will be in communication with both the conduction and valence bands [165,178]. In addition to the recombination centres there may be normal electron and hole trapping centres.

3.3.2. Plasma Injected into Semiconductors

At sufficiently high applied voltages, the injected carriers outnumber the defect states and approximately neutralise each other making up the injected plasma. In a semiconductor, however, there will be sufficient number of thermally generated free carriers to relax the injected space charge [179].

Consider an n-type semiconductor with equilibrium electron and hole concentrations n_o and p_o respectively. $n_o - p_o = N_D - N_A$, where N_D and N_A are the donor and acceptor densities respectively. If n and p are the total free electron and free hole densities, then under injection conditions, the injected components are everywhere equal.

$$n - p = n_o - p_o = N_D - N_A$$

At high injection levels

$$n \gg n_o, \quad p \gg n_o, \quad n \simeq p.$$

The current density is then given by [164]

$$J = \left(\frac{9}{8} \right) e \, (n_o - p_o) \mu_n \mu_p \, \bar{\tau} \, (V^2/d^3) \qquad (3.22)$$

where μ_n and μ_p are the electron and hole mobilities respectively and $\bar{\tau}$ is the common average life time for injected electrons and holes.

Equation (3.22) is found valid for the effective life time, τ_{eff}, of the carriers also [180].

3.3.3. Negative Resistance

Localised defect states can play an important role in double injection. The capture and immobilisation of injected carriers may be expected to affect

the double injection current-voltage characteristic drastically. One of the potentially useful effects of this is the current controlled negative resistance (CCNR) regime in the characteristic deriving from a free carrier life time. The negative resistance of this type can be explained by the analysis of two possible levels [181] for the recombination centres.

Consider a single set of recombination centres lying well below the Fermi level and therefore completely occupied by electrons in thermal equilibrium. At low applied field, the injection level is very low and the occupancy of these states is negligibly perturbed, resulting in an infinite electron life time and relatively short hole life time. The injection current will be a trap free electron SCL current which recombines with the injected holes within the diffusion length of the hole injecting contact. As the field is increased holes will be driven across the system and hole life time increases. A stage is reached where the injected electron and hole concentrations exceed the occupancy of recombination centres and the hole injection level increases. The more holes injected, the easier it is for them to traverse the system.

the voltage required actually decreases as the current increases. Thus a region of negative resistance of current controlled type is obtained in the characteristic. This mechanism of CCNR was first pointed out by Stafeev [182].

If a single set of recombination centres are lying not too far below the Fermi level, then the centres are partially occupied by electrons. As in the previous case, the hole life time increases with increasing injection level, allowing the voltage across the system to drop, producing a current controlled negative resistance. The difference from the previous problem appears at low injection levels. Here, since there are empty centres as well as filled centres, there is a recombination barrier to the transit of electrons as well as holes, as a consequence of which there is a voltage threshold for current flow. In both cases, the CCNR is an irreversible process.

3.4. Activation Energy Analysis

3.4.1. Localised Levels

The measurement of thermal activation energies for both ohmic and SCL conduction over a broad

temperature range enables to evaluate both depth and concentration of localised levels in a semiconductor. For a simple activation energy in electrical conduction, specific energy levels must contribute overwhelmingly to partition functions of electrons and holes [183]. At each temperature there must be only one such level for each carrier. These are termed the 'dominant levels'. In narrow band gap materials the dominant levels tend to be the transport bands where as in wider band gap materials some localised level within the gap tends to be dominant instead.

The concentrations of the dominant levels and their locations in energy together with the concentration of electrons contributed by excess donors determine the location of the Fermi energy. A schematic energy level diagram for a solid containing dominant electron and hole states labelled by E_m and E_q respectively is shown in figure 3.4.

3.4.2. Roberts - Schmidlin Model

Both ohmic and SCL currents are thermally activated and the corresponding activation energies give the information regarding the localised levels in the band gap of the material [184]. Thermal

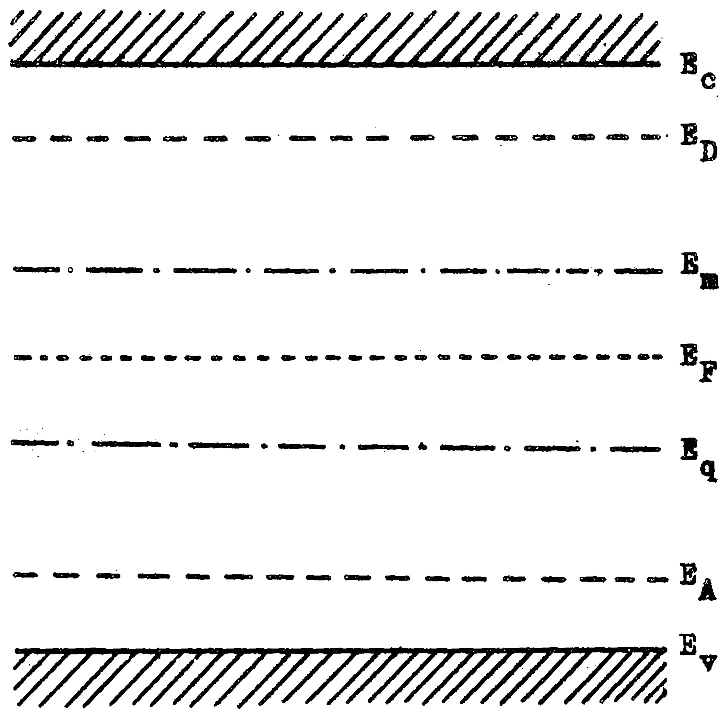

Figure 3.4. Schematic energy level diagram for a solid containing dominant electron and hole states.

activation energy for electrical conduction in semi-conductors is usually interpretted in one of the three possible ways, viz., half the band gap (material-intrinsic), some trap depth (material-extrinsic) or half the trap depth (material - highly doped). According to Roberts and Schmidlin [185] the position and population of the dominant levels can make two situations termed as extrinsic and non-extrinsic.

The analysis can be carried out for an n-type material. The extrinsic condition corresponds to common usage to the extent that the location of the Fermi energy depends on the excess donor concentration ($N_D - N_A$). All the not-extrinsic cases can together be called non extrinsic. This general term include intrinsic (both transport bands dominant), half intrinsic (one transport band dominant) and compensated (neither transport bands dominant).

If the excess donor concentration is small in comparison with the concentration of electrons excited from the dominant hole level to the dominant electron level, then the Fermi energy is located in such a way as to make the concentration of electrons in the dominant electron level equal to the concentration

of holes in the dominant hole level. This is called the "non-extrinsic" situation. The extrinsic condition arises when the electron (hole) concentration contributed by excess donors (acceptors) exceeds twice the non-extrinsic electron (hole) concentration. In this case the Fermi energy is determined by the extend to which the contributed electron (hole) concentration fills the dominant electron (hole) level.

The activation energy for non-extrinsic conduction is half the energy separation between the dominant levels plus the depth of the dominant level for majority carrier, while the activation energy for extrinsic conduction is just the depth of the dominant level for majority carrier alone. The activation energy required to populate the dominant levels is half the energy separation between the dominant levels if the conditions are non-extrinsic and zero if the conditions are extrinsic.

The total activation energies for ohmic and SCL conduction which are fully contained in n and θ_m, can be computed as follows.

For the extrinsic case

$$n = X N_c \exp(-E_e/kT)$$

$$\text{i.e., } n = \frac{(N_D - N_A)\, N_c}{N_m} \exp\left[-(E_c - E_m)/kT\right] \qquad (3.23)$$

and

$$\theta_m = \frac{N_c}{N_m} \exp\left[-(E_c - E_m)/kT\right] \qquad (3.24)$$

In this case, the activation energies for Ohmic and SCL conduction are identical [186] and equal to the dominant trap depth.

For the non-extrinsic case

$$n = N_c \left(\frac{N_c}{N_m}\right)^{\frac{1}{2}} \exp - \left[(E_c - E_m) + \tfrac{1}{2}(E_m - E_q)\right]/kT \qquad (3.25)$$

and

$$\theta_m = \frac{N_c}{N_m} \exp\left[-(E_c - E_m)/kT\right] \qquad (3.26)$$

The activation energies for ohmic and SCL conduction are different. However, the activation energy for SCL conduction is same for both the cases because the injected space charge converts non-extrinsic conduction to extrinsic conduction.

The above analysis provides the Roberts-Schmidlin theorem [185,187]. "Different (or identical)

activation energies for ohmic and SCL conduction is both necessary and sufficient condition for ohmic conduction to be non-extrinsic (or extrinsic)".

The dominant level approach is also useful in accounting for temperature induced changes in activation energies for electron conduction [187]. A decrease in slope of an activation energy plot as the temperature increases implies that the initial condition is non-extrinsic. This model have been applied to evaporated films of CdTe [188], Pentacene [189] etc. to determine the location of dominant energy levels in the system.

CHAPTER FOUR

DIELECTRIC PROPERTIES OF THIN FILMS

The dielectric response of solids provides information about the orientational adjustment of dipoles and the translational adjustment of mobile charges [190] present in the dielectric medium on application of an electric field. Theoretically the dielectric constant of a material should be preserved down to few atomic layers [191] and hence no thickness dependence is expected. However, in thin films the dielectric constant is found to fall rapidly with decreasing thickness [192] especially for very low thicknesses. This property is dependent on the deposition technique and deposition conditions of thin films.

4.1. Dielectric Losses

When the electric polarisation in a dielectric becomes unable to follow the varying electric field, dielectric losses occur [193]. Any metal - thin film dielectric - metal system can be considered as a parallel plate capacitor whose capacitance is given

by

$$C = \frac{\varepsilon \varepsilon_0 A}{d} \tag{4.1}$$

where ε is the relative permittivity, ε_0 is the permittivity of free space, A is the electrode area and d is the electrode separation which is the thickness of the film. Then the dielectric loss is

$$\tan \delta = \frac{1}{\omega RC} \tag{4.2}$$

where R is the finite parallel resistance of the system which is very large and ω is 2π times the frequency. Dielectric loss is a bulk property and does not depend on film thickness unless the defect structure of the film take part in the relaxation process. Deviations from stoichiometry may modify the dielectric losses exhibiting strong dependence on deposition conditions. In the studies of alkali halide films [194,195] the dielectric losses were found to decrease steadily with aging time after deposition. However, significantly lower losses have been reported in single crystal epitaxial films [196].

4.1.1. Frequency Dependence

Dielectric relaxation peaks are observed in thin films at very low frequencies, near 0.01 Hz.

However, at higher frequencies loss peaks have been observed which are due to relaxation of pairs of point defects [197] and caused by structural vibrations. As temperature is raised the relaxation peaks are observed to move towards higher frequencies [198]. Dielectric materials possessing significant densities of mobile charge carriers do not show any loss peaks down to the lowest attainable frequencies [199-201]. According to Debye [202] the concentration of dipoles increases exponentially with temperature and the relaxation decreases with temperature and also depends on frequency.

4.1.2. Cole-Cole Diagram

The dielectric data such as permittivity and loss as a function of frequency and temperature can be displayed in the form of graphs for the real and imaginary parts of the permittivity. A semicircular graph can be obtained by plotting the imaginary part of permittivity ε'' at a particular frequency against the real part ε' at the same frequency. Cole and Cole [203] was the first to introduce this method to explain the relaxational behaviour of certain dielectrics in accordance with the Debye theory. However, the Cole-Cole diagram of most solids do not give the

simple semicircular arcs expected of Debye responses and the most meaningful representation for a homogeneous media is the frequency dependence of the real and imaginary components of the dielectric permittivity [190,204].

4.2. Dielectric Polarisation

Large number of dielectric polarisation mechanisms are possible in polycrystalline or amorphous thin films. They can generally be classified into two groupings [205], one due to the presence of interfaces and the other a characteristic of the thin film material itself.

4.2.1. Interface Phenomena

The concentration of various charged species present near the interfaces of thin film structures contribute to the modification of dielectric properties. Even in the absence of any current there can be space charge regions and built-in-potentials at the interfaces of thin films [206-208]. The interfacial effects can be determined by measuring the effective polarisation currents induced by a small ac signal applied across the film. However, the dc effects also have to be

considered which complicates the problem due to the band bending even at zero applied field [209].

Two approaches to the problem of determining the effective ac polarization currents arising from interface effects are found in the literature. One approach [210,211] neglects the existence of regions of large band bending (> kT) at the interface. A modification of this approach treats the band as being flat thus ignoring completely the band bending. This approach may be characterized by saying that the effective polarization arises from the motion of mobile charges back and forth under the action of the ac field. In a second approach, any modification in concentration of charge carriers which take place in the region of band bending less than kT is neglected either completely [212,213] or partially [214]. However, if the interfaces at the electrodes did not modify the concentrations adjacent to them, then there would be no interface effect.

4.2.2. Bulk Phenomena

The polarization effects due to the bulk of the material include dipole and dipole-like polarization which result when dipolar molecules and ions

are capable of occupying several closely spaced positions in the given region. Another polarisation mechanism is that arising from imperfections. The polarisation caused due to the distortion of the special configuration of tightly bound electrons is also a bulk effect.

The polarisation can be made to vary, and information on the dielectric properties can be obtained by varying the field (either by application of an ac signal [215] or by application of a pulse [216]) or by thermally stimulating the frozen-in-polarisation [217,218]. The studies on the polarisation phenomena can provide very useful information on the structure and electronic properties of thin films.

4.3. Permittivity

The permittivity of a dielectric is little dependent on structure or loss. It is an intrinsic property of the constituent ions. In the absence of the electrode effects or interfacial effects the permittivity has four components.

$$\varepsilon = f(\varepsilon_{ex}\ \varepsilon_{e}\ \varepsilon_{n}\ \varepsilon_{d}) \qquad (4.3)$$

where ε_{ex} is the extrinsic contribution, ε_{e} is the

contribution of electronic polarisability, ε_n is the contribution of ionic polarisability caused by vibration of the nuclei and ε_d is the contribution of the deformation of the ion.

4.3.1. Extrinsic Permittivity

The extrinsic permittivity, ε_{ex}, is that part of the permittivity which does not arise from the constituent ions and electrons of the substance. This permittivity is rarely determined to better than one percent absolute and is usually insufficient to reveal any extrinsic components.

4.3.2. Intrinsic Permittivity

(i) Electronic Contribution

The electronic term ε_e dominates in the case of systems with less number of relatively nondeformable constituent ions. Such phenomena is observed in polymers and group IV semiconductors [198]. In group IV elements the permittivity is found to increase with the atomic number.

(ii) Nuclear Ionic Contribution

Both the ionic terms ε_n and ε_d appear only at and beyond the infrared. For ionic compounds like alkali halides ε_n dominates. This value of ε_n is

found to be inversely proportional to the square of the infrared absorption frequency.

(iii) Deformation Ionic Contribution

In oxides, since the oxide ion is large and very deformable, the permittivities are dominated by the deformable ionic contribution ε_d. The contribution of ε_d increases with atomic number. For almost all amorphous dielectrics having permittivity greater than ten, ε_d is found to dominate.

4.4. Temperature Coefficient of Capacitance and Permittivity

The temperature coefficient of capacitance γ_c is defined by the equation

$$\gamma_c = \frac{1}{C}\frac{dC}{dT} \qquad (4.4)$$

The temperature coefficient of permittivity, γ_p, defined by the equation

$$\gamma_p = \frac{1}{\varepsilon}\frac{d\varepsilon}{dT} \qquad (4.5)$$

is related to γ_c by

$$\gamma_c = \gamma_p + \alpha \qquad (4.6)$$

where α is the linear expansion coefficient of the dielectric.

4.4.1. Extrinsic Behaviour

If the loss peak near the room temperature is exceptionally broad, then its contribution to the γ_p is extrinsic [219] and is due to inhomogeneities. Then,

$$\gamma_p = A^* \tan\delta \tag{4.7}$$

where A^* is a constant dependent on the relaxation time, τ, of the inhomogeneity [220].

$$A^* = \frac{2}{\pi T} \ln\left(\frac{\tau}{\tau_0}\right) \tag{4.8}$$

where τ_0 is a constant and τ is dependent on the activation energy of the dipole.

The extrinsic behaviour is characterised by high loss ($\tan\delta > 0.1\%$).

4.4.2. Intrinsic Behaviour

All the three intrinsic contributions of permittivity change with temperature. The Clausius-Mosotti equation relates the intrinsic permittivity ε to the polarisability α_m of a macroscopic volume $\bar{V}$ [198].

i.e., $$\frac{\varepsilon - 1}{\varepsilon + 2} = \frac{\alpha_m}{3\varepsilon_0 \bar{V}} \tag{4.9}$$

For the intrinsic behaviour, loss is small and the temperature coefficient of capacitance is dependent on the permittivity value. For the vacuum case, $\varepsilon = 1$, γ_c is zero. If the permittivity lies between 1.5 and 2.5, the electronic term dominates [221]. These materials are generally plastics with negative value for γ_c. For materials having permittivity between 2.5 and 10, ionic and electronic polarisabilities are comparable. With increasing values of ε, γ_c will pass from negative values through zero to positive values. In the case of $\varepsilon \geq 10$, the ionic deformation permittivity dominates. Since ε is large, $\alpha\varepsilon \gg \varepsilon$, and the value of γ_c [222] is given as

$$\gamma_c \simeq \text{a constant} - \alpha\varepsilon \qquad (4.10)$$

Experimental results on high permittivity glasses [223] show positive values of temperature coefficient of capacitance.

CHAPTER FIVE

METHODS OF THIN FILM PREPARATION

Thin solid films are prepared by various methods [224-229] depending on the type of the film required. The methods, however, in general, can be classified into two: (A) the chemical methods and (B) the physical methods. The chemical methods depend on a specific chemical reaction yielding the required film whereas physical methods depend on the evaporation or the ejection of the material from a source.

A. Chemical Methods

The chemical methods have broadly been classified into two, chemical vapour deposition and electro deposition.

5.1. Chemical Vapour Deposition

In the chemical vapour deposition (CVD) the substrate is exposed to one or several vaporised components, or reagent gases, some or all of which contain the constituents of the material to be deposited. A chemical reaction is then initiated,

preferably near or on the substrate surface, resulting in the condensation of the desired material on the substrate as a solid-phase reaction product. The chemical reaction can be activated by various means such as electron bombardment, catalytic action of the substrate surface, or application of an RF field, heat, X-ray or light radiation [230,231]. The working pressure for most CVD processes is a few torrs and single crystal films of semiconducting compounds [232,233] have been obtained by this method.

5.1.1. Pyrolysis

Pyrolysis is the process in which a deposit of a stable residue of a compound is yielded by the thermal decomposition

$$AB \longrightarrow A + B$$

Epitaxial films of silicon and germanium have been prepared by the pyrolysis of silane (SiH_4) and germane (GeH_4) [234,235].

5.1.2. Polymerization

Polymer films—both organic and inorganic—can be prepared from the monomer vapour by the use of electron beam, ultraviolet irradiation or glow

discharge. The polymerisation process results in loss of hydrogen or dissociation by breaking the carbon chain in a hydrocarbon. Replacing some or all of the carbon atoms in organic polymers by Si, P, N, B, As etc. can produce inorganic polymers which are stable at relatively high temperatures.

5.2. Electrodeposition

5.2.1. Electrolytic Deposition

Under the influence of an applied electric field, the metallic ions in an electrolyte migrate towards the cathode and get deposited. The deposition rate is proportional to the time and the current density and can be influenced by the geometry of the cathode, the temperature and the agitation of the electrolyte. The structure of the deposit depends sensitively on the rate of deposition and the characteristics of the electrolyte [236] and may vary from well oriented single crystal to highly disordered.

5.2.2. Electroless Deposition

Metal films may be deposited by the chemical reduction of a suitable compound in solution, without the application of any external potential [237]. This

method is called electroless deposition or chemical reduction plating. The rates of deposition depend on the pH of the solution and the temperature [238,239]. Structurally the films grow as nucleated islands. According to Schlesinger [240] different growth patterns are observed in metal films prepared by electroless deposition rather than in vacuum deposition because the substrates have to be catalytic with respect to the specific metal deposited and the metal deposition occurs with the substrate immersed in a solution. An important property of electroless deposition is its ability to deposit metals selectively [241].

5.2.3. Anodisation

Anodisation is a technique that depends on the presence of a substrate on which a film can be grown from the substrate itself. For this substrate-dependent growth, a suitable substrate, conditions for the correct chemical activity for the growth to occur, and the coherence in the growing film are required. Anodisation is an assisted form of thermal growth [242]. The metal to be anodised is made the anode in a bath of electrolyte so that negative ions are attracted to its surface. Growth of the layer will

stop when the potential across the film is no longer large enough to drive these negative ions through the film [243]. For obtaining a coherent film the pH of the electrolyte is important. The final thickness will depend on the metal, voltage applied to the anode, temperature of the bath and the time the metal is immersed in the electrolyte.

5.3. Other Methods

5.3.1. Langmuir-Blodgett Technique

Monolayer films of fatty acids are prepared by the Langmuir-Blodgett technique. A well defined monolayer oriented outward at the surface of a solution can be obtained on a glass substrate raised out of the solution [244]. The orientation can be altered depending on the direction of the dipping. This method is used to prepare uniform oriented organic films of known and controllable thicknesses.

5.3.2. Chemical Spray Method

Certain reagents like thiourea, selenourea or thioacetamide can interact with salt solutions of heavy metals and precipitates can be formed when heated at a suitable pH value. This method is used to

prepare photoconducting films of certain II-VI compounds [245].

B. Physical Methods

The two important physical methods of thin film preparation are sputtering and thermal evaporation.

3.4. Sputtering

Ejection of the surface atoms from a surface is possible if the surface is bombarded with energetic particles. This process is known as sputtering. A thin film can be formed on a substrate by the condensation of these ejected atoms. Alloy films can be prepared by this method without the fractionation of the components. There are various types of sputtering depending upon the method used to eject the atoms.

3.4.1. Glow Discharge Sputtering

In this method an electric field applied between two electrodes in a gas at low pressures provides the source of ions for sputtering. The factors influencing this sputtering technique are the pressure of the system, the current and voltage dependence and the cathode area.

5.4.2. Bias Sputtering

A small negative bias is given to the film with respect to the anode so that it is subjected to the ion-bombardment throughout its growth. This effectively cleans off the adsorbed gases [246] and a less contaminated film is obtained.

5.4.3. Triode Sputtering

Electrons are injected into the discharge by some means to accelerate the effectiveness of the glow discharge system. This allows to produce sputtered films at lower pressures of the order of 10^{-2} torr.

5.4.4. Ion Beam Sputtering

A specific ion source is used instead of using a discharge system and this enables to grow films sputtered from targets in a residual pressure as low as 10^{-5}torr.

5.4.5. R F Sputtering

By applying an RF field between the cathode and anode it is possible to sputter directly from insulators [247]. The principle behind this technique is that since very high frequency is used, the negative

charge accumulated on the insulating target will not be sufficient during the half cycle in which the target is positive to prevent positive ions bombarding the target during the half cycle in which the target is negative.

5.4.6. Reactive Sputtering

Deposition can be obtained of a completely reacted material such as an oxide or nitride, if the residual gas in a discharge system is taken so that a large proportion of the residual gas is a reactive species relative to the film being deposited. This can effectively be used in glow discharge systems or triode sputtering systems.

5.5. Evaporation

For the preparation of thin solid films the evaporation techniques are commonly used. This is effected in a vacuum system which lowers the evaporation temperature considerably so that a large number of materials can be evaporated with less contamination. Since the vapour goes out from the source in straight line in vacuum, well defined patterns of the films can be deposited on substrates by using proper masks in between the substrate and the source. Rates of

evaporation and the condensation can vary over very wide limits depending upon the type and temperature of the source and the material used.

5.5.1. Evaporation Theory

Majority of the metals and dielectrics are evaporated from the liquid phase while some are evaporated from the solid state. The maximum number of molecules dN_e evaporating from a surface area A_e during a time dt, according to Knudsen [248], is

$$\frac{dN_e}{A_e dt} = (2\pi m k T)^{-\frac{1}{2}} p_e \qquad (5.1)$$

where p_e is the equilibrium pressure. The free evaporation rate of the vapour atoms, m_e, from a clear surface of unit area in vacuum is given by the Langmuir expression [249,250].

$$m_e = 5.83 \times 10^{-2}\ p_e (M/T)^{\frac{1}{2}} \text{ gm cm}^{-2} \text{ sec}^{-1} \qquad (5.2)$$

where T is the temperature, M is the molecular weight of the vapour species and p_e is taken as less than 10^{-2} torr. In terms of the molecules ejecting out of the source, the evaporation rate is

$$N = 3.513 \times 10^{22}\ p_e (1/MT)^{\frac{1}{2}} \text{ molecules cm}^{-2} \text{ sec}^{-1} \qquad (5.3)$$

The rate of deposition of the vapour on the substrate depends on the source geometry, position of the source relative to the substrate and the condensation coefficient. According to Knudsen cosine law, the rate of deposition varies as cos θ / r^2, for the ideal case of the deposition from a clear uniformly emitting point source to a plane substrate, where r is the radial distance of the substrate from the source and θ is the angle between the radial vector and the normal to the substrate direction.

5.5.2. Evaporation Methods

(i) Resistive Heating

The material is heated with a resistively heated filament or boat, made of refractory metals such as tungsten, molybdenum or tantalum. Such vapour sources of various geometries, types and sizes are commonly in use [224,251,252]. Knudsen sources (point vapour sources) are widely used due to its highly directional property. If the vapour pressure of a material to be evaporated is too high, then it will sublime before the melting occurs. In such cases it is difficult to control the rate of evaporation.

(ii) Three-temperature Method

Thermal evaporation of alloys or compounds

usually result in the production of nonstoichiometric thin films due to (i) the rate of evaporation of the components vary owing to their difference in vapour pressures, (ii) the possible thermal decomposition of the parent material and (iii) the different tendencies of the components to react with the support material. In the preparation of the compound semiconductor films, the different stages of condensation, namely adsorption, surface diffusion and nucleation are greatly dependent on the deposition rate, substrate temperature and interfacial energies [253,254].

If an alloy of two components A and B is evaporated, the ratio of the evaporation rates of A and B may be obtained from Langmuir's expression (equation 5.2),

i.e., $$\frac{N_A}{N_B} = \frac{C_A P_A}{C_B P_B} \left(\frac{M_B}{M_A} \right)^{\frac{1}{2}} \qquad (5.4)$$

where C's are the atomic fractions of the components. Generally this relation is not obeyed because of the strong interaction between the components of the alloy [225].

An efficient method of preparing thin films of alloys and compounds with controlled compositions

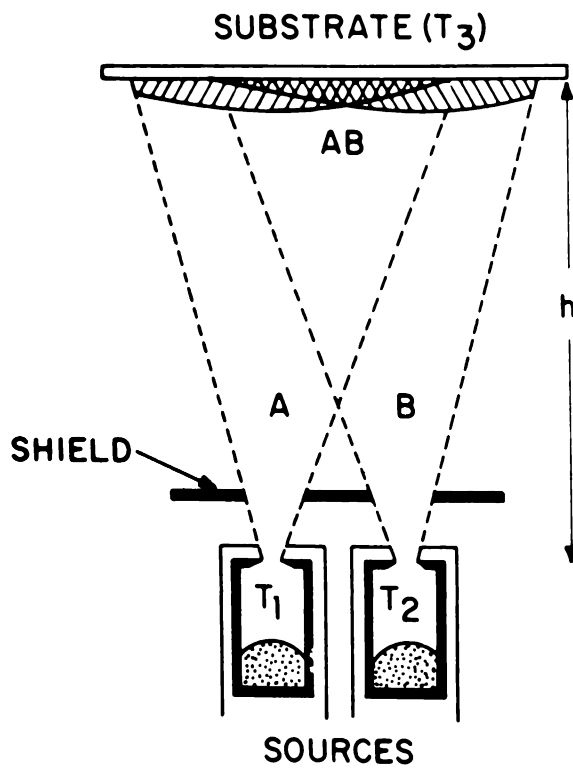

Figure 5.1. Two source evaporation.
h - source-substrate distance.

is to evaporate each component from a separate source with reaction and homogeneity brought about at the substrate at elevated temperature. (Figure 5.1). This method is called Gunther technique [255] or three temperature method and is used for preparation of semiconducting compound layers [21,256-259].

According to Gunther, a critical condensation flux exists for every substrate temperature at which spontaneous nucleation occurs. After nucleation, the condensation flux quickly reaches a maximum value. The dependence of condensation flux, N_K, on the substrate temperature for two incident components A and B having constant incident fluxes is shown in figure 5.2. T_c values are the critical values for the condensation components. At a constant substrate temperature, the condensation diagram for two incident components A and B can be shown as in figure 5.3. With a suitable substrate temperature and adequate incident rates of both components stoichiometric compound layers can be prepared by this method.

(iii) Flash Evaporation

A rapid evaporation of the alloy or the compound is used to minimise the dissociation of

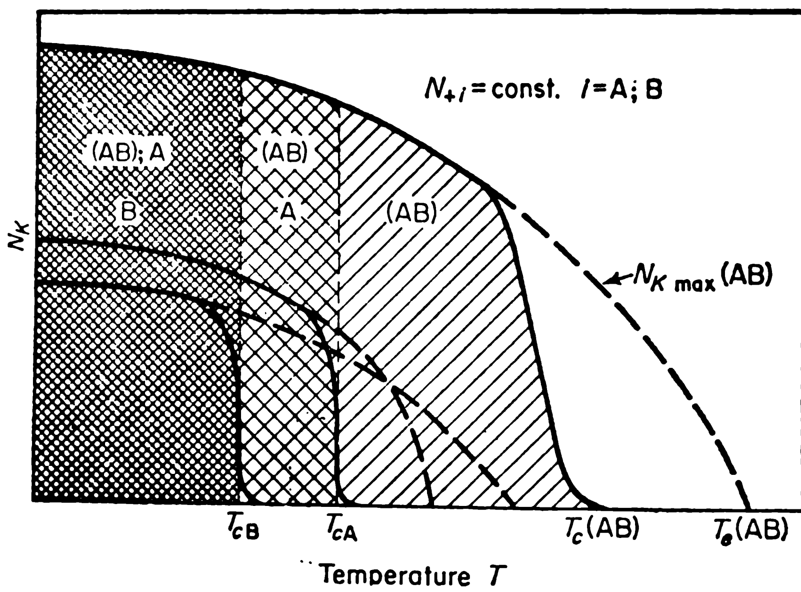

Figure 5.2. Condensation flux as a function of temperature with two incident components A and B.

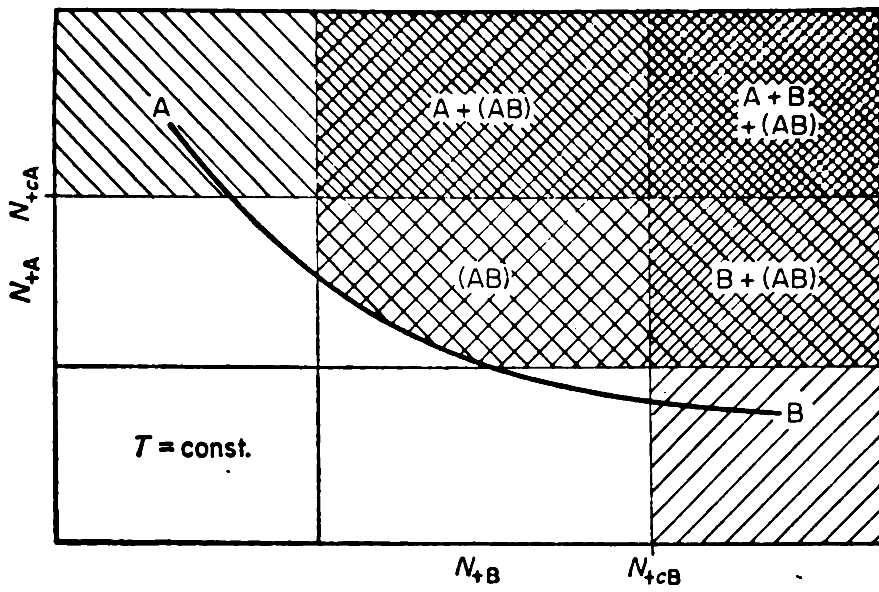

Figure 5.3. Condensation diagram of two incident components A and B.

the component elements. This may be obtained by continuously dropping fine powdered particles of the compound on to a very hot surface so that numerous discrete evaporations occur [260,261]. The powdered material is fed into the heated boat using different types of material feeders such as mechanical, electromagnetically vibrating, rotating etc. This method has been used to prepare semiconducting thin films of certain III-V [256,262] and V-VI [263] compounds. Recently, Platakis and Gatos [264,265] developed a new flash evaporation technique using a U-tube type source which permits the preparation of compound semiconductor films with high structural and chemical homogeneity.

(iv) Laser Evaporation

An intense beam of laser can be used to heat and vapourise the materials. The laser source can be placed outside the vacuum system and focussed on to the substance to be evaporated. The evaporation takes place at the surface only, since the laser penetration depth is small.

(v) Electron Bombardment Heating

Vapourisation of materials is caused by using electron bombardment. A stream of electrons

are accelerated by applying a positive potential and focussed on to the material to be evaporated. The electrons lose their energy in the material rapidly. The range of electrons is determined by their energy and the atomic number of the material. The surface of the material becomes a molten drop and evaporates.

(vi) R F Heating

RF or induction heating can be provided to the material by suitable arrangement of RF coils. This avoids the contamination of the film by the support material to a greater extent.

(vii) Arc Evaporation

Very high temperatures can be generated to evaporate refractory materials by striking an arc between two electrodes. This method is used for carbon evaporation for electron microscope specimens.

(viii) Reactive Evaporation

Oxides and nitrides of metals are prepared by evaporating the metals in relatively high oxygen and nitrogen pressures [266]. This method of

reactive evaporation produces films at low deposition rates and is effective in preparing oxide films using low temperature sources.

5.5.3. Molecular Beam Epitaxy

The newest development in the evaporation process is the molecular beam epitaxy [267-269] used for the epitaxial growth of films on single crystal substrates by slowly evaporating the constituent elements of the film from Knudsen effusion cells on to substrates held at appropriate temperatures needed for chemical reaction, epitaxy and reevaporation of excess constituents. Knudsen effusion cells are deep crucibles in furnaces with cooled shrouds. Epitaxial films of compound semiconductors are prepared by this method.

CHAPTER SIX

GROWTH AND STRUCTURE OF THIN FILMS

The growth of the evaporant atoms on a substrate to form a continuous film emerges from a number of processes [270] such as the nucleation and the formation of island structure, the coalescene of islands and channel formation and finally formation of the continuous film. The condensation of a vapour can occur if the partial pressure of the film material in the gas phase is equal to or larger than its vapour pressure at that temperature [271]. The initial stages of condensation starts with the adsorption of vapour atoms on the substrate surface.

6.1. Film Nucleation

The process of the combination of several adsorbed atoms on the substrate surface to form small clusters is called nucleation. The Langmuir-Frenkel condensation model [272,273] suggests that the adsorbed atoms move over the surface during their life times to form pairs which in turn act as condensation centres for other atoms. If the

impinging atoms are not adsorbed, they re-evaporate into the vapour phase. Hence condensation is the net result of an equilibrium between the adsorption and desorption processes [274]. According to Semenoff [275] hetrogeneous nucleation proceeds by the formation of an amorphous film followed by the nucleation of crystallites within the amorphous film.

6.1.1. Theories of Nucleation

The effects of monomer depletion by capture by growing clusters is the principal basis of the nucleation theory [276]. The nucleation theories suggest that if a cluster has reached a critical size, it will not dissociate into monomers but will grow to form stable condensates. However, the two principal models of nucleation—the capillarity model and the atomistic model—differ in their approach to evaluate the energy of formation of the clusters.

(i) Capillarity Model

The classical droplet model for homogeneous nucleation from the vapour phase [277,278] has been extended to the nucleation of thin film clusters by Hirth and Pound [279].

According to this theory, clusters can be formed by collisions of adatoms on the substrate surface if the supersaturation is sufficiently high in the vapour phase. With the increase in free energy these clusters will develop until a critical size is reached. The growth continues above this size with a decrease in free energy. The radius of the critical nucleus r^* is given by

$$r^* = -\frac{2\sigma_{cv}}{\Delta G_v} \qquad (6.1)$$

where σ_{cv} is the interfacial free energy and ΔG_v is the Gibbs free energy difference. The free energy corresponding to this critical size, according to Rhodin [280] is

$$\Delta G^* = \frac{16\pi}{3} \frac{\sigma_{cv}^3}{\Delta G_v^2} \phi(\theta) \qquad (6.2)$$

where $\phi(\theta)$ expresses the relative values of the specific interfacial energies between the substrate, the crystal and the vapour. The effective supersaturation varies rapidly with the change of substrate temperature and the nucleation rate depends on the impinging flux.

This approach is called the capillarity model, since the free energy of nucleation is expressed

directly in terms of relative changes in specific interfacial energies corresponding to the formation of a hemispherical cap on the substrate.

(ii) Atomistic Model

The capillarity model has applied bulk surface free energies to clusters of very small sizes, which according to Walton and Rhodin [281–283] is not correct. Walton et al [284] used the dissociation energy, Q_i, of a cluster containing i atoms into i adsorbed monomers to modify the free energy formation of a cluster. The rate of formation of critical nucleus is

$$I^* = R a_o y N_o \left(\frac{R}{\nu_1 N_o}\right)^{i^*} \exp\left[\frac{(i^* + 1)Q_{des} - Q_d + Q_i^*}{kT}\right] \tag{6.3}$$

where R is the impingement rate, a_o is the jump distance of the adsorbed monomer, y is the available cluster periphery for impingement, N_o is the density of monomer adsorption site, ν_1 is the attempt frequency of the adsorbed monomer for desorption, i^* is the number of monomers in a critically sized aggregate, Q_{des} is the activation energy for desorption, Q_d

is the activation energy for diffusion and Q_i^* is the dissociation energy of a critical cluster.

According to this model, at low substrate temperatures or very high super-saturations, the critical nucleus may be a single atom which forms a pair with another to form a stable cluster. Also, the nucleation rate depends on the impingement rate.

6.1.2. Comparison of Nucleation Theories

The fundamental concepts up on which both the capillarity theory and the atomistic theory are based, are identical. The difference between the models is that the atomistic model uses only discrete arrangements of atoms, whereas the capillarity model employs simple idealised geometrical shapes for the cluster [285]. The capillarity model predicts a continuous variation rate with supersaturation, while the atomistic model predicts discontinuous changes if the size of the critical cluster is small.

In the case of epitaxial growth, the temperature should be significantly below the melting point and the super-saturation should be sufficiently low to suppress misoriented nuclei and other crystallographic defects and to give a low nucleation density [286].

6.2. Stages of Growth

There are different stages of growth of the film after the nucleation on the substrate surface. The process of growth contains the capture and decay of clusters [287] which depends on their size and thermodynamic properties.

The impingement of vapour atoms on the substrate surface is followed by its condensation to form small nuclei. Subsequently, these nuclei grow three dimensionally, however, its growth parallel to the substrate surface will be greater than that normal to it. This is due to the surface diffusion of the clusters and its interaction with few single atoms as proposed by Halpern [288], which result in the formation of islands.

As the size of the islands increase, due to coalescence of smaller ones, larger islands will be formed. During this process, a considerable transfer of mass takes place between the islands by diffusion and their density decreases considerably.

The growth of the islands changes their circular shape and the islands become elongated and

join to form a continuous network structure in which deposit material is separated by long, irregular, narrow channels.

Further, secondary nucleations occur in the channels which finally grow and touch the sides of the channel. The empty channels will thus be filled and a continuous film with small holes results. The secondary nucleation now takes place at these holes and these nuclei grow and coalesce with the film to form a holes free continuous film.

6.3. Factors Affecting the Growth of Films

The growth and structure of the evaporated film are strongly dependent on factors such as the nature of the substrate, substrate temperature, contamination etc.

An increase in the binding force between the substrate and the evaporant atom increases the film adhesion and decreases the mobility of adatoms on the substrate surface. It also increases the density of nuclei formation which affects the coalescence process and the structure and size of islands.

The mobility of condensed atoms on the substrate increases with the substrate temperature which affects the crystalline structure of the film formed.

Contamination due to impurity in the vacuum system affect the film to a greater extent. An important effect of the contamination is the loss of adequate adherence of the deposited film. Contamination increases the number of initial nuclei, which causes them to coalesce early in film growth, influencing the orientation of a continuous film [289].

A dc electric field in the plane of the substrate surface can induce coalescence at an early stage of film growth. Chopra and Khan [290] showed that an electric field can affect the re-orientation and recrystallisation of the nuclei in CdS films, which in turn affects the film structure.

6.4. Structure of Films

A very thin metal film will have a structure with voids which make these films less dense than the bulk material. However, in the case of non-metallic

- G 3608 -

films very thin continuous films (thickness ~ 10 Å) can be produced by evaporation [291]. The structure of the film, either amorphous, polycrystalline or single crystal, depends on the nature of the substrate, substrate temperature, angle of incidence of the vapour atoms etc. For single crystal films it is important to know the orientation relationship with respect to the substrate. Also particle size and perfection of crystallites are important in the study of the structure of films.

Generally two methods—diffraction and image formation—are used for the structure determination of thin films. In both cases electrons or X-rays which penetrate the volumes of the film are used as tools. However, high scattering probability of electrons make them an important tool for the investigation of thin films. An important advantage of electrons is the existence of electron lenses to construct an image whereas X-ray lenses are not possible. Large area topography using X-rays and scanning electron microscopy are two important microscope techniques used to study the structure of thin films.

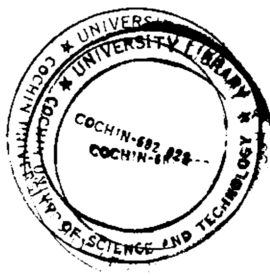

CHAPTER SEVEN

EXPERIMENTAL DETAILS

This chapter describes in detail the experimental set up and the procedures used for the preparation and characterisation of antimony tri-sulphide films for the present investigation.

7.1. Vacuum Coating Unit

The films for the present study have been prepared in a vacuum coating unit capable of producing a vacuum better than 10^{-5} torr. The coating unit consists of a vacuum chamber which rests on a collar fitted on a cabinet containing the pumping system. The schematic layout of the unit is as shown in figure 7.1.

7.1.1. Pumping System

The pumping system consists of a four stage fractionating oil diffusion pump backed by a two stage rotary pump. A water cooled baffle D isolates the diffusion pump from the work chamber. The diffusion pump is a six inch, water cooled, fractionating pump

with a specified baffle pumping speed of 1000 litres per second and has got an oil charge of 500 ml. Silicon DC 704 oil is used as the pumping fluid. The two stage rotary pump has got a pumping speed of 540 litres per minute, which is used to back the diffusion pump.

The roughing and the backing valves F and G in the figure 7.1 in turn connects the vacuum chamber and the diffusion pump to the rotary pump. Keeping the baffle valve E closed, the roughing valve, allows to evacuate the work chamber initially with the rotary pump.

All the interconnecting vacuum lines are copper tubes having one inch diameter and the distance between the components such as valves and pumps are kept as short as possible to ensure maximum pumping speed. The pumping line is connected to the rotary pump with a neoprene tubing so as to reduce the transfer of vibrations from the rotary pump to the other parts of the system. All the couplings are made of demountable screw seals which compress neoprene O-rings.

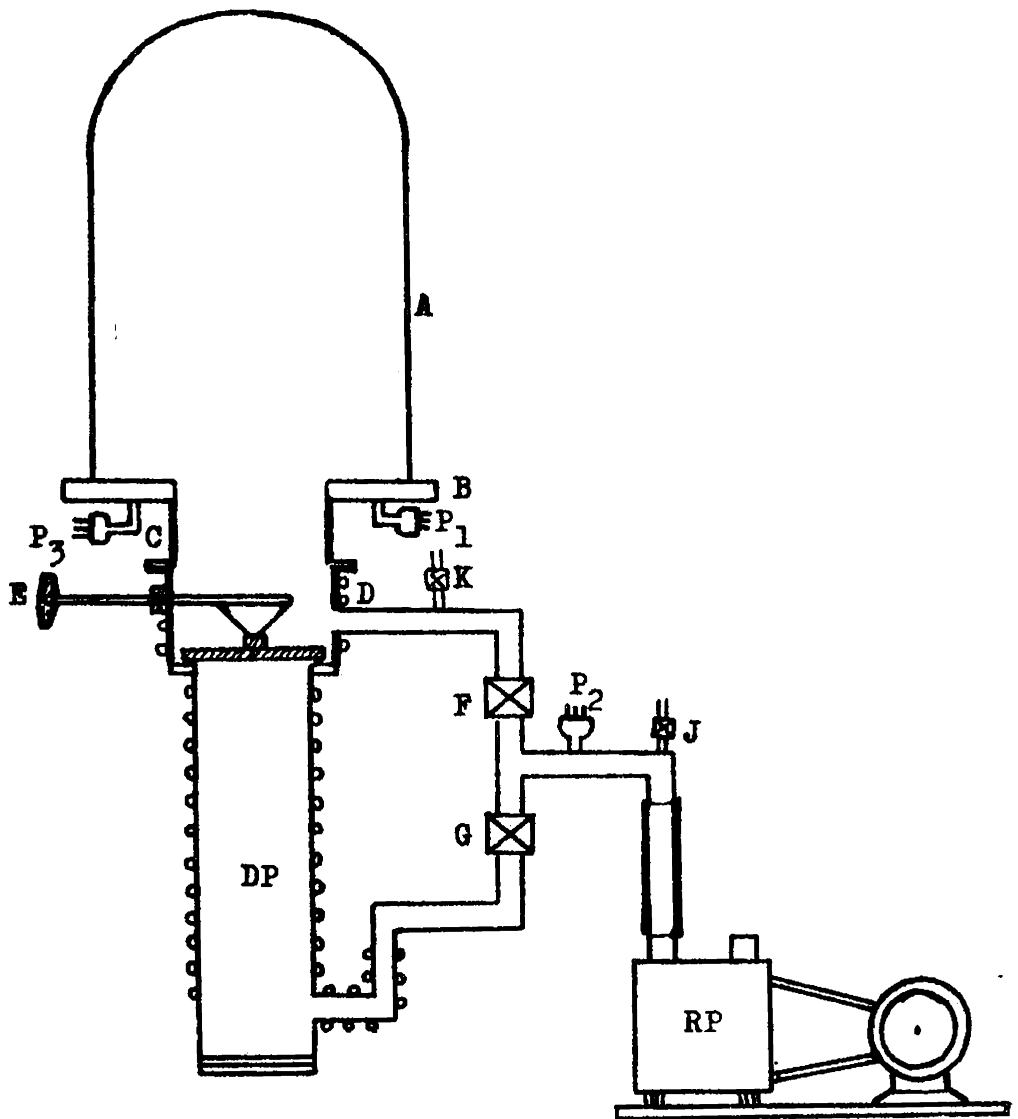

Figure 7.1. Schematic diagram of the vacuum coating unit. A - Vacuum chamber, B - Base plate, C - Collar, D - Baffle, E - Baffle valve, F - Roughing valve, G - Backing valve, DP - Diffusion pump, RP - Rotary pump, J,K - Air admittance valves, P_1P_2 - Pirani gauge heads, P_3 - Penning gauge head.

An air admittance valve J, connected above the rotary pump, allows to admit air into the rotary pump while switching off. Another air admittance valve K is fitted on the base plate to admit air into the work chamber.

7.1.2. Work Chamber

The vacuum chamber consists of a 12 inch glass bell jar resting on a stainless steel base plate. A neoprene L gasket attached to the bell jar provides the vacuum seal with the base plate.

The base plate has provisions to attach electrical feed throughs, gauge heads etc. These feed throughs use neoprene O-rings to provide vacuum sealing with the base plate. Four numbers of high current feed throughs are used in the system which are electrically insulated by teflon tubings. Two teflon insulated high voltage feedthroughs provides the electrical supply for ion bombardment cleaning in the vacuum system. A source shutter which can be operated externally is fitted to the base plate through a Wilson seal. The Penning gauge head and the Pirani gauge head are both attached to the base plate with demountable adapters.

An ion bombardment cleaning unit is fitted inside the chamber on a tripod fixed on the base plate. This consists of two shielded annular rings of high purity aluminium. A stainless steel baffle plate is fitted within the tripod above the base plate. The filaments or boats are connected to the high current feed throughs using thick copper strips.

The substrate holder is kept above the source so that the source-substrate distance can be adjusted. For metal evaporations a source-substrate distance greater than 15 cms have been used and for the coevaporation and the flash evaporation of the semiconductor 12 cms was taken as the source substrate distance. The substrate holder was made using a square shaped aluminium plate, the central portion of which is made hollow to place three glass slides side by side. When the coevaporation is carried out, a shield is placed in between the two sources.

7.1.3. Measurement of Vacuum

The lower vacuum in the range 1 to 10^{-3} torr is measured using the Pirani gauge attached to the chamber. The higher vacuum is indicated with a Penning

gauge capable of measuring vacuum upto 10^{-6} torr. The ultimate vacuum attained in the system has been better than 1×10^{-5} torr.

7.2. Film Deposition

7.2.1. General

(i) Evaporant Materials

High purity materials have been used for preparing thin films. In the preparation of antimony trisulphide films by the three temperature method, antimony (99.999 %) and sulphur (99.98 %) have been used for the coevaporation. In the flash evaporation method antimony trisulphide having purity 99.999 % (Koch Laboratories, England) has been used. Different metals, aluminium (99.999 %), silver (99.999 %), indium (99.99 %), tin (99.99 %), bismuth (99.999 %) and antimony (99.999 %) have been used in the investigation of electrical characteristics and metal-Sb_2S_3 contacts.

(ii) Evaporant Sources

The evaporation source is the support to the evaporant material supplying the heat of vapourization.

The source should maintain the material at sufficiently high temperature to produce the vapour pressure required for the condensation. However, it should avoid contamination of the deposits from its own vapourization or dissociation. Hence, a source must be of negligible vapour pressure and dissociation pressure at the operating temperature and should be available at the desired shape. In view of all these requirements refractory metals are commonly used as evaporant sources.

Coiled tungsten filament fabricated using 0.5 mm diameter tungsten wire was used for the evaporation of aluminium. All other metals—antimony, silver, indium, tin and bismuth—were evaporated from molybdenum boats. The molybdenum boats were made using molybdenum foils of length 6 cm, breadth 1.1 cm and thickness 0.1 mm. To keep the material required for evaporation a small dimple was made at the centre of each foil by pressing.

For evaporating sulphur, resistively heated glass crucible was used. A small crucible of length about 2 cms was drawn from Corning glass tube and

the open end was fire polished. A basket shaped heater coil was wound using tungsten wire and was used to support and heat the V-shaped glass crucible (figure 7.2). For the evaporation of low melting point materials such externally heating methods are reported to be convenient [292].

(iii) Substrates

Microscope glass slides of size 7.5 cm x 2.5 cm x 0.12 cm have been used as substrates for preparing the thin films. Glass slides are widely used as substrates since they can be cleaned thoroughly and have got good electrical insulation.

(iv) Substrate Cleaning

Cleanliness of the substrate surface has got a very decisive influence on the adhesion and growth of films. Contaminants on the substrate generally include those from the manufacturing processes, airborne dust, lint, oil particles, finger prints etc. Number of cleaning procedures have been discussed in the literature [220,293-295]. The bonds between the contaminant molecules and that

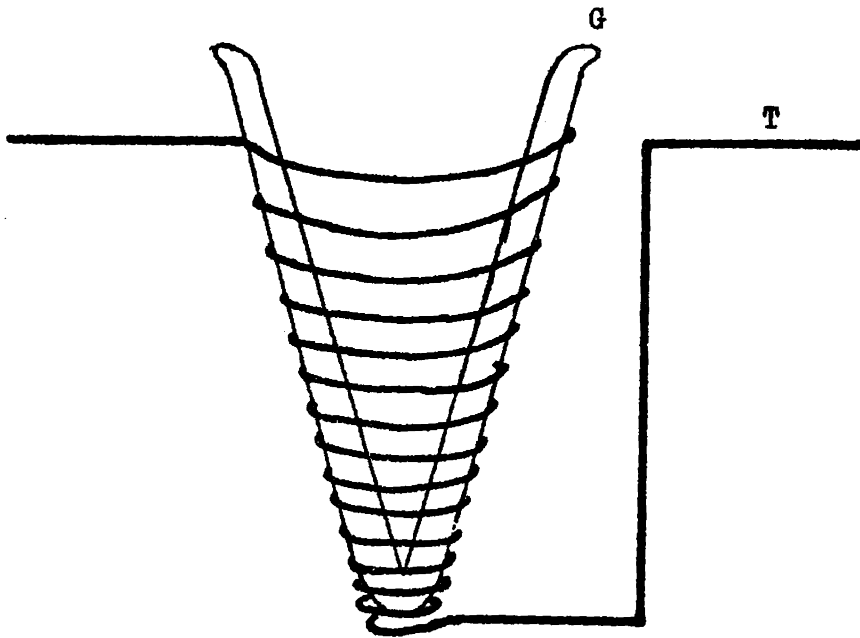

Figure 7.2. Resistively heated glass crucible.
G - Glass crucible; T - Basket shaped tungsten coil.

between the contaminant molecule and substrate have to be removed in the cleaning process. This can be done by chemical methods using reagents or by heating or agitating the substrate to remove the contaminants by supplying the sufficient energy to release the bonds.

The following procedure was used for cleaning the glass substrates. The glass slides were scrubbed several times with fine cotton in a strong teepol solution. These were then cleaned in distilled water followed by isopropyl alcohol and acetone. This chemical cleaning process removed majority of the contaminants on the substrate. Further, the substrates were agitated ultrasonically in distilled water for about 15 minutes using an ultrasonic cleaner. After this process the substrates were well rinsed with distilled water and dried in a slow stream of hot air. Immediately after this they were removed to the work chamber where they were subjected to ion bombardment for about 10 minutes in a vacuum $\sim 10^{-2}$ torr. Besides removing the last traces

of impurities, the ion bombardment cleaning modifies the glass surface for an enhanced nucleation during the film deposition [296].

7.2.2. Three Temperature Method

The antimony trisulphide films were prepared by the coevaporation of antimony and sulphur from separate sources so that the compound Sb_2S_3 was formed in the vapour phase and deposited on the substrate kept at a particular temperature. Antimony was evaporated from a molybdenum boat and the evaporation temperature was 683K. The sulphur evaporation was carried out from the resistively heated glass crucible whose temperature was maintained at 363K. In the case of films prepared for conductivity measurements the substrates were kept at different temperatures ranging from 303K to 423K. For all other studies the substrate temperature, T_s, was kept at 345 ± 2K. The substrates were heated radiantly using a substrate heater. The substrate heater was fabricated with heating filaments made of tightly wound nichrome wire on mica sheet which was pressed in between two steel plates. The heater

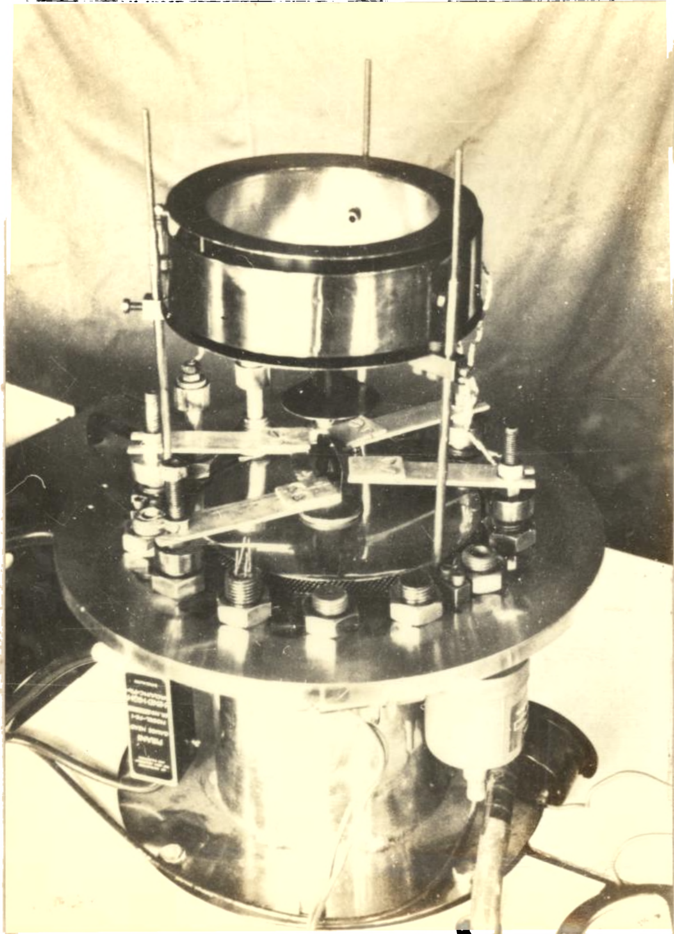

Figure 7.3. (a) Layout of the coevaporation set up in the work chamber.

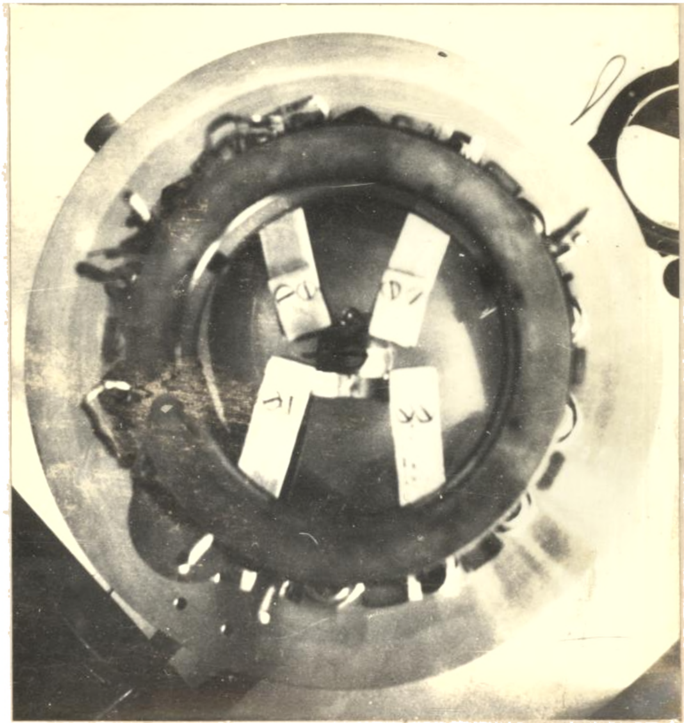

Figure 7.3. (b) Top view of the coevaporation sources.

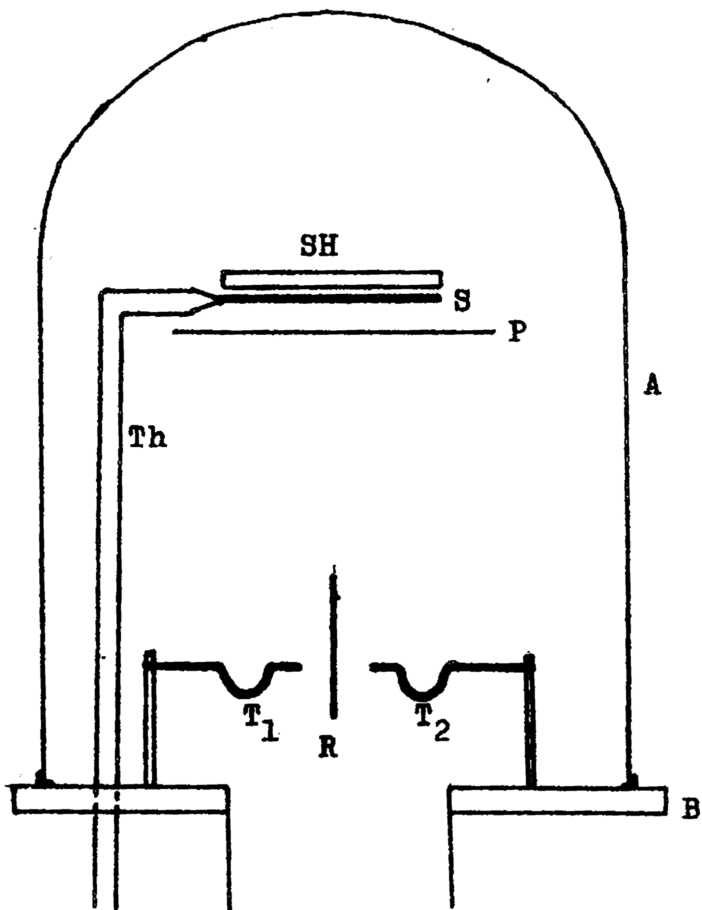

Figure 7.4. Schematic diagram of three temperature method. A - Bell jar; B - Base plate; T_1, T_2 - Two sources; S - Substrate; SH - Substrate heater; P - Shutter; R - Shield; Th - Thermocouple.

was kept about 0.5 to 1 cm above the substrates. The substrate temperature was measured using a chromel-alumel thermocouple kept on the substrate surface.

A mica sheet was used as a shield between the two sources. The shutter was positioned just below the substrates to monitor the deposition. Both the materials were then allowed to vaporise and when there was enough vapour for the compound formation, the shutter was removed and the vapours were allowed to fall and form the compound on the substrate surface. A layout of the work chamber with the coevaporation set up is shown in figure 7.3. A schematic diagram of the preparation of films by the three temperature method is as in figure 7.4.

7.2.3. Flash Evaporation

Compound semiconductor films can be prepared by the flash evaporation without the decomposition of the constituent elements. Agasiev et al [297] used laser beam for the flash evaporation of antimony trisulphide films.

For the present study powdered antimony trisulphide was allowed to fall on to a heated molybdemum boat (temperature > 850K) using an electromagnetically vibrating material feeder. The powder then quickly evaporated without any dissociation since the temperature of the boat was very high.

The electromagnetically vibrating material feeder, similar to that used by Campbell and Hendry [298], fabricated for the flash evaporation consists of a mild steel rod, serving as an electromagnet. A mild steel plate which can be adjusted by screws on a pivot is attracted by the electromagnet whenever the current flows through the coil. Intermittant passage of current through the coil makes the mild steel plate vibrate at a desired frequency. A pipe-shaped narrow glass tube made of corning glass fixed to the mild steel plate serves to drop the powdered material. This tube was made by drawing it from a thick walled corning glass tube and fire polishing the edges. A schematic diagram of the set up is shown in figure 7.5. The whole system was enclosed in an aluminium cover and was used inside the vacuum system.

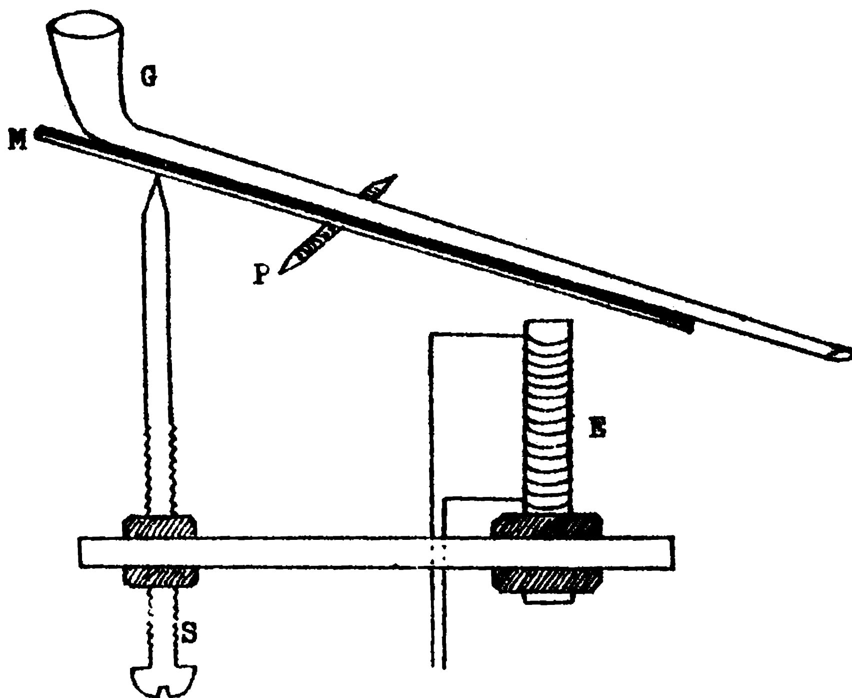

Figure 7.5. Schematic diagram of flash evaporator.
E - Electromagnet; M - Mild steel plate;
G - Pipe shaped glass tube; P - Pivot;
S - Screw.

The power to the winding of the electromagnet was fed from an astable multivibrator working at a frequency 2 c/s. The multivibrator was constructed using a timer circuit consisting of an IC 555 and the output was amplified with a power transistor to feed the windings of the electromagnet.

Antimony trisulphide powder was taken in the pipe shaped glass tube and was vibrated on to the molybdenum basket. Several trials were made to ensure that the powder fell continuously through the tube into the basket. Keeping the substrates in position, the unit was evacuated to a pressure less than 10^{-5} torr. The molybdenum basket was heated and the Sb_2S_3 powder was vibrated into it using the material feeder. Only sometime after the evaporation commenced, the shutter was removed to allow the film to deposit on the substrate. The substrate temperature was maintained at $345 \pm 2K$ for all films prepared by the flash evaporation technique.

7.2.4. Determination of the Type of Conductivity

The type of conductivity of the films was determined by the hot-probe technique [299]. In this method one probe of a microvoltmeter is heated and

both probes are touched on the sample and the meter deflection is observed. If the hot-probe voltage is positive with respect to the cold-probe, the sample is n-type and if the hot-probe voltage is negative, the sample is p-type. As a temperature gradient exists in the sample, the carriers near the hot probe will have higher velocities than that near the cold probe and a current flows. The direction of the flow depends on the type of the carriers in the sample.

In the present case, thick films of antimony trisulphide prepared at substrate temperature $T_s = 345 \pm 2K$ were used to determine the conductivity type. The sample was touched with the hot positive probe of a dc microvoltmeter along with the cold negative probe. The meter deflection was towards the negative side indicating the semiconductor to be p-type. In the case of both coevaporated and flash evaporated films this test showed that the films were of p-type.

7.3. Structure Fabrication

7.3.1. For Resistance Measurements

Two well cleaned glass substrates were placed on the substrate holder with proper masks. The masks

made of freshly cleaved mica exposed a rectangular surface having 5 cm length and 0.4 cm width and thus Sb_2S_3 films of the mask size were made to form on the glass substrates. Another glass substrate, partially covered with a mask was also placed very close to the other substrates in order to determine the film thickness. Antimony and sulphur were coevaporated on to these substrates. Antimony trisulphide films of this pattern prepared keeping the substrates at temperatures, T_s, ranging from 303K to 423K were used for resistivity measurements.

The electrode films of either aluminium or antimony were evaporated over these Sb_2S_3 films at both ends so as to get an effective length of 3 cm semiconductor film. The thickness of the electrode films were of the order of 2000 Å. The film-electrode structure is shown in figure 7.6(a).

7.3.2. M S M Structure

The current-voltage measurements and the dielectric measurements of the antimony trisulphide films have been carried out using the metal-semiconductor-metal (MSM) sandwich structures. For all MSM structures, antimony film was used as the base electrode.

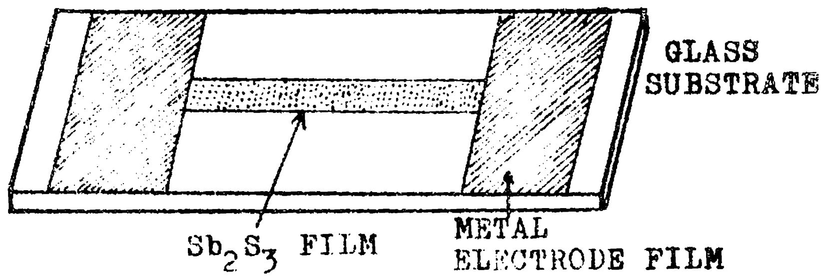

(a)

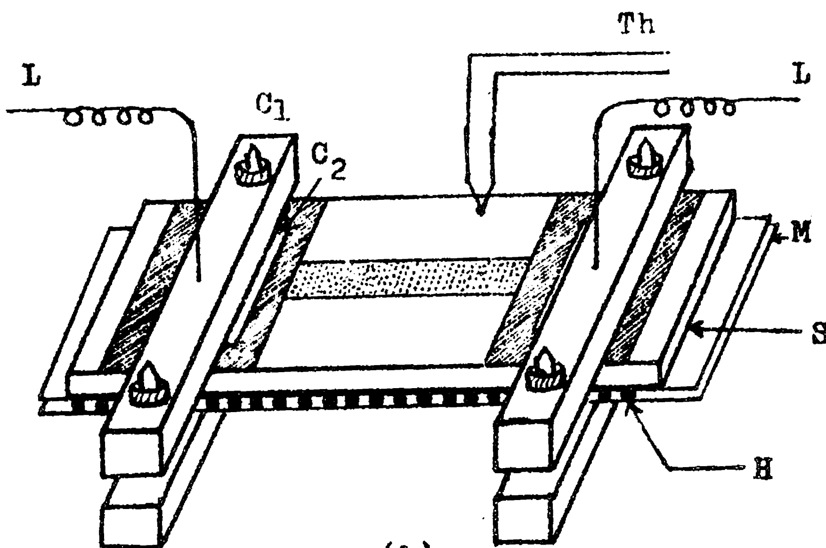

(b)

Figure 7.6. (a) Film-electrode structure used for the resistance measurements.

(b) Film-electrode structure with pressure contacts and heating arrangement.
C_1 - Copper block, C_2 - Thin copper foil,
S - Glass substrate, M - Mica sheet,
H - Heater windings, L - Contact leads,
Th - Thermocouple.

Three clean glass substrates were mounted side by side on the substrate holder in the vacuum chamber with masks of exactly the same size. These masks exposed a rectangular surface of size 6 cm in length and 0.2 cm in breadth on each glass substrate at the centre, for evaporation. After evacuating the chamber, antimony was evaporated from a molybdenum boat, over these substrates so that the thickness of the antimony film was of the order of 3000 Å. Antimony trisulphide film was then evaporated over each of these substrates, keeping the substrates at 345 ± 2K, so that the Sb_2S_3 film covered about 3/4th of the base electrode film in length. For this, separate masks having a 4.5 cm x 0.4 cm slot at the centre were used. Prior to the evaporation of the semiconductor film, the substrates with antimony as base electrode were annealed at 345 ± 2K for about 15 minutes. A clean glass substrate partially covered with a mask was also kept side by side with the substrates to use this for the thickness measurement. The thickness of the antimony trisulphide film prepared in the study varied from 900 Å to 9000 Å.

Such $Sb-Sb_2S_3$ systems were used for preparing $Sb-Sb_2S_3$-metal structures. Antimony, aluminium, bismuth,

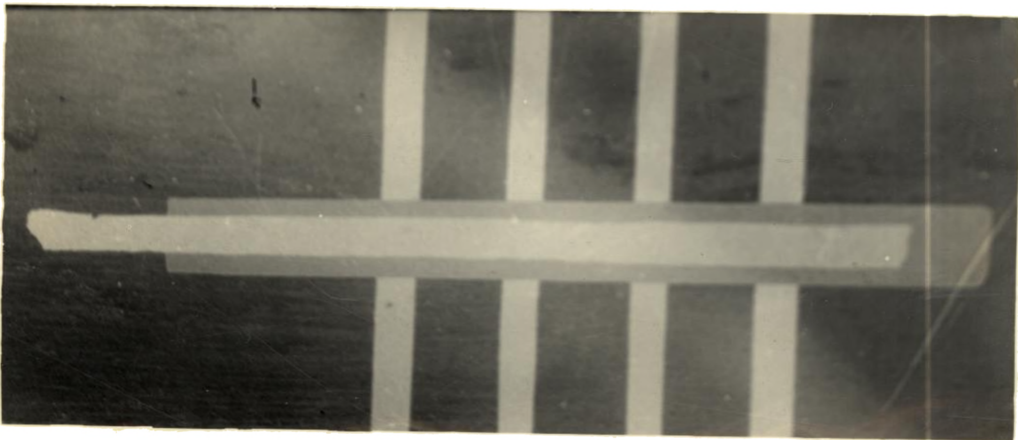

Figure 7.7. Photograph of the MSM structure used for measurements.

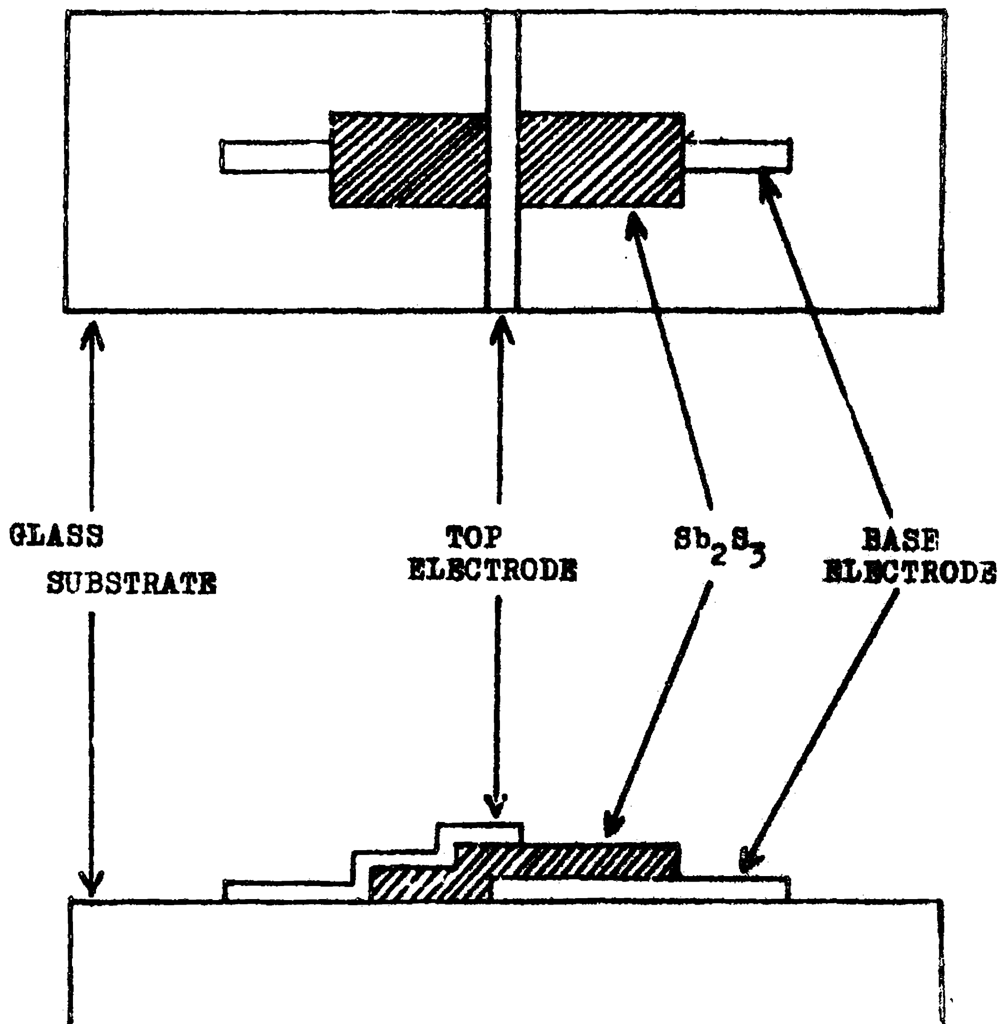

Figure 7.8. Schematic diagram of the MSM structure.

indium, silver and tin were used as top electrodes. During each evaporation four MSM structures were obtained in a single pumpdown using mask with four slots of 0.2 cm width and 0.5 cm apart. A photograph of the MSM structure used for the measurements is shown in figure 7.7. A schematic diagram is shown in figure 7.8. The thickness of the overlay films were of the order of 1000 Å in all the cases. The effective area of each MSM structure was 4×10^{-2} cm^2.

7.4. Film Thickness Measurement

7.4.1. General

The measurement of thickness of thin films is of great importance for examining their properties. Methods of measuring thickness can be divided into two, direct measurement and indirect measurement [300]. In the indirect method the rate of deposition is controlled and a film of desired thickness can be produced. In the direct measurement technique a direct measure of the thickness of the film is obtained after deposition.

Monitoring the thickness of a film using a quartz crystal thickness monitor is an indirect method. There are different direct measurement

techniques such as stylus, X-ray fluorescence, multiple beam interferometry etc. In the stylus method, the movement of a stylus attached to a lever and a fulcrum along a substrate-film step is amplified and recorded. The intensity of secondary X-rays, obtained after directing a beam of X-rays into a film, is used to estimate its thickness in the X-ray fluorescence method.

7.4.2. Method of Measurement

Film thicknesses were measured using the multiple beam interferometry of Tolansky [301,302]. A beam of light reflected many times between the two surfaces will have an intensity large enough to affect total interference. The method of Fiseau fringes of equal thickness has been used to measure the thickness of the films throughout this investigation.

To produce fringes, a uniform, opaque and high reflectivity coating was made over the film prepared for thickness measurement. The Fiseau interferometer was formed by placing a semisilvered reference plate on top of the step at a small angle to the substrate surface so that the reflecting surface

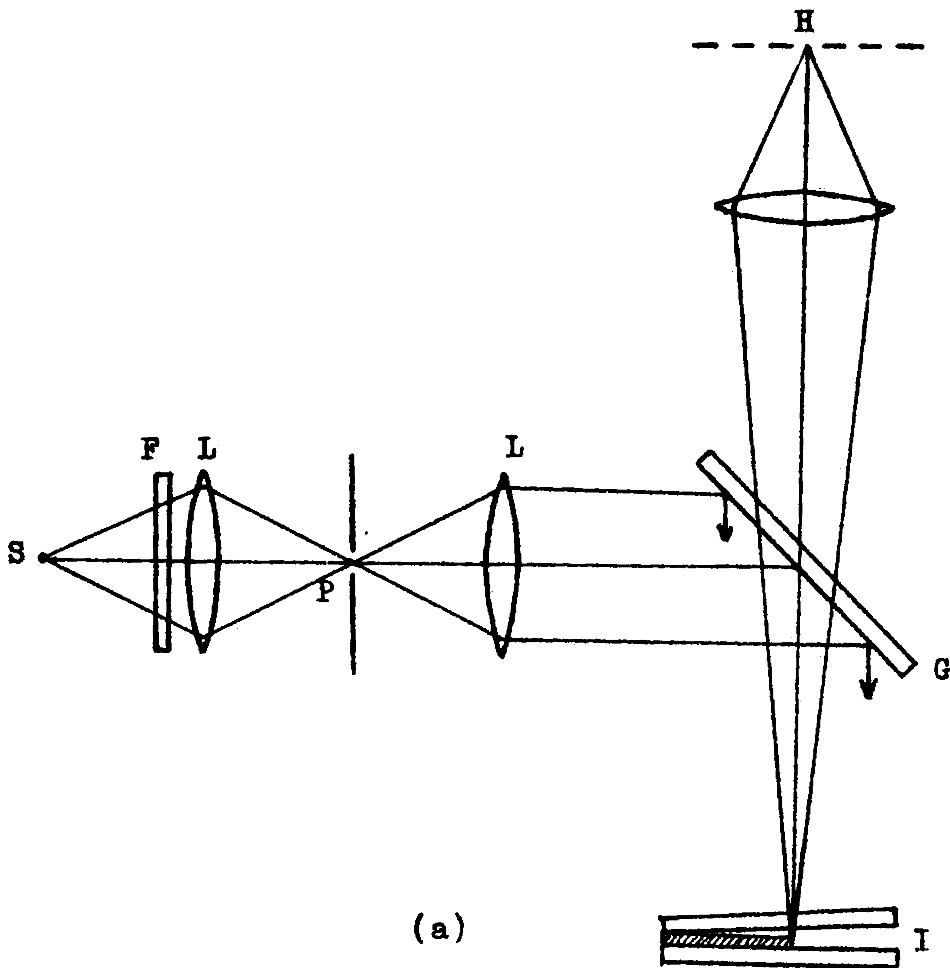

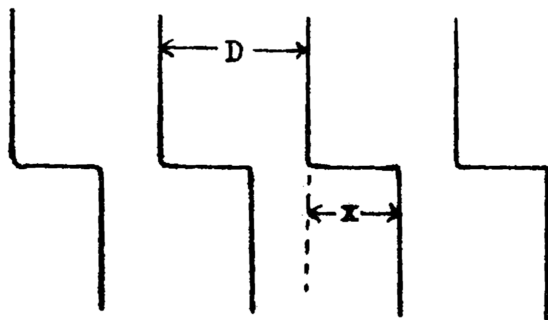

Figure 7.9 (a) Interferometer arrangement for Fizeau fringes of equal thickness. S - Source, F - Filter, L - Lens, P - Pinhole, G - Semisilvered glass plate, I - Interferometer, H - Image plane.
(b) Fringes produced by interferometer, D - Fringe spacing, x - Fringe displacement.

faced each other. The interferometer was illuminated with a monochromatic light, mercury green (λ = 5460 Å). The fringe system was viewed in a microscope. This interferometer arrangement is shown in figure 7.9(a). Figure 7.9(b) shows the fringe pattern. If λ is the wavelength of the monochromatic light, the distance between two successive dark fringes corresponds to $\lambda/2$. The film thickness, d, is given by

$$d = \frac{x}{\text{fringe spacing}} \times \frac{\lambda}{2} \qquad (7.1)$$

where x is the fringe displacement. For highly reflective surfaces, the width of the fringe can be about 1/40th of the fringe separation in the Fizean's method.

7.5. Electrical Measurements

All the electrical measurements were carried out in a vacuum cell made of corning glass, with provisions for heating the film and keeping the film at any desired atmosphere. The desiccator type cell has got feed through arrangements at the opposite sides for making electrical connections. Chromel-alumel thermocouple leads and thick copper wires are fixed through these feed throughs and then vacuum sealed.

All the measurements were carried out at a pressure $\sim 10^{-2}$ torr and keeping the cell in a dark environment to avoid any light induced effects.

7.5.1. Conductivity Measurements

Pressure contacts using copper blocks were given to the electrode-semiconductor film combination shown in figure 7.6(a). A layer of silver conducting paint was used carefully at the contact surface of the electrode film and copper block, to make the contact resistance minimum. A heating element wound of nichrome tape was used to heat the film. A chromel-alumel thermocouple was placed on the substrate surface side by side with the film to measure the temperature. This entire arrangement (figure 7.6(b)) was kept inside the vacuum cell and the external connections were given. The whole set up including the vacuum cell was kept in a rectangular copper box which was perfectly earthed to give proper shielding.

The cell was evacuated using a rotary pump. The electrical resistance of the film was measured by a BPL million meg ohm meter at three test voltages, 10V, 50V and 100V. The initial temperature of the

system was found to be 302-303K by measuring the thermocouple voltages. The film system was then heated slowly. At each 5 degree interval of the temperature the resistance was measured after attaining a steady temperature. This resistance measurements were continued upto a temperature of 373K and then the system was cooled and the resistance at each temperature was again measured. The average value of resistance of both heating and cooling cycle was taken. For all the films, prepared at substrate temperatures ranging from 303 to 423K, resistance measurements as described above were carried out.

7.5.2. Current-Voltage Measurements

U-shaped copper electrodes of 0.4 cm width and 0.3 cm thick were used to give external electrical contacts to the MSM structure. These copper electrodes were tightened to the bottom and top metal layers of the structure with thin copper foil in between and a thin layer of silver conducting paint was used at the interfaces (figure 7.10). This was kept inside the vacuum cell and external connections were made. A heating element wound of nichrome wire was used to heat the film system and a chromel-alumel thermocouple

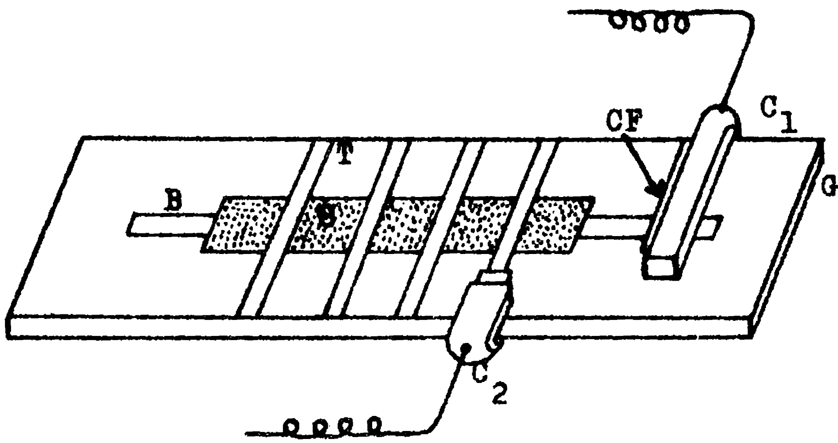

Figure 7.10. Set up of the MSM system for the current-voltage measurement.
C_1, C_2 - U-shaped copper electrodes, CF - Thin copper foil, B - Base metal electrode film, T - Top metal electrode film, S - Semiconductor Film, G - Glass substrate.

was placed on the substrate surface to measure the temperature. The vacuum cell was then kept in a dark environment and evacuated.

A high input impedence (> 10 meg ohm) digital voltmeter was used to measure the voltage across the specimen. In order to measure the current, a standard 1000 ohms resistance was kept in series in the circuit and the voltage developed across it was measured using a DC microvoltmeter. For the Sb-Sb_2S_3-Sb/In systems, the current-voltage characteristics were measured at different temperatures ranging from 303K to 353K.

After electrical measurements, the surface of the effective area of all the systems were examined under reflected light with a Carl-Zeiss metallurgical microscope. In the case of Sb-Sb_2S_3-Al system certain features like discontinuities were observed on the surface and the microphotographs were then taken.

7.5.3. Dielectric Measurements

For the dielectric measurements of the Sb-Sb_2S_3-Sb systems, the electrical connections were made similar to that in the current-voltage measurements. The

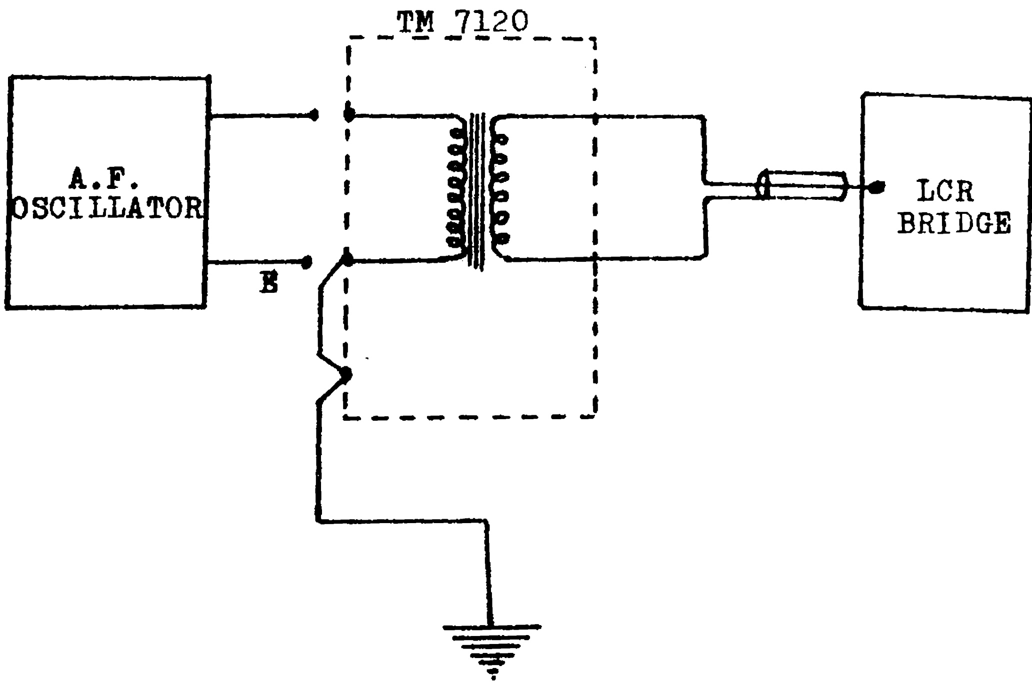

Figure 7.11. Connection diagram for adapting external oscillator with the LCR Bridge.

capacitance and the dielectric loss were measured using a Marconi TF 2700 LCR Bridge keeping the system in a vacuum $\sim 10^{-2}$ torr. The capacitance at different frequencies ranging from 100 c/s to 20 k c/s was measured using an external audio frequency source in conjunction with a Marconi isolating transformer TM 7120. The connection diagram of the set up is as in figure 7.11. The dielectric loss was measured at a fixed frequency of 1 k c/s available from the internal oscillator of the bridge.

The capacitance of the MSM systems was measured at different temperatures ranging from 303 to 353K also. These measurements were carried out for films of varying thicknesses. From the capacitance value measured, knowing the effective area and thickness of the film, the dielectric constant was calculated.

7.6. Thin Film Transistor

Many attempts to make field effect transistors and space charge limited triodes using metal-semiconductor thin film layer combinations resulted in fabricating insulated gate thin film transistor.

Successful results have been reported in the literature using semiconductor materials like CdS [303], CdSe [304], p-type Te [305], PbS [306], Silicon [307], PbTe [308] etc. for the preparation of thin film transistors (TFT). As such, an attempt was made to use antimony trisulphide thin film for the fabrication of a thin film transistor, since the material is a low band gap semiconductor.

There are two types of insulated gate thin film transistors [309], the coplanar-electrode type and the staggered-electrode type. In the coplanar-electrode structure, the source, the drain and the gate of the TFT are evaporated on the same side of the semiconductor, while in the staggered-electrode type the source and the drain are on one side and the gate on the other side. The structure used in the present investigation was a staggered electrode type.

7.6.1. Structure Fabrication

The thin film transistor structures were fabricated on clean glass substrates. Aluminium thin film strips having a thickness of about 1500 Å were used as gate electrodes. Antimony films which make ohmic contact with antimony trisulphide were used as

source and drain electrodes. Aluminium oxide layer prepared by reactive oxidation over the aluminium film and a polymer film of para toludine were used as insulator layers. However, the aluminium oxide layer was found to be ineffective, probably be due to the porosity of the film.

A clean glass substrate was kept on the substrate holder with proper mask in the vacuum system and the aluminium was evaporated from a tungsten filament. The substrates with aluminium films of 0.1 cm width was then taken out for the insulator film deposition.

The insulator film of poly-p-toludene of thickness about 1000 Å was deposited over the aluminium film, by the glow discharge plasma polymerisation of the monomer para toludene, in a glow discharge sputtering unit.

The substrate with gate and gate insulator film structure was then put inside the vacuum chamber and antimony trisulphide film was evaporated by the coevaporation method, keeping the substrate at a temperature 345 ± 2K. Proper masks were used such

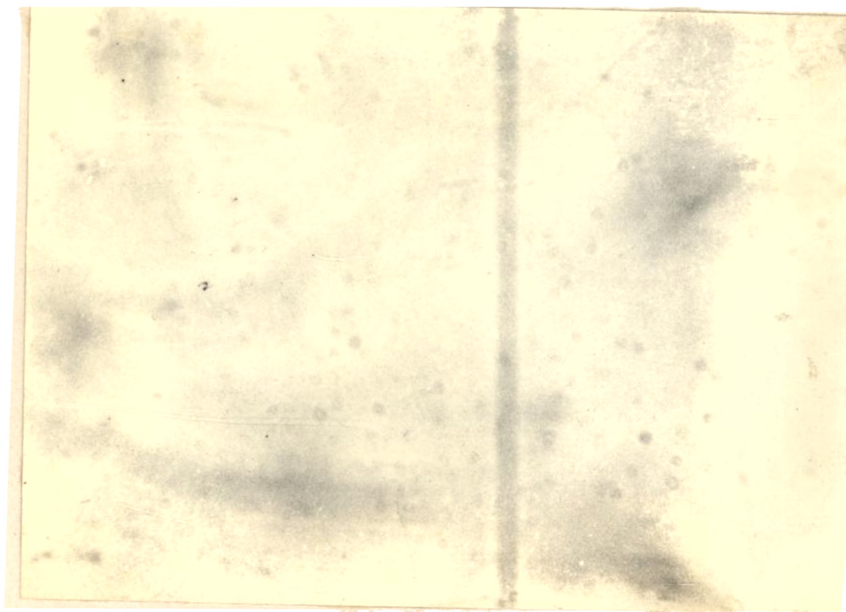

Figure 7.12. Micrograph showing the source-drain separation of the fabricated TFT. Separation - 15 μm.

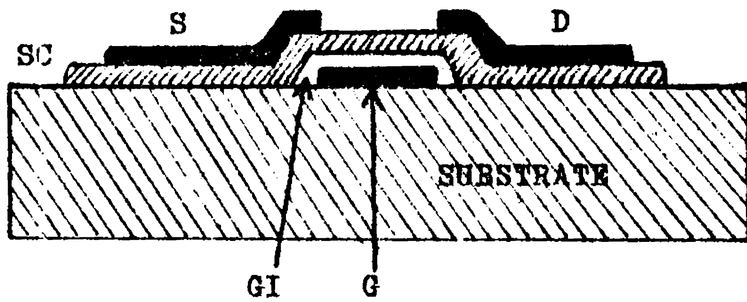

Figure 7.13. Schematic diagram of the structure of Thin Film Transistor. S - Source, D - Drain, G - Gate, SC - Semiconductor, GI - Gate insulator.

that Sb_2S_3 films of 0.4 cm x 0.4 cm were formed over the Al-insulator structure.

To deposit the source and the drain electrodes, utmost care was taken in preparing the masks. The separation between the source and the drain have to be small and quiet uniform. Antimony was evaporated over the Al-insulator-Sb_2S_3 structure using a carefully prepared suitable mask to form a uniform gap width of 15 µm. Figure 7.12 shows the source-drain separation. A schematic diagram of the structure of the TFT prepared is shown in figure 7.13.

7.6.2. Evaluation of the TFT

The electrical contacts to the source, drain and gate were given using U-shaped copper contacts and silver conducting paint. The drain current was measured by varying the source-drain voltages for zero gate voltage and for fixed gate voltages. The drain current was also measured for both polarity to the gate.

The thin film transistor can be converted to a thin film field effect diode by shorting the gate and the drain. The TFT fabricated as described above was studied as a field effect diode also, by shorting the gate and the drain and measuring the characteristics.

CHAPTER EIGHT

RESULTS AND DISCUSSION

The present investigation mainly consists of four parts---the temperature dependence of electrical conductivity of coevaporated antimony trisulphide films prepared at different substrate temperatures, a study of different metal - Sb_2S_3 contacts by analysing the current-voltage characteristics, space charge limited conduction and the analysis of dielectric properties of antimony trisulphide films. For evaluating the dominant levels by activation energy analysis and for dielectric studies both coevaporated and flash evaporated antimony trisulphide films were used and the results compared.

Antimony trisulphide is found in orange and black colours and it changes its orange colour to black when it is crystallized [310]. Hanafi and Ismail [311] reported that at room temperature the sample is having a brownish-black colour. The antimony trisulphide films prepared by both the coevaporation and flash evaporation methods were of brownish-black colour with a reddish-brown transparency.

8.1. Conductivity Studies

8.1.1. Dependence on Substrate Temperature

The electrical conductivity of the films studied was found to increase with the increase of temperature. However, this increase in the conductivity with temperature was found to be dependent on the substrate temperature, T_s, at which the films were prepared. The rate of increase in conductivity was small up to about 330K and further the increase was found to be larger in all cases. For films prepared at $T_s = 303K$, larger increase in conductivity was observed in the temperature range 330 to 373K. Films having higher T_s value showed less rate of increase in conductivity. But for all films prepared at substrate temperature, $333 < T_s < 368K$, the change in conductivity with temperature was uniform. For $T_s > 368K$, the rate of increase in conductivity was found to be decreasing as T_s increases. Figure 8.1 shows the log conductivity versus reciprocal temperature curves for films prepared at different substrate temperatures.

Thermally activated electrical conductivity, σ, is

$$\sigma = \sigma \exp - \frac{\Delta E}{kT} \qquad (8.1)$$

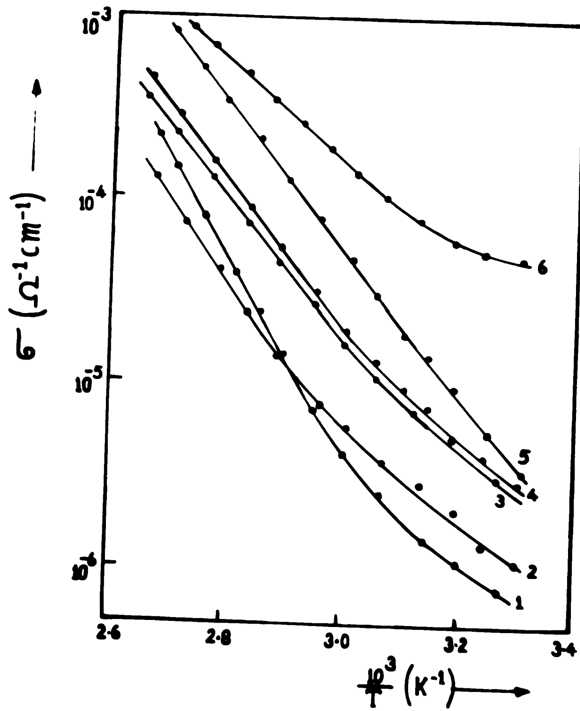

Figure 8.1. Conductivity versus inverse temperature for films prepared at different substrate temperatures; curve 1 - T_s = 303K, curve 2 - T_s = 316K, curve 3 - T_s = 338K, curve 4 - T_s = 323K, curve 5 - T_s = 368K, curve 6 - T_s = 423K.

where ΔE is the activation energy. From the slope of the log conductivity versus 1/T plots, the values of thermal activation energy, ΔE, were calculated for films prepared at different substrate temperatures. These ΔE values for different substrate temperatures are tabulated in Table 8.1. It can be observed that films prepared at different substrate temperatures differ in their thermal activation energy. However, at 338K $< T_s <$ 368K, the activation energy gives a constant value of ΔE = 0.75 eV. This is in agreement with the ΔE value 0.77 eV obtained by Budinas et al [312] for antimony trisulphide. A graph of the activation energy ΔE versus substrate temperature, T_s, was plotted (figure 8.2) which showed a plateau region at the substrate temperature 330 to 370K.

The uniform activation energy, ΔE = 0.75 eV, can be attributed to the stoichiometric uniformity of the films prepared at these substrate temperatures. According to deKlerk and Kelley [21], the condensation of excess sulphur on the substrate is possible if it is placed at substrate temperature less than 323K. As such, the films prepared at $T_s <$ 323K may have excess sulphur content. At higher substrate temperatures, $T_s >$ 373K, the reevaporation of sulphur from

TABLE 8.1

Activation energy values for films prepared at different substrate temperatures.

Substrate Temperature T_s K	Activation Energy ΔE eV
303	1.02
316	0.89
323	0.76
338	0.75
345	0.75
358	0.75
368	0.75
393	0.67
423	0.53

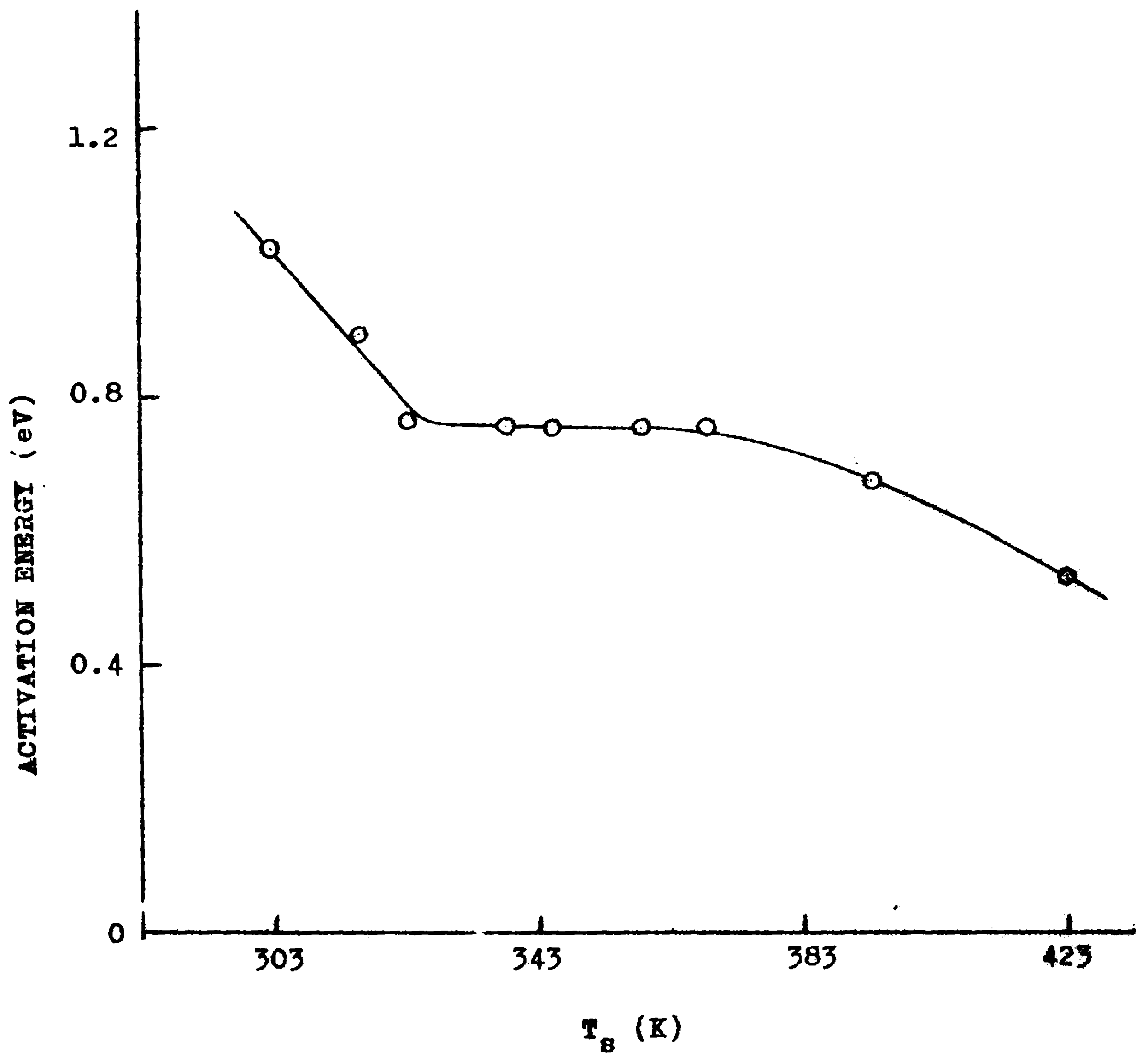

Figure 8.2. Activation energy , ΔE, versus substrate temperature, T_s.

the substrate results in the nonstoichiometric films. Hence, the range of substrate temperature at which the plateau is observed in figure 8.2 can be considered as the T_s value for the formation of stoichiometric films.

8.1.2. Optimum Substrate Temperature

The temperature T_s of the substrate during deposition is one of the most critical parameters determining the structure and properties of thin films.

According to Vincett, Barlow and Roberts [313,314] (hereafter called VBR), there exists an optimum substrate temperature, T_{os}, at which the exact stoichiometric film is formed in the case of compound semiconductors, such that this T_{os} is related to the boiling point T_b of the material by $T_{os}/T_b = 0.33$. However, it has been shown by VBR [313], that the ratio T_{os}/T_m can be from 0.44 to 0.32, where T_m is the melting point. A correction applied considering the boiling energies of the compounds gives the ratio T_{os}/T_b to be 0.33.

From the earlier works on compound semiconductors such as ZnTe [315] and CdTe [316], Vincett et al obtained T_{os}/T_m values of 0.42 and 0.40

respectively. From the range of substrate temperatures for which stoichiometric films have been obtained (338K to 368K), the optimum substrate temperature, T_{os}, has been taken, according to VBR theory, as 345K such that $T_{os}/T_m = 0.42$, where $T_m = 823K$ [317,318] is the melting point of Sb_2S_3. This T_{os} value has been used throughout the entire study for preparing antimony trisulphide films.

The coevaporation technique has several advantages [319] for preparing compound semiconductor films, the stoichiometry can be adjusted by varying the individual evaporation rates, low substrate temperature can be tolerated for polycrystalline growth, thickness can be controlled and the film growth can be started and stopped abruptly. Recently, coevaporation method has been used by Fleisch and Abermann [320] to prepare stoichiometric Ag_2S films and by Best et al [321] for preparing high quality HgSe films.

8.2. Metal-Semiconductor Contacts

One of the major methods of analysis of the metal-semiconductor contacts is by measuring the current-voltage characteristics of the systems.

According to Smith [13], low work function metals are considered to make ohmic contacts to semiconductors. However, heats of reaction at the interface is also relevant in determining the contacts [322].

The work function of Sb_2S_3 is reported to be 4.7 - 4.9 eV [323,324]. The current-voltage characteristics of Sb-Sb_2S_3-metal thin film structures using contact metals having work functions less than that of antimony trisulphide—antimony (ϕ = 4.1 eV), indium (ϕ = 3.8 eV), tin (ϕ = 4.2 eV), aluminium (ϕ = 4.1 eV), silver (ϕ = 4.5 eV) and bismuth (ϕ = 4.3 eV)—were analyzed to investigate the behaviour of these metal contacts. Since antimony film was used as the base electrode, the behaviour of the base electrode—semiconductor interface remains the same, and any difference in the characteristics observed can be attributed to the effect of the metal-Sb_2S_3 interface at the top electrode. Depending upon the top electrode metal, the current-voltage characteristics of the Sb-Sb_2S_3-metal structures showed wide variations.

8.2.1. Antimony Contact

The current-voltage characteristics of Sb-Sb_2S_3-Sb structures showed an ohmic region at low

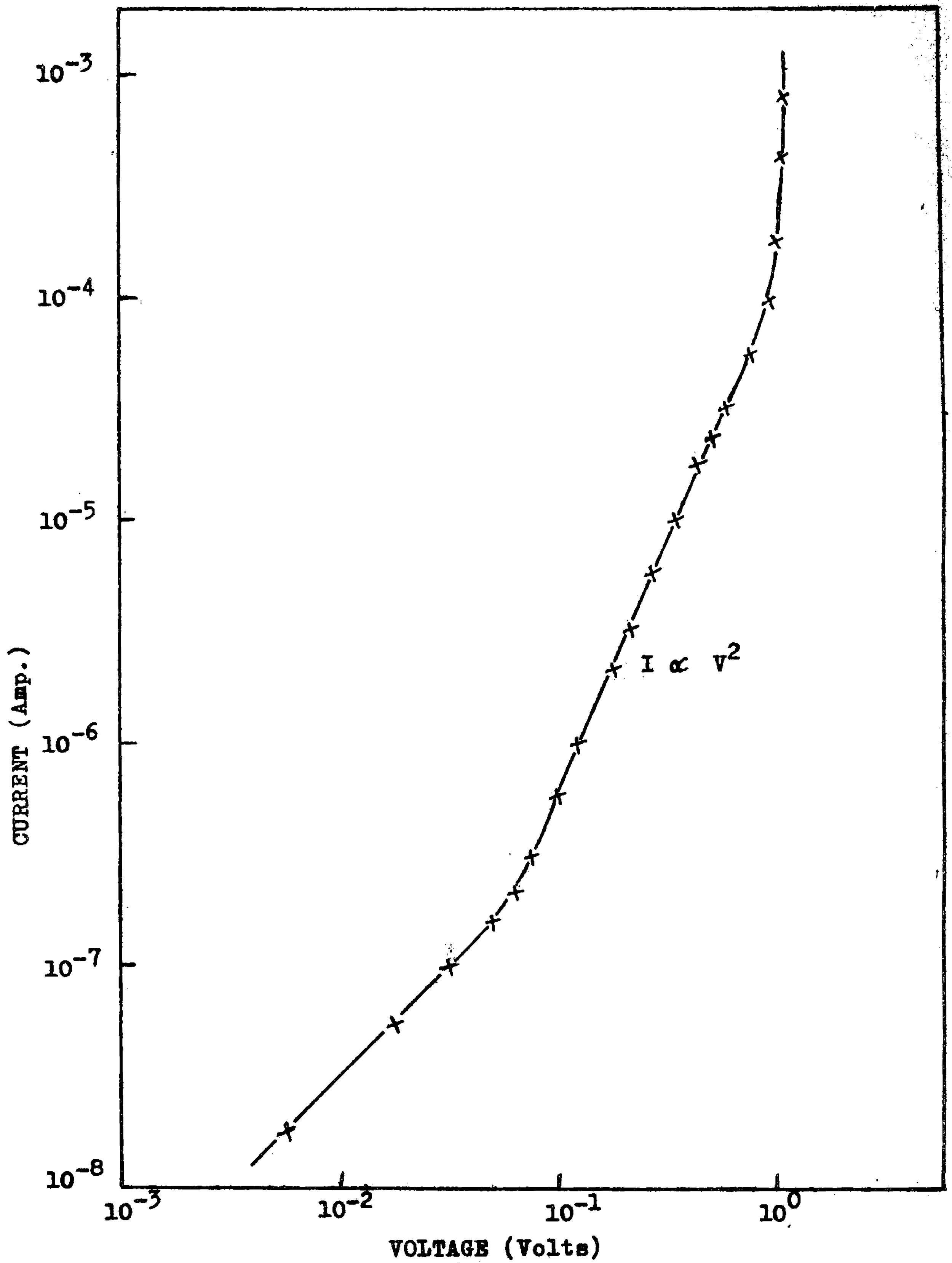

Figure 8.3. Current-voltage characteristics of $Sb-Sb_2S_3-Sb$ structure.

fields followed by a square law region at high fields as in figure 8.3. After the square law region a sharp increase in the current was observed. No change in the characteristics was observed by reversing the polarity of the electrodes. The nature of the characteristics remains the same for the entire range of thicknesses of the Sb_2S_3 films studied. At the square law region the characteristics showed a $I \propto d^{-3}$ dependence on thickness. The thickness dependence of current at the square law region for different voltages is shown in figure 8.4.

The $I \propto V^2/d^3$ dependence indicates that a space charge limited conduction is predominant in the film system. The space charge injection into the semiconductor needs an ohmic contact [160] between the electrode metal and the semiconductor. Since the Sb_2S_3 is sandwiched between two antimony films, both the Sb-Sb_2S_3 interface and Sb_2S_3-Sb interface are to be considered. However, since the nature of the characteristics remains the same independent of the polarity of the top electrode, both these interfaces can be considered as of the same nature. Hence antimony can be considered as making an ohmic contact to antimony trisulphide.

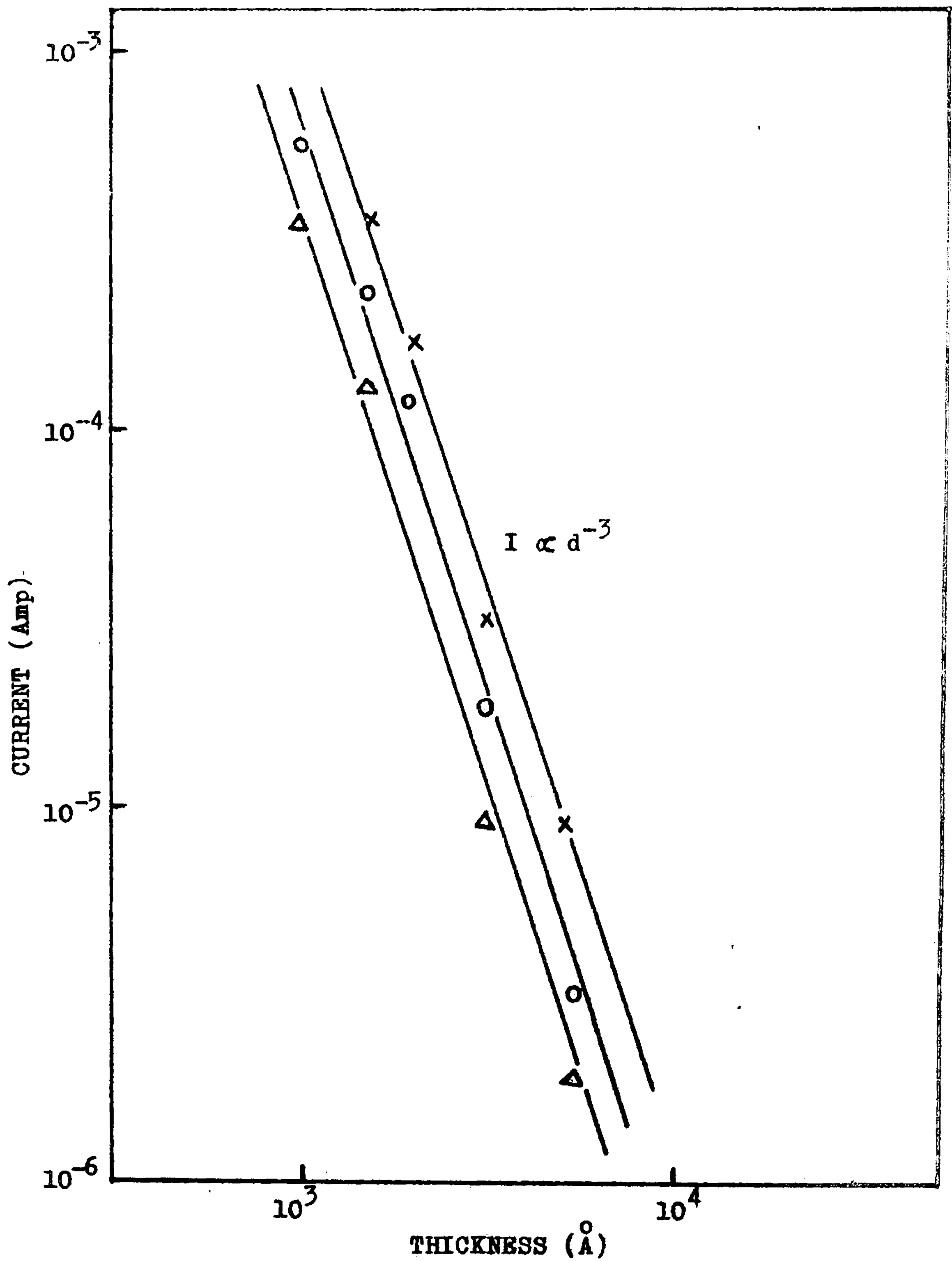

Figure 8.4. Current versus thickness for $Sb-Sb_2S_3-Sb$ systems. Δ - at 400 mV; O - at 500 mV; X - at 600 mV.

8.2.2. Indium Contact

In the case of indium film as top electrode, the system showed a behaviour similar to that of the $Sb-Sb_2S_2-Sb$ structures. Figure 8.5 is the current-voltage characteristics of the $Sb-Sb_2S_3-In$ structures at different temperatures. The characteristics shows an ohms law region followed by a square law region at high fields. In this case also no variation in the characteristics was observed by changing the polarity of the indium electrodes. Figure 8.6 shows the thickness dependence of the current at the square law region of the characteristics indicating a d^{-3} dependence.

The observed characteristics explains a space charge limited conduction in this film system also. The SCL conduction needs atleast one ohmic contact to the semiconductor. $Sb-Sb_2S_3$ contact is ohmic as discussed earlier. Since no effect for reversing the polarity was observed in the characteristics, for both directions of current flow in the system, space charge injection takes place. This needs both contacts to be ohmic. Hence indium can be considered as making ohmic contact to Sb_2S_3. This is in quiet confirmity with Mitchel and Denure [324].

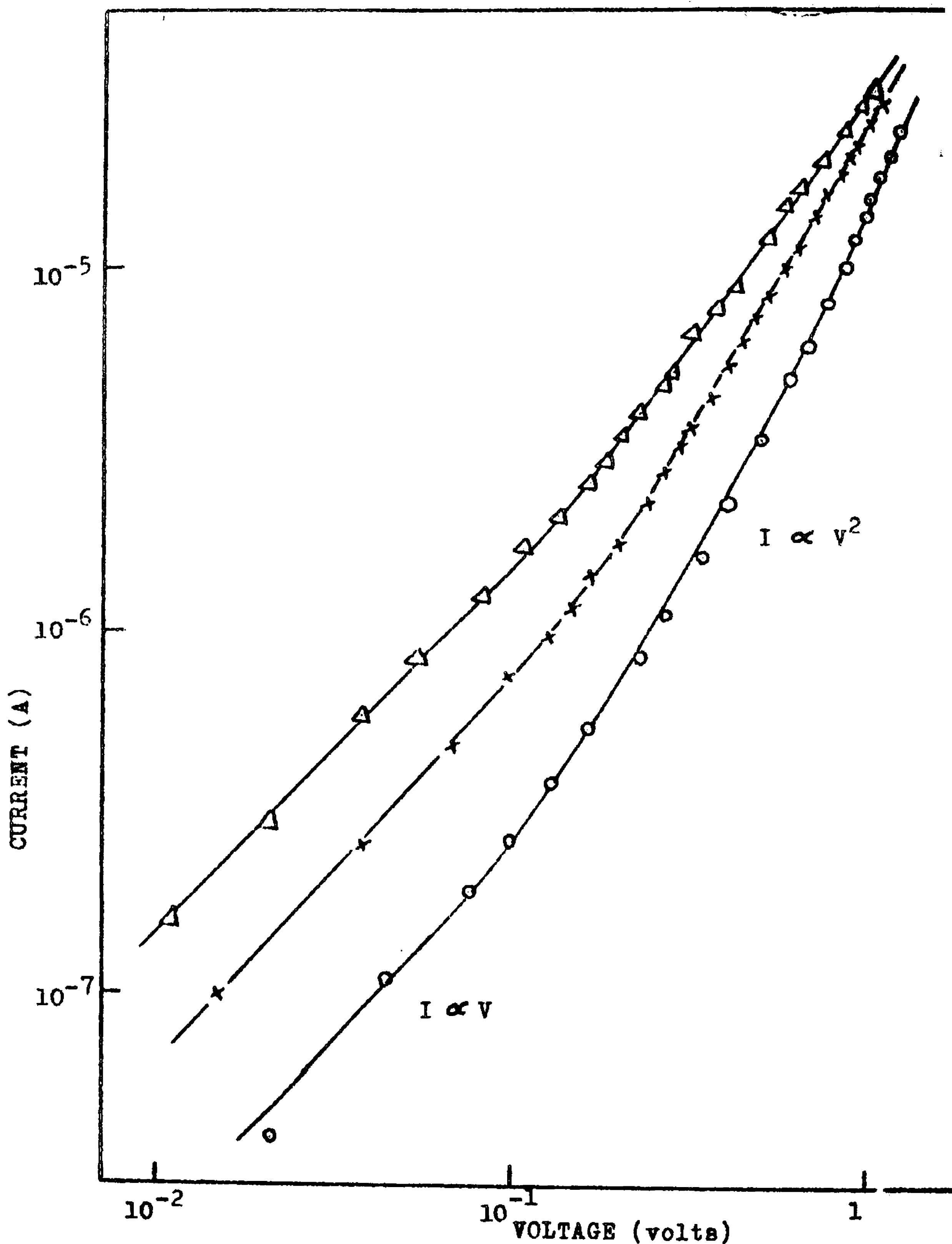

Figure 8.5. Current-voltage characteristics of the $Sb-Sb_2S_3-In$ structure at different temperatures. O, at 303K, X, at 323K, Δ, at 348K.

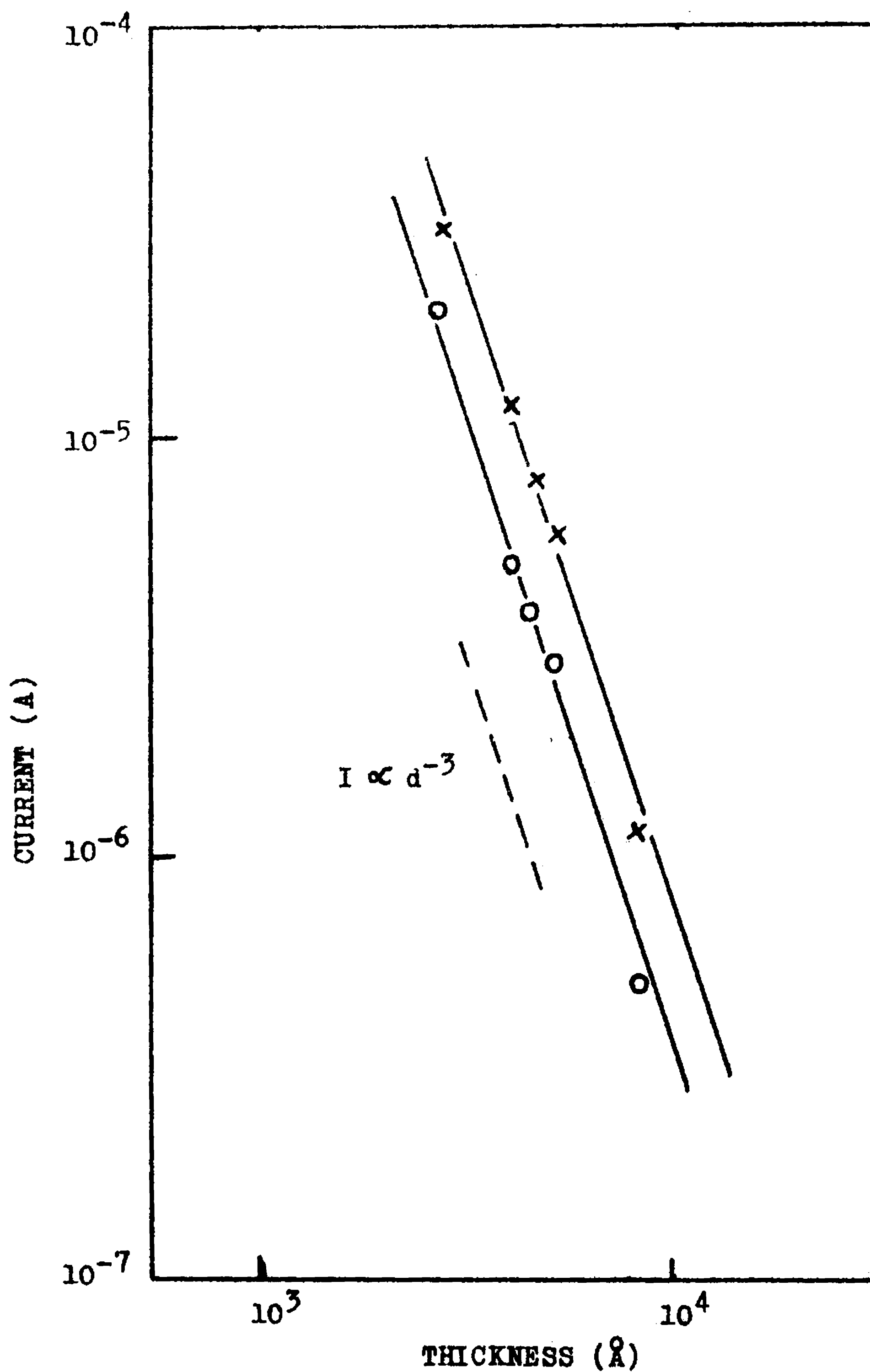

Figure 8.6. Current versus thickness characteristics of $Sb-Sb_2S_3-In$ systems. O at 500 mV, X at 700 mV.

where indium is treated as making very good ohmic contact with antimony trisulphide. Also several other studies using indium electrodes [325-327] report it to be making good ohmic contact with most materials. However, the deposition of indium over Sb_2S_3 has got a predominant effect in making the contact. Indium may perhaps diffuse to Sb_2S_3 so that the In-Sb_2S_3 junction is a diffused barrier forming an ohmic contact.

8.2.3. Tin Contact

As in the case of antimony and indium as top electrodes, Sb-Sb_2S_3 structure with tin as top electrodes also showed an ohms law region followed by a square law region (figure 8.7) for both polarity to the tin electrode. The characteristics shows an inverse cube dependence on thickness at the square law region as illustrated in figure 8.8.

This $I \propto V^2/d^3$ dependence of the film system for both polarity to the tin electrode indicates both interfaces to be of similar nature. As such, since Sb-Sb_2S_3 contact is ohmic, tin can also be considered as making ohmic contact to antimony trisulphide. The tin metallisation may be strong enough to make a diffused barrier at the interface due to the higher kinetic energy of the tin atoms.

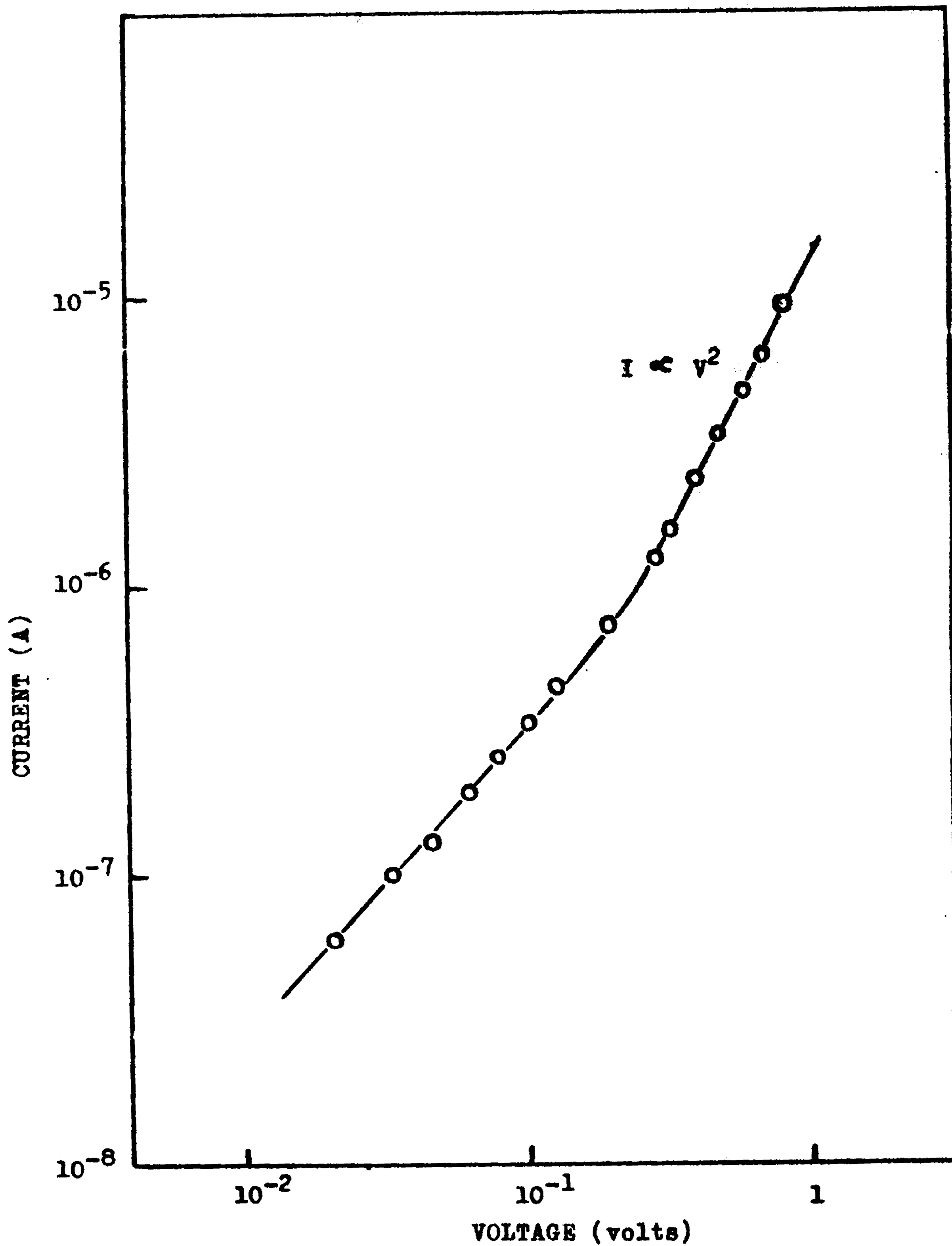

Figure 8.7. Current-voltage characteristics of Sb-Sb_2S_3-Sn structure.

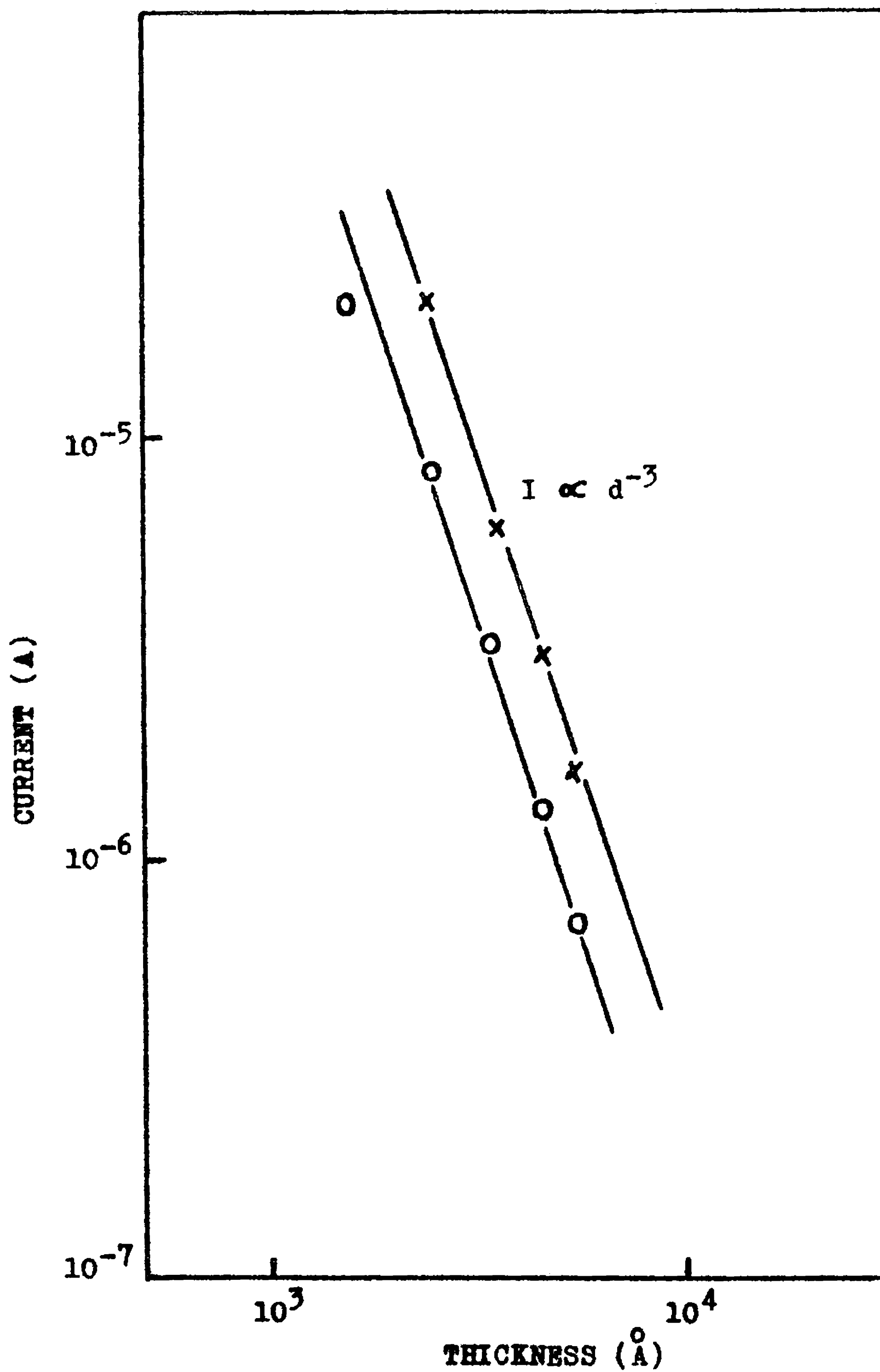

Figure 8.8. Current versus thickness characteristics of $Sb-Sb_2S_3-Sn$ systems. O at 500 mV, X at 700 mV.

8.2.4. Aluminium Contact

The current-voltage characteristics of Sb-Sb_2S_3-Al structures were found to be strongly dependent on the polarity of the electrode for the entire range of thicknesses of the film studied. A higher current in the system was observed when the aluminium electrode was negatively biased compared to a positively biased aluminium electrode. Figure 8.9 shows the I-V characteristics of such a system. A similar characteristics have been reported by Hafis et al [328] while using aluminium electrodes to germanium films.

Analysing the two interfaces, it can be seen that the Sb-Sb_2S_3 contact is ohmic and hence it offers low resistance to current flow in both the directions. This means that the variation in the characteristics observed while changing the polarity is due to the Al-Sb_2S_3 interface. However, with the aluminium electrode negatively biased, the large current indicates that the aluminium-antimony tri-sulphide junction offers a smaller resistance to the current flow than when the aluminium electrode is positively biased. Such an interface which offers low resistance to one direction of current flow

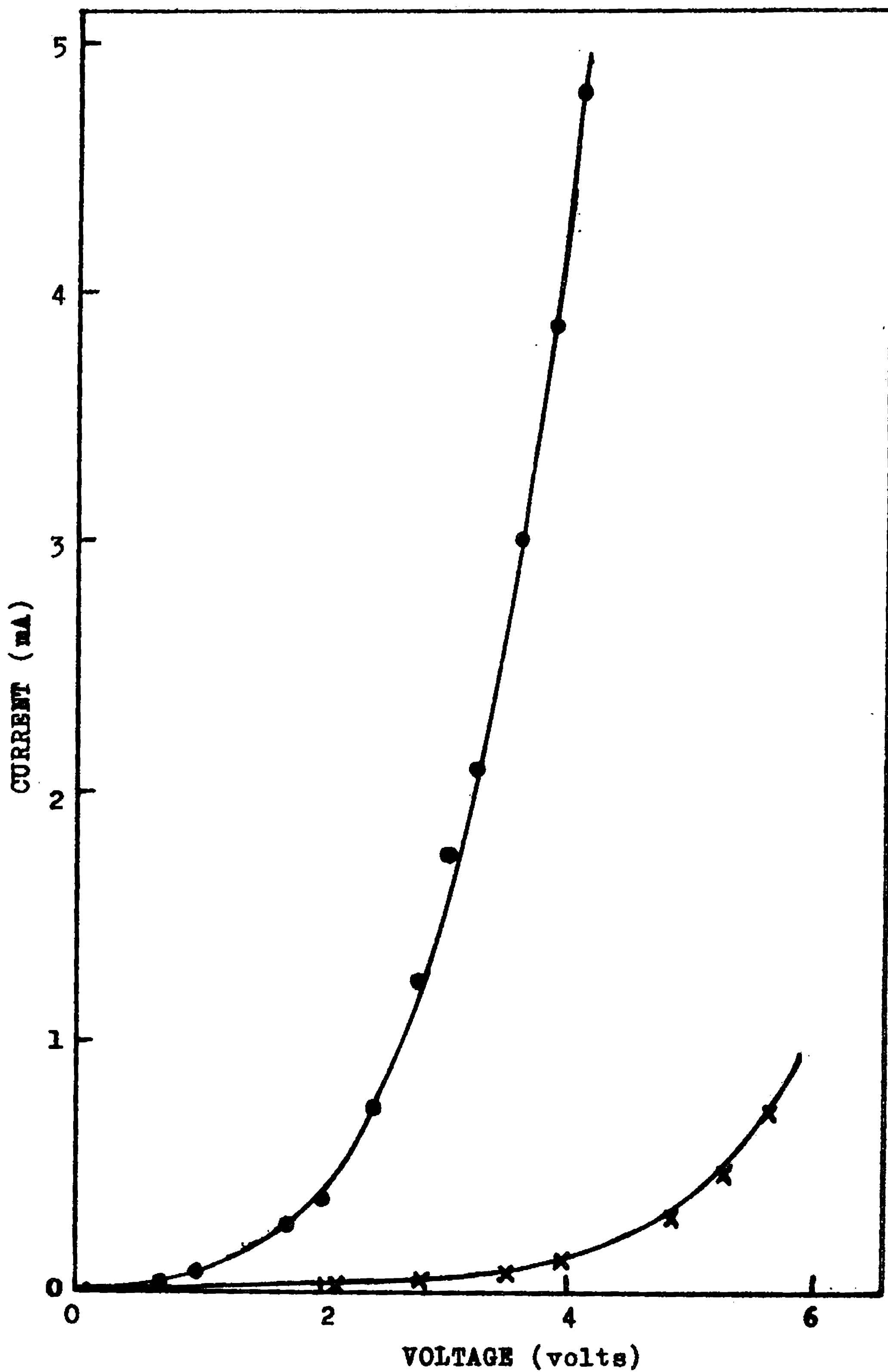

Figure 8.9. Current-voltage characteristics of the $Sb-Sb_2S_3-Al$ structure. ● Al negative; ×, Al positive.

and high resistance of the current flow in opposite direction is called a Schottky barrier as already discussed in chapter two. Hence Al-Sb_2S_3 interface can be treated as a Schottky barrier. A similar Schottky contact at the Nb_2O_5-Au interface has been reported in the case of Nb-Nb_2O_5-Au thin film structures by Sciri and Chabicovsky [329].

(i) Poole-Frenkel conduction

The current-voltage characteristics of the structures replotted as log I versus $V^{\frac{1}{2}}$ for different film thicknesses are shown in figure 8.10. The nature of the characteristics suggests either Schottky or Poole-Frenkel type conduction in the film system [89,94]. In both the cases, the current is field dependent

$$I = I_o \exp\left(\frac{\beta E^{\frac{1}{2}}}{kT}\right) \tag{8.2}$$

where β is either the Schottky factor (β_S) or the Poole-Frenkel factor (β_{PF}) depending upon the conduction. The value of β was calculated using the formula

$$\beta_{PF} = 2\beta_S = \frac{e^3}{\pi \epsilon_o \epsilon} \tag{8.3}$$

where e is the electronic charge, ε is the permittivity

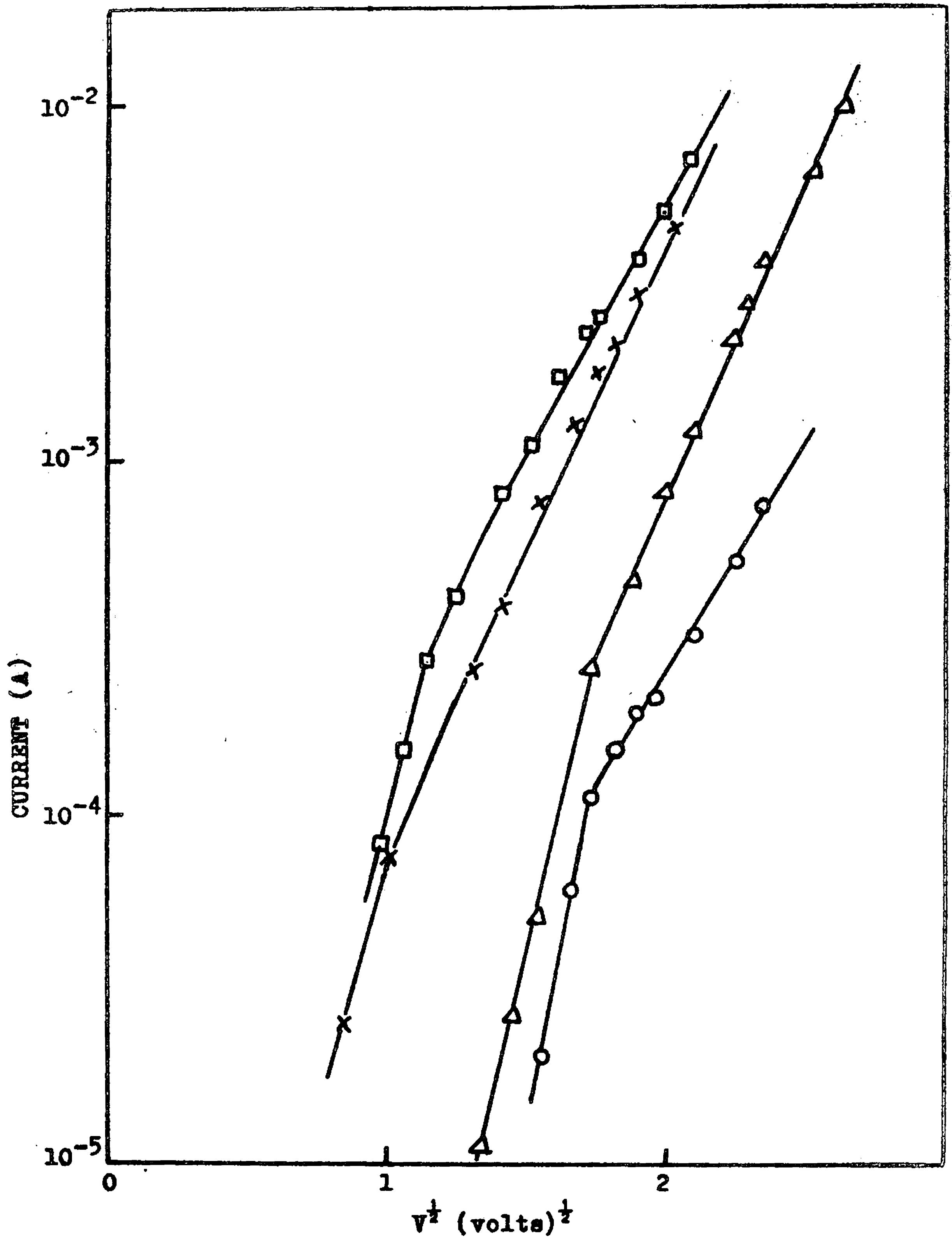

Figure 8.10. Log I versus $V^{\frac{1}{2}}$ graph of the Sb-Sb_2S_3-Al film structure. O , film thickness 2450 Å; X film thickness 1810 Å; △ film thickness 1650 Å; □ , film thickness 2275 A.

of free space and ε is the high frequency dielectric constant. Also from the slope of the log I versus $V^{\frac{1}{2}}$ graph (figure 8.10), the value of β was determined. The experimentally determined and theoretically calculated values of β are tabulated in table 8.2. Comparing these β values it is suggested that the bulk-limited conduction is predominant in the film system. Bulk limited conduction using aluminium contacts has been reported by Gogoi and Barua [330] in CdSe films and Krause and Grunler [331] in SiO_2 films.

(ii) Surface features

After applying large fields (greater than 9×10^5 V cm^{-1}) the top surface of the effective area of Sb-Sb_2S_3-Al structure was found to be damaged. Figure 8.11 is an optical micrograph of such a damaged film system viewed under reflected light. It has been observed that once this damage is initiated at the surface, it spreads rapidly and covers the entire surface of the effective area. The damage causes the current in the system to fall down and the current-voltage characteristics of a system from the virgin state to the damaged state is shown in figure 8.12.

TABLE 8.2

β values for different film thicknesses

Film Thickness d Å	$\beta_{expt} \times 10^{-4}$ eV $V^{-\frac{1}{2}} cm^{\frac{1}{2}}$	Average $\beta_{expt} \times 10^{-4}$ eV $V^{-\frac{1}{2}} cm^{\frac{1}{2}}$	$\beta_{theor.} \times 10^{-4}$ eV $V^{-\frac{1}{2}} cm^{\frac{1}{2}}$
1650	1.62		
1810	1.84	1.79	1.98
2275	1.99		
2450	1.71		

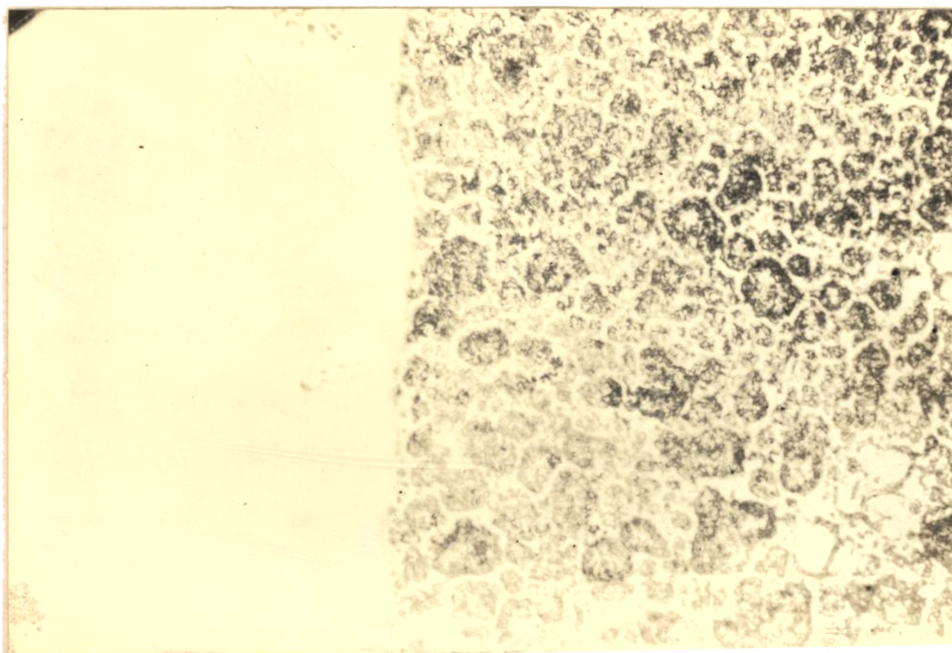

Figure 8.11. Optical micrograph of the damaged area of the $Sb-Sb_2S_3-Al$ structure. Right - damaged area. (Magnification 300X).

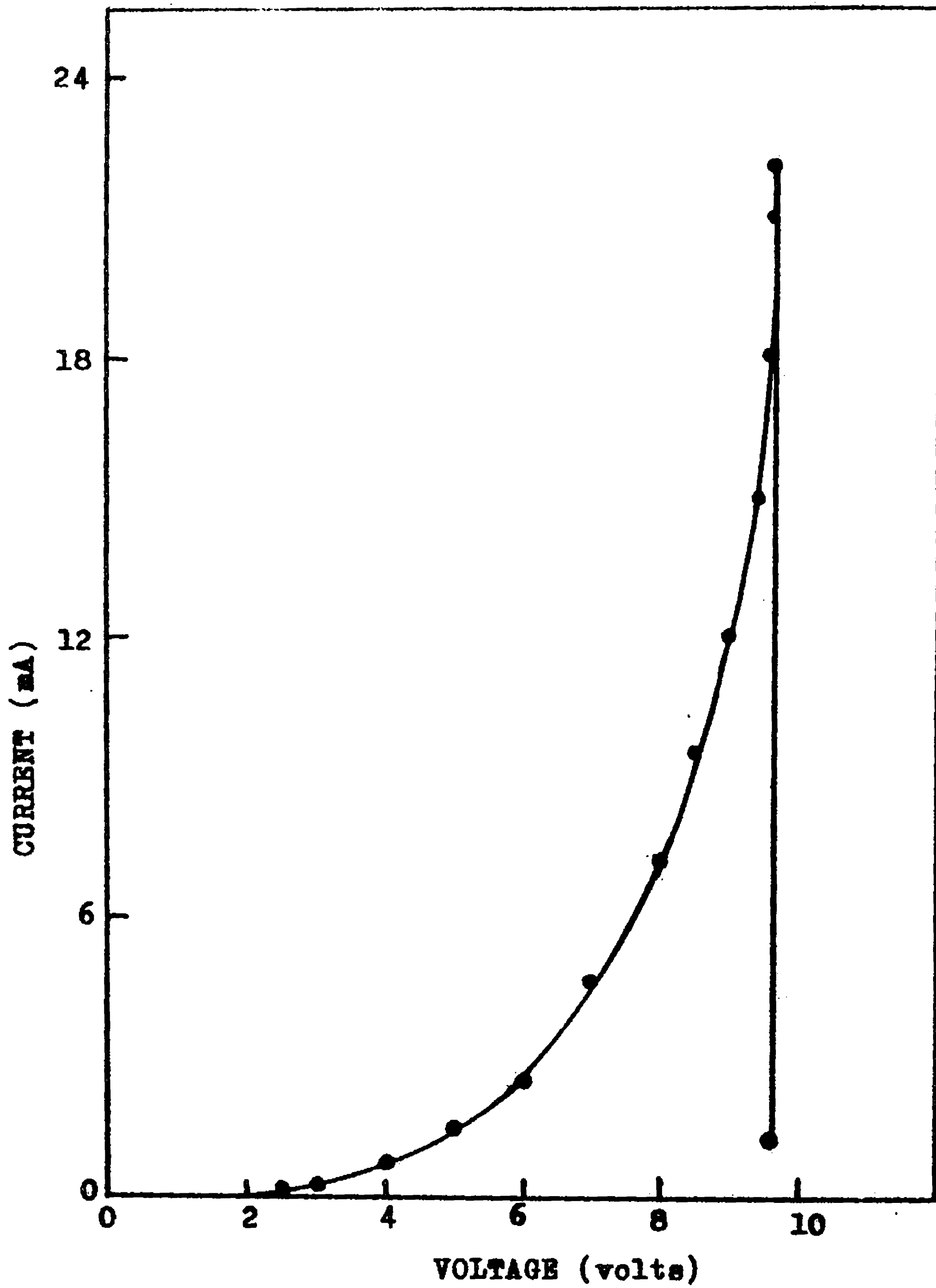

Figure 8.12. Current-voltage characteristics of the $Sb-Sb_2S_3-Al$ system from virgin state to damaged state.

According to Budinas et al [312] antimony trisulphide cannot withstand a field greater than $(7.5 - 9.5) \times 10^5$ V cm.$^{-1}$ This is in agreement with the present observation. The observed damage might also have been assisted by the joule heating at the metal-semiconductor junction.

8.2.5. Silver Contact

Figure 8.13 is the current-voltage characteristics of the Sb-Sb_2S_3-Ag structure. No detectable current was observed upto 0.1 volt potential and then the current was found to increase sharply near about 0.1 to 0.5 volt, irrespective of the polarity of the electrodes. None of the systems observed with silver as top electrode was capable of withstanding a field greater than 10^3 V cm.$^{-1}$ This may be due to the poor stability of the silver electrode. Mitchell and Demure [324] have also reported that silver electrodes to antimony trisulphide are highly unstable.

8.2.6. Bismuth Contact

In the case of bismuth film as top electrode, an ohmic region followed by a square law region was

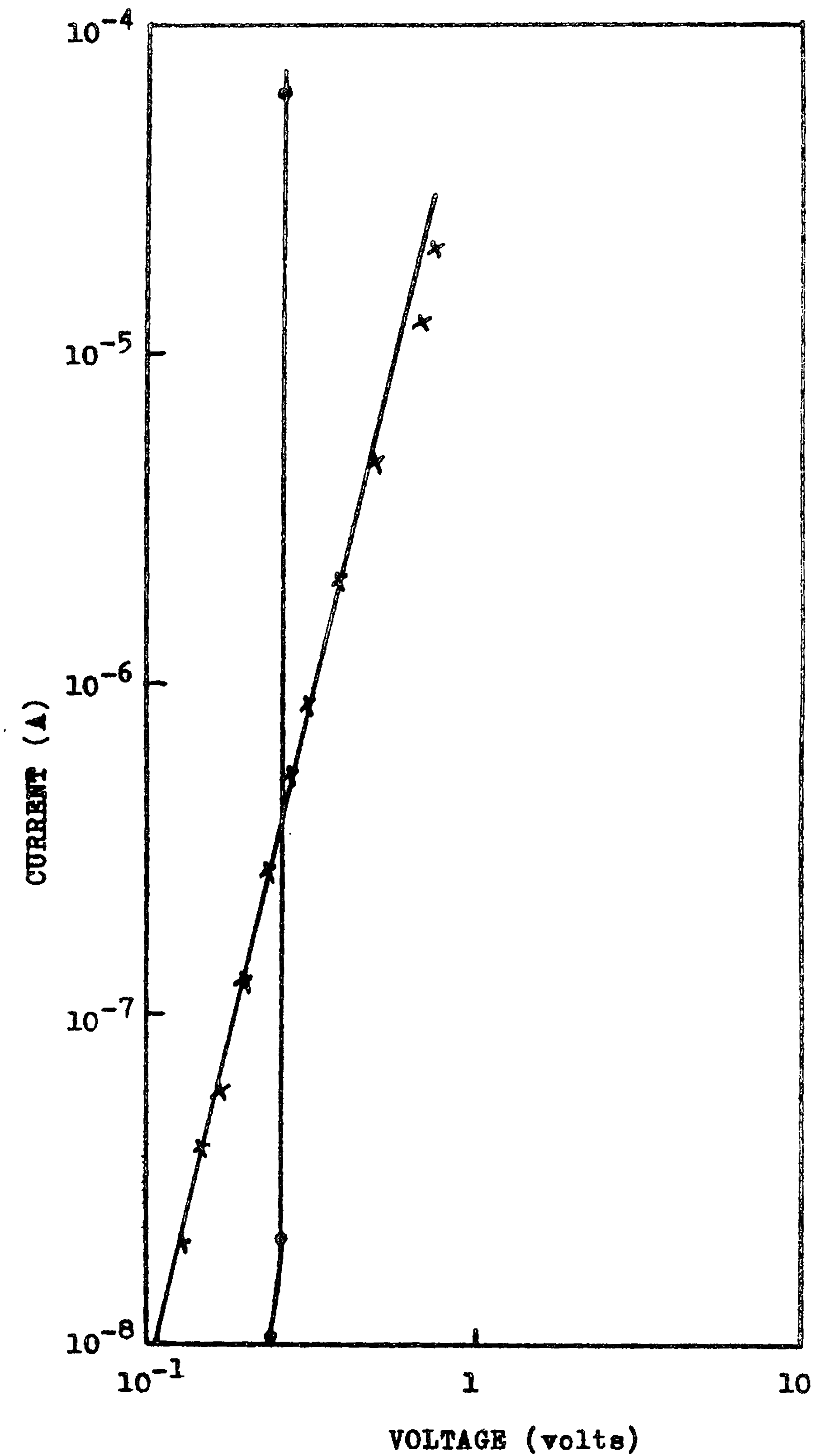

Figure 8.13. Current-voltage characteristics of the $Sb-Sb_2S_3-Ag$ structure.

● Ag negative; ✕ Ag positive.

observed for both polarity to the bismuth electrode. However with a positive polarity voltage applied to the bismuth electrode, a negative resistance region was observed after the square law region as shown in figure 8.14. In the square law region the current shows d^{-3} dependence on thickness (figure 8.15). After the negative resistance region, again the characteristics followed a $I \propto V^2$ relation. The I-V characteristics was found to be irreversible after the negative resistance region.

The $I \propto V^2/d^3$ dependence observed for both polarities to the bismuth electrode indicates that a SCL conduction is predominant in the film system. The irreversible negative resistance behaviour is a current controlled phenomenon [332]. This current controlled negative resistance (CCNR) can be explained by Lampert's double injection model [160,165]. The holes can be injected from the bismuth anode and will form a space charge in the semiconductor enhancing the field towards the antimony cathode which in turn enhances the charge carrier injection from the antimony electrode causing a double injection. Hence bismuth can be treated as an ohmic injecting contact to antimony

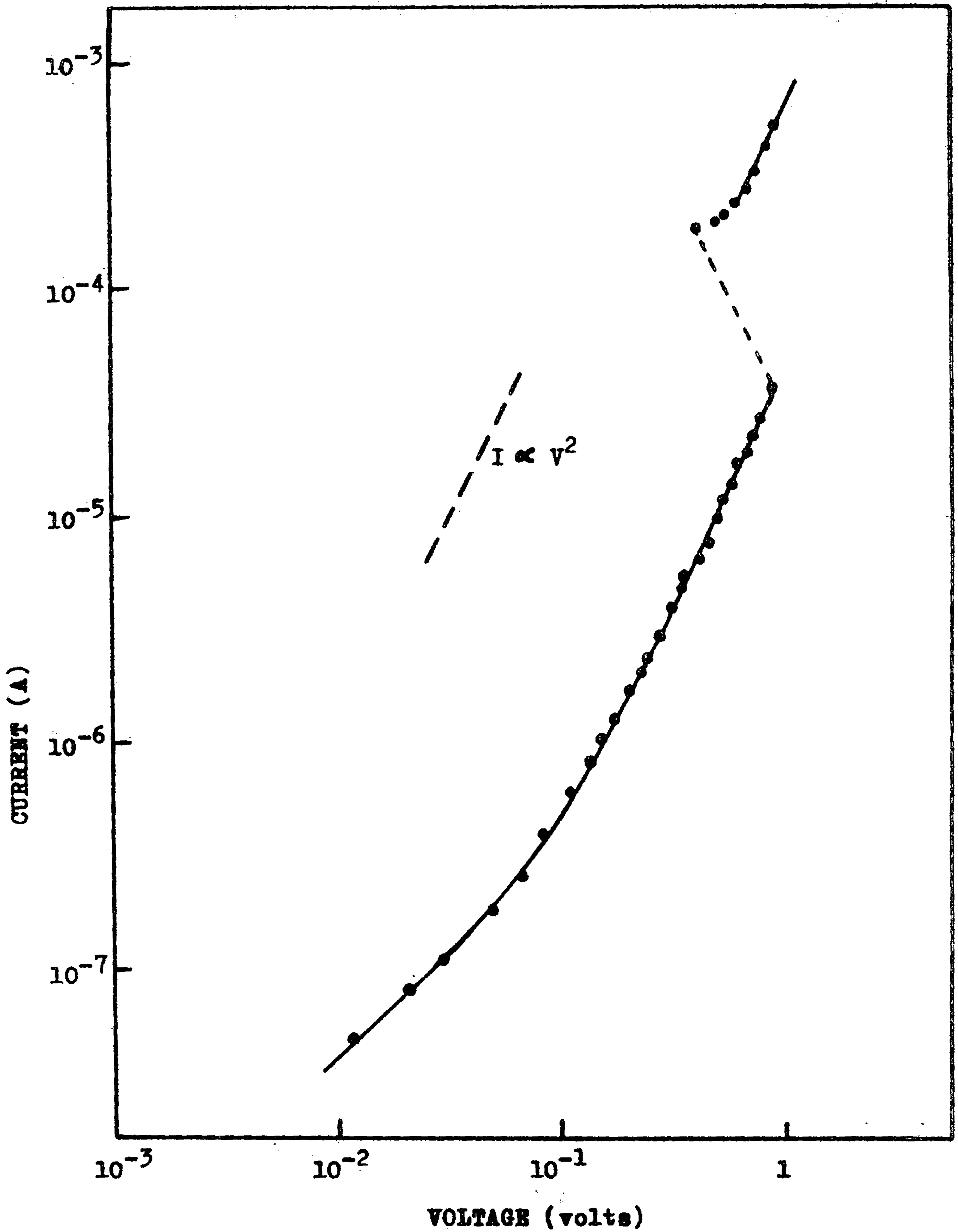

Figure 8.14. Current-voltage characteristics of the $Sb-Sb_2S_3-Bi$ structure showing the negative resistance behaviour.

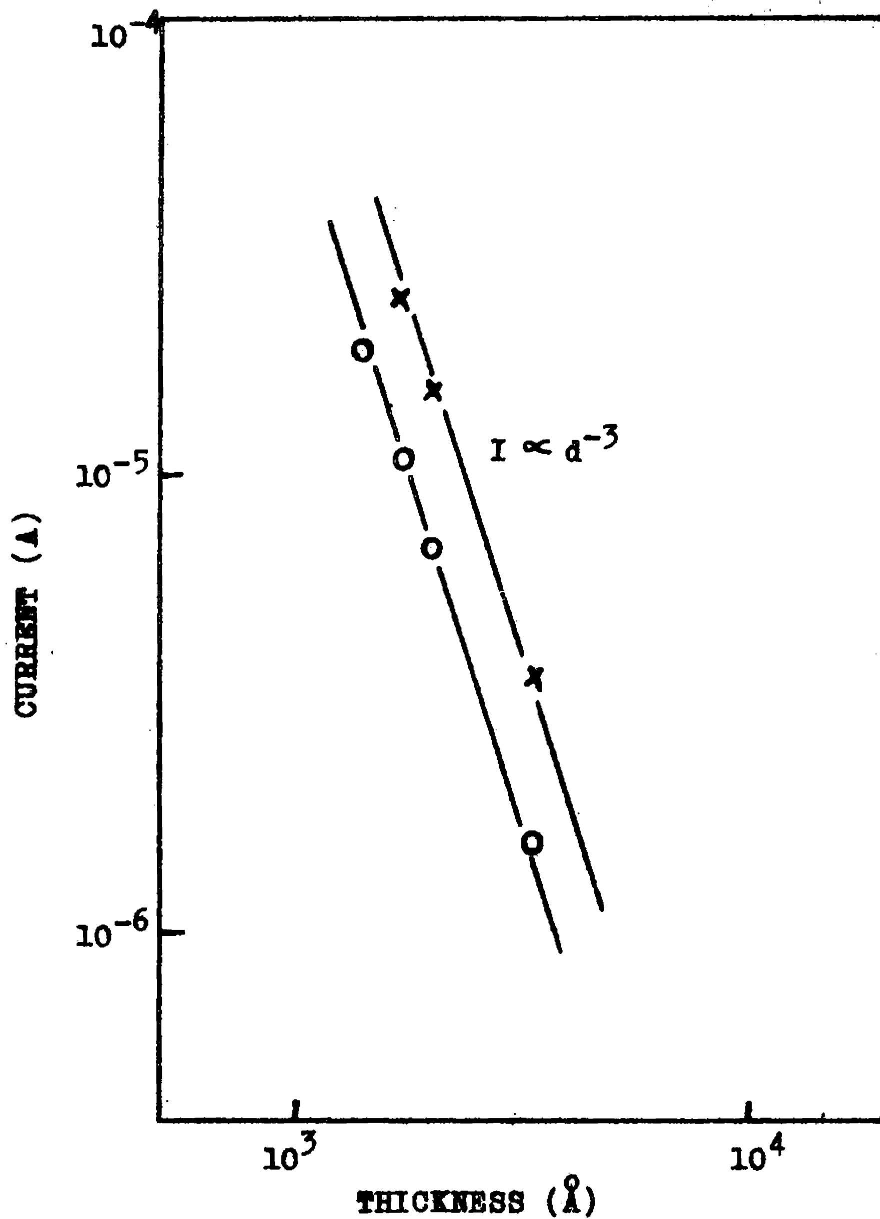

Figure 8.15. Current versus thickness characteristics of $Sb-Sb_2S_3-Bi$ systems. O at 400 mV, X at 600 mV.

trisulphide. Budinas et al [312] have also reported bismuth as an injecting contact to Sb_2S_3. The CCNR characteristics due to double injection have been reported by Arya and Singh [333] for Bi_2O_3 films and Omura and Miyata [334] in the case of Si-SiC film devices.

8.2.7. Remarks

All the contacts studied with metals having work function less than that of antimony trisulphide did not show similar behaviour. The behaviour of the metal contacts to antimony trisulphide are summarised in Table 8.3. Even though, according to Smith [13] and Mitchell and Denure [324], low work function metals make ohmic contacts with semiconductors, it is observed that not all low work function metals make ohmic contact with Sb_2S_3.

8.3. SCL Conduction and Dominant Level Analysis

Both the coevaporated and flash evaporated antimony trisulphide films exhibited space charge limited conduction while sandwiched between antimony electrodes. The current-voltage characteristics showing this SCL conduction measured for films of

TABLE 8.3

Type of contact made by different metals

Electrode Metal	Work function ϕ eV	Type of contact
Antimony	4.1	Ohmic
Aluminium	4.2	Schottky barrier
Bismuth	4.3	Ohmic injecting type
Indium	3.8	Ohmic
Tin	4.2	Ohmic
Silver	4.5	Unstable

different thicknesses were used to determine the trap densities and trap energy levels in the system. The dominant electron and hole levels in the semiconductor were determined from the temperature dependence of I-V characteristics.

8.3.1. Trap Density and Trap Depth

The current-voltage characteristics for $Sb-Sb_2S_3-Sb$ systems of different thicknesses is shown in figure 8.16. The characteristics show an ohms low region at low fields followed by a square law region. After the square law region a steep increase in the current is observed. At the square law region both the coevaporated and the flash evaporated films show an inverse cube dependence on thickness as in figure 8.17, indicating that the current flow in the film system is space charge limited as discussed earlier. In such a case the knee observed between the ohms law and the square law region in the current-voltage characteristics can be considered as the cross-over voltage, V_x, and the voltage at which the sharp increase in current occurs can be treated as the trap filled limit voltage, V_{TFL}. Table 8.4 gives the values of V_x and V_{TFL} for different thicknesses of both

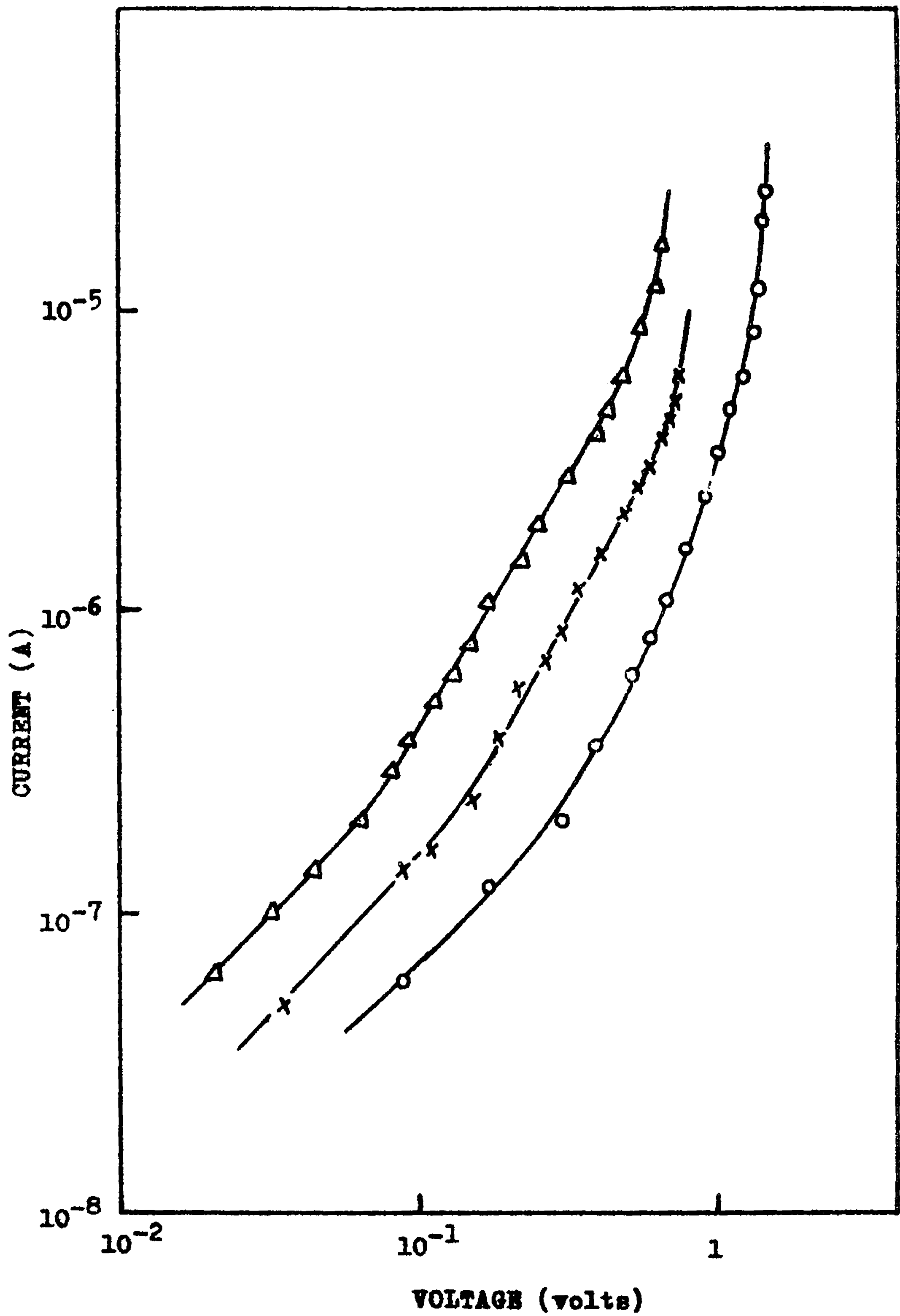

Figure 8.16. Current-voltage characteristics of Sb_2S_3 films of different thicknesses. O, 3240 Å X, 2175 Å; Δ, 1730 Å.

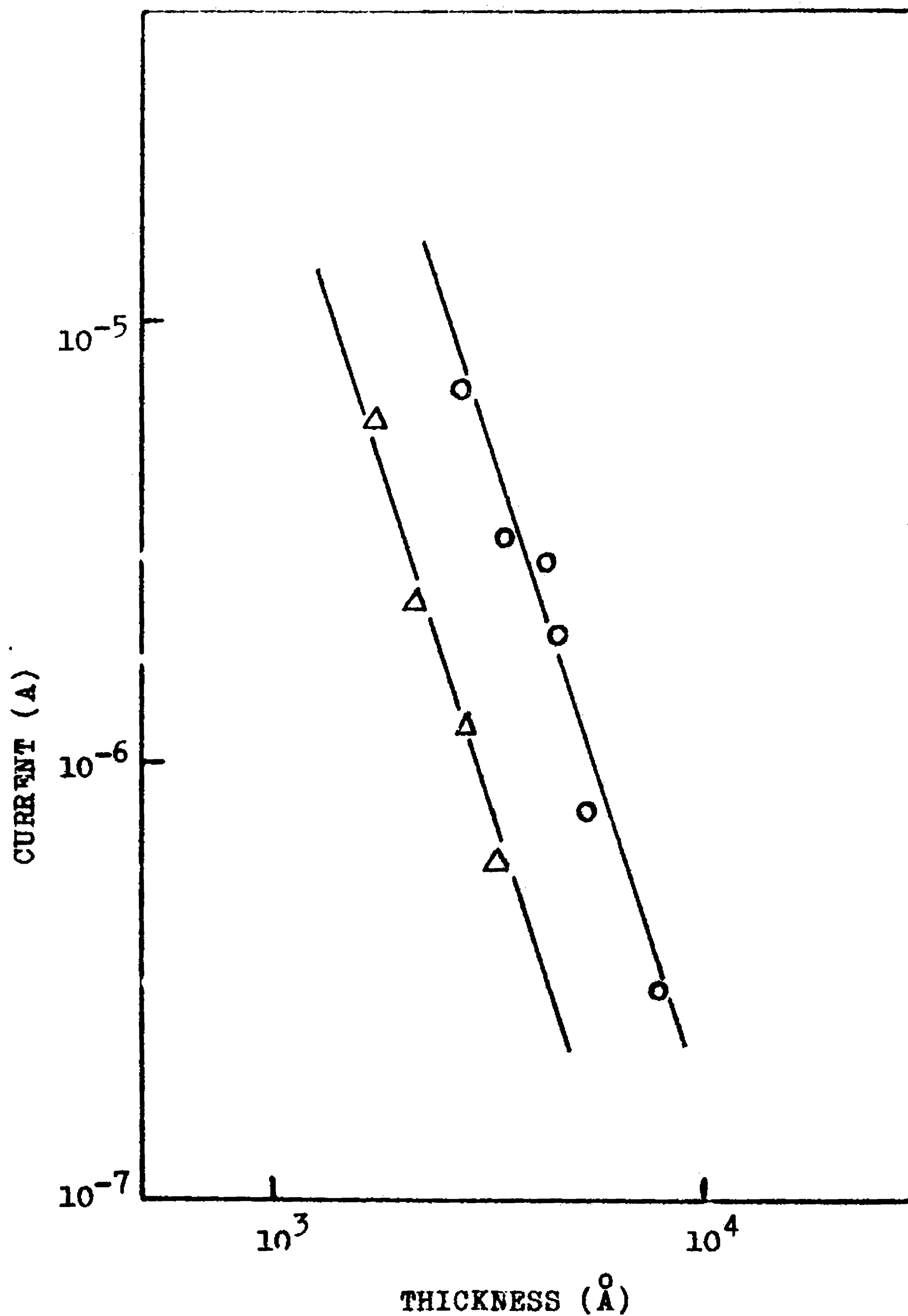

Figure 8.17. Current versus thickness characteristics of Sb_2S_3 films in the square law region. O, coevaporated; Δ, flash evaporated. Slope = -3.0.

TABLE 8.4

V_x and V_{TFL} values for films of different thicknesses

Type of the system	Film Thickness d Å	Cross over voltage V_x volts	Trap filled limit voltage V_{TFL} volts
Coevaporated	2700	1.8×10^{-1}	$9.x\ 10^{-1}$
	3070	9×10^{-2}	1.0
	4560	2×10^{-1}	2.9
	5400	2.5×10^{-1}	3.25
Flash evaporated	1730	6.4×10^{-2}	6.5×10^{-1}
	2175	1.5×10^{-1}	7.5×10^{-1}
	2800	1.8×10^{-1}	1.0
	3240	3×10^{-1}	1.35

coevaporated and flash evaporated films. The trap filled limit voltage V_{TFL} shows a square law dependence on thickness as shown in figure 8.18. This V_{TFL} enables to evaluate the density of the traps, N_t [157]

$$V_{TFL} = \frac{eN_t\, d^2}{2\varepsilon} \qquad (8.4)$$

According to Lampert and Mark [160], the trap density can be calculated with the practical values of V_{TFL}, using the formula

$$N_t = \frac{1.1 \times 10^6\ \varepsilon\ V_{TFL}}{d^2}\ cm^{-3} \qquad (8.5)$$

where ε is the dielectric constant. The trap density thus calculated, using $\varepsilon = 14.5$ [335] for films of different thicknesses is $N_t = 1.44 - 2.22 \times 10^{16}\ cm^{-3}$ for coevaporated and $N_t = 2.03 - 3.40 \times 10^{16}\ cm^{-3}$ for flash evaporated film systems.(Table 8.5). These trap density values are in agreement with that obtained by Bube [336] for stoichiometric antimony trisulphide films.

Since the nearly vertical section of the characteristics is directly preceded by the square law section, it can be considered that the traps lay in

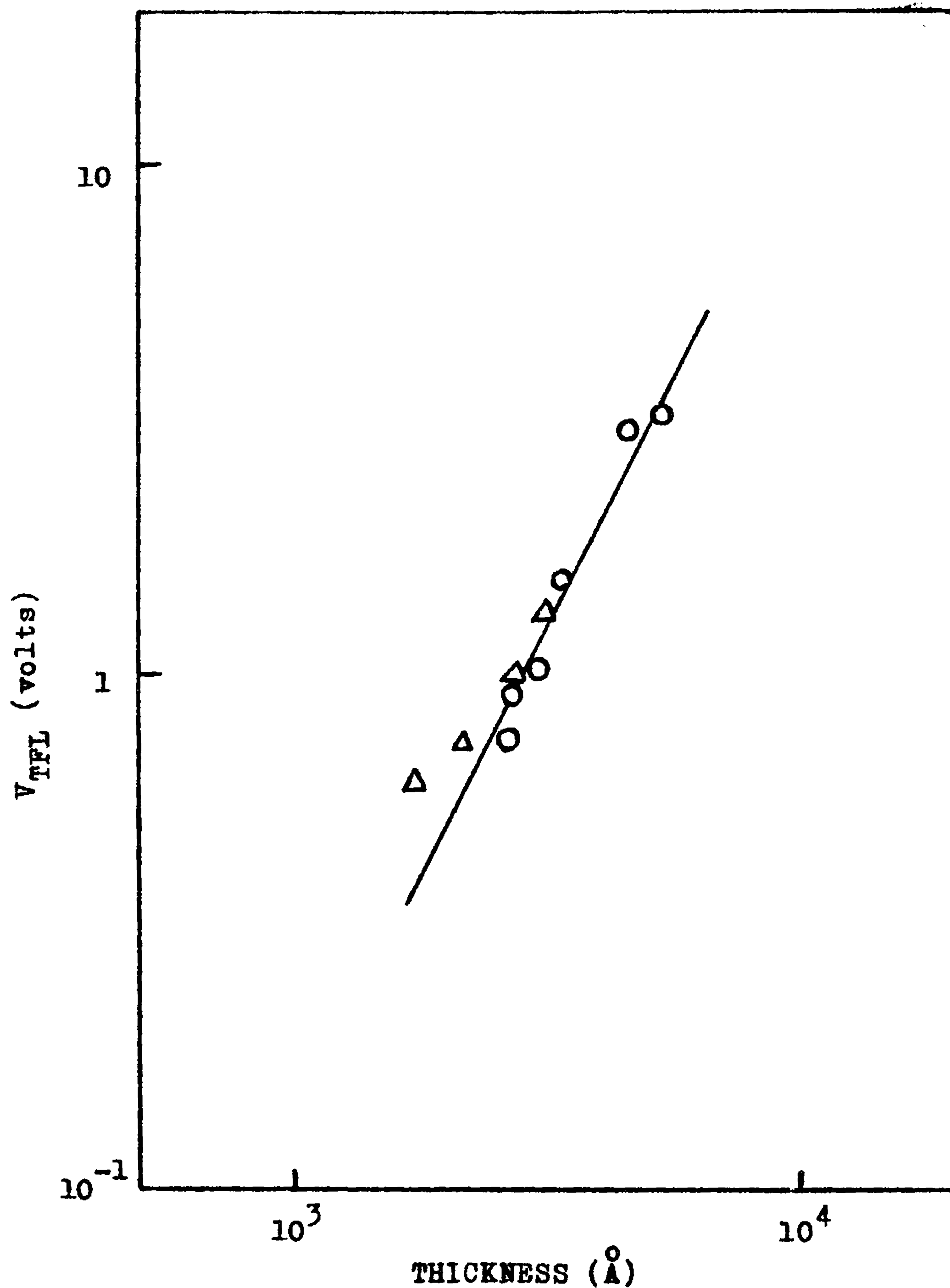

Figure 8.18. Thickness dependence of the trap filled limit voltage V_{TFL} for the Sb_2S_3 films. O , coevaporated; Δ ,flash evaporated. Slope = 1.96.

TABLE 8.5

N_t, θ and E_t values for different film thicknesses

Type of the film	Film Thickness d Å	N_t $\times 10^{16}$ cm^{-3}	θ $\times 10^{-10}$	E_t eV
Coevaporated	2700	1.97	2.06	0.75
	2725	1.44	2.1	0.75
	3070	1.69	5.33	0.73
	4560	2.22	5.29	0.72
	5400	1.77	5.93	0.73
Flash evaporated	1730	3.46	2.34	0.75
	2175	2.53	1.92	0.74
	2480	2.76	1.72	0.74
	2800	2.03	2.21	0.74
	3240	2.04	1.79	0.75

between the Fermi level and the top edge of the valence band (p-type). This square law region, called the shallow trap square law region, gives the information about the trap depth in the film system. The trap depth, E_t, has been calculated using the relation

$$E_t = kT \ln \frac{N_v}{\theta g N_t} \qquad (8.6)$$

where N_v is the effective density of states in the valence band ($N_v = 2.5 \times 10^{19} cm^{-3}$), k the Boltzmann constant, T the temperature, $g \simeq 2$ the degeneracy factor of the traps and θ is the reduction factor. The reduction factor θ was determined for films of different thicknesses using the relation

$$\theta = 1.8 \times 10^{-6} \, p_o \, d^2/\varepsilon V_x \qquad (8.7)$$

where V_x is the cross over voltage from ohms law to square law region and p_o is the thermally generated free carrier concentration. Assuming the Fermi energy to be 0.82 eV [312], the value of p_o was obtained as 4.1×10^5 cm^{-3}. The values of determined are tabulated in Table 8.5. The trap depth E_t calculated for films of different thicknesses, using equation (8.6) yielded values of E_t = 0.72 to

0.75 eV for coevaporated and E_t = 0.73 to 0.75 eV for flash evaporated films (Table 8.5). The average value of trap depth, E_t, was taken as 0.74 eV from the valence band edge. This trap remains shallow since the thermal width of the energy gap, E_g, is 1.55 eV for Sb_2S_3 [337] which is greater than twice the trap depth.

8.3.2. Dominant Level Analysis

The temperature dependence of ohmic and SCL conduction was used to analyse the activation energy of localised levels in the film system. In the current-voltage measurements of the Sb-Sb_2S_3-Sb film systems at different temperatures, in order to prevent the damage of the film systems, the fields were not applied beyond the square law region.

Figure 8.19 and 8.20 are the I-V characteristics of the coevaporated and the flash evaporated antimony trisulphide films respectively sandwiched between antimony electrodes at different temperatures. Both ohmic and SCL currents are thermally activated. Their corresponding activation energies can be determined from the temperature dependence of the characteristics. Figure 8.21 shows the log I versus 1/T

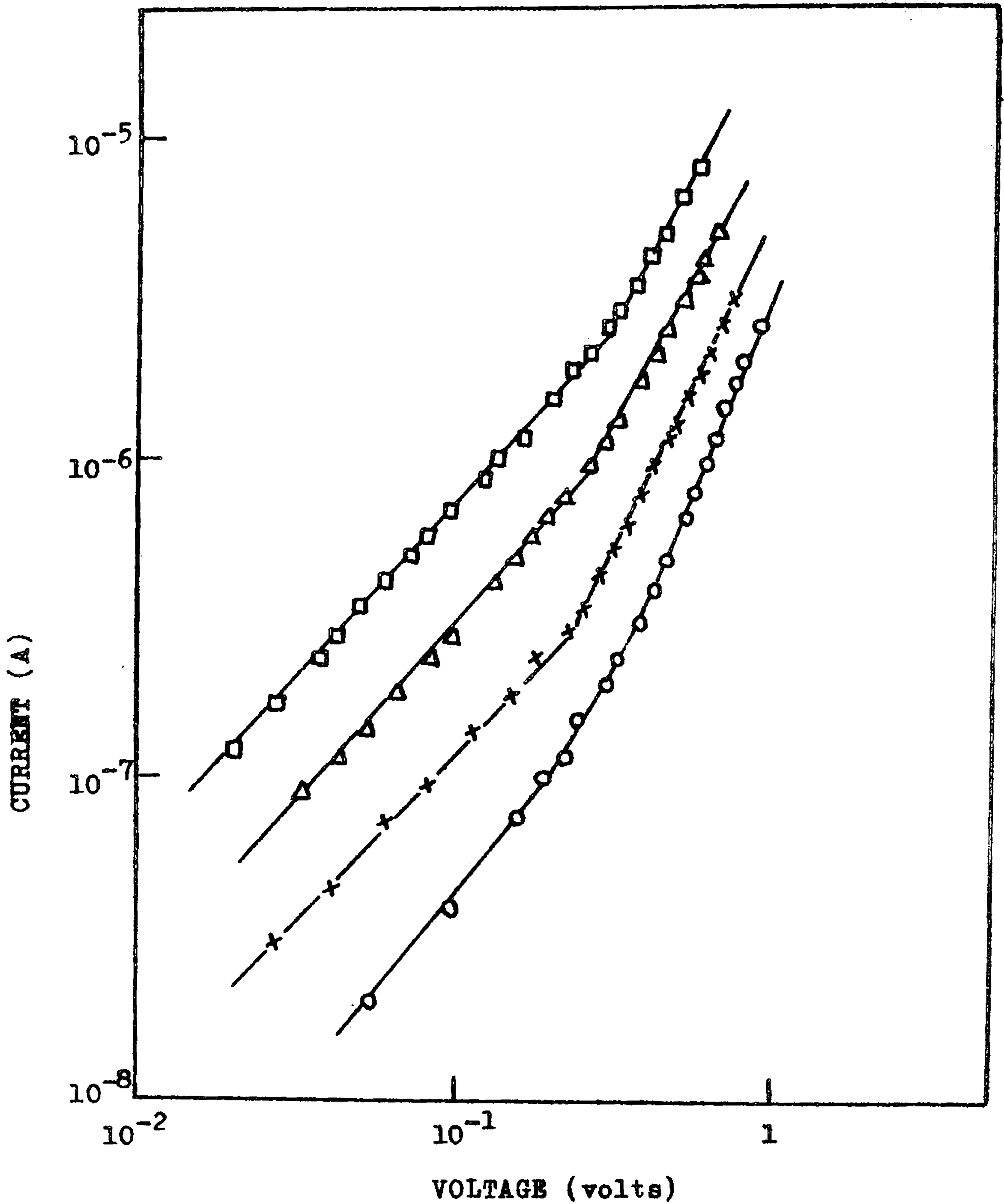

Figure 8.19. Current-voltage characteristics of the coevaporated Sb_2S_3 film system at different temperatures. O, 301K; X, 315K; Δ, 328K; □, 343K. Film thickness 5400 Å.

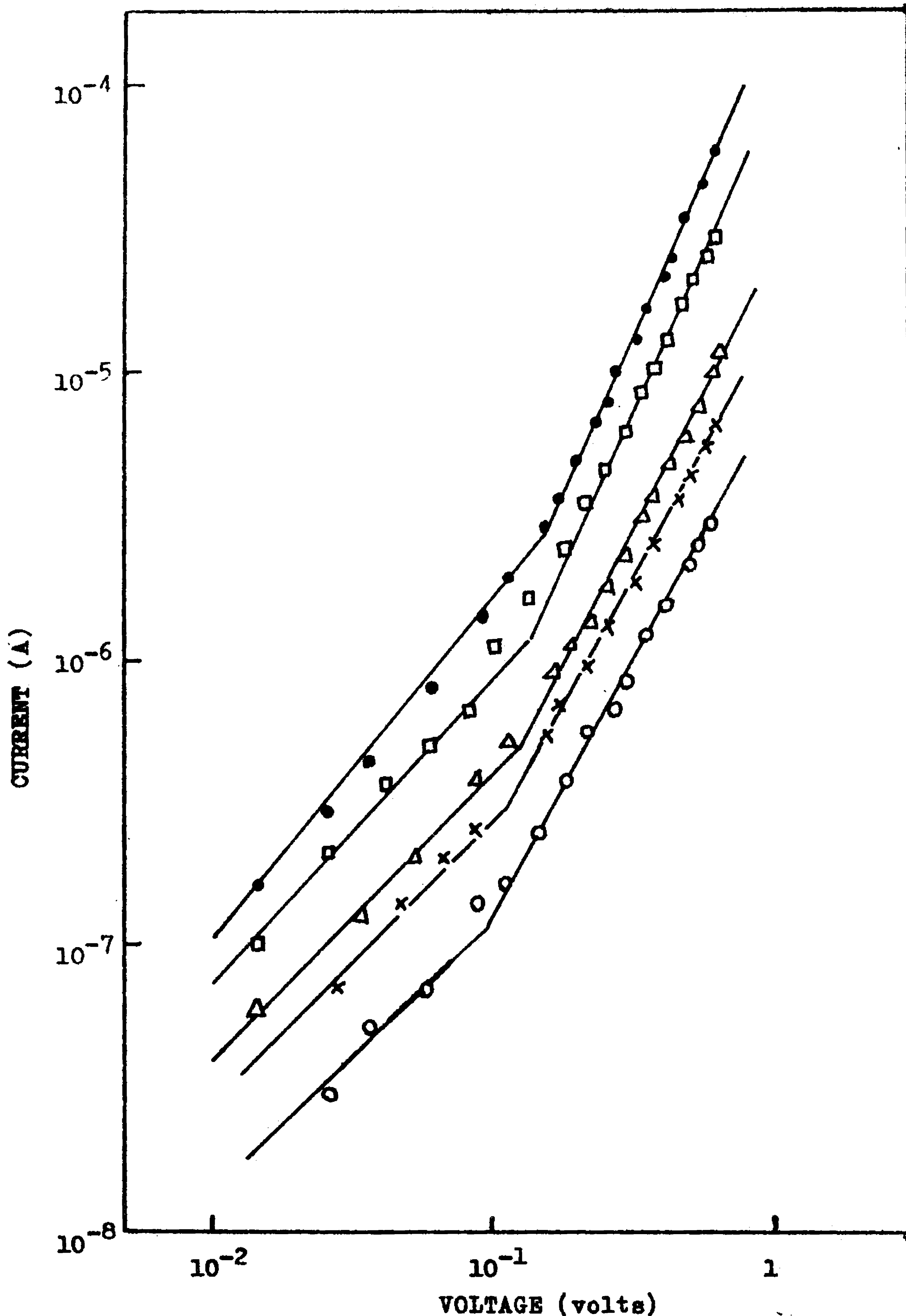

Figure 8.20. Current-voltage characteristics of the flash evaporated Sb_2S_3 film system at different temperatures. ○, 301K; ×, 311K; △, 318K; □, 333K; ●, 343K. Film thickness 2175Å.

plot for the sandwiched Sb_2S_3 film systems (both coevaporated and flash evaporated) for ohmic region and SCLC region. An activation energy of 0.58 eV in the ohmic region and 0.52 eV in the SCL region were obtained for coevaporated systems while for flash evaporated systems they are 0.61 eV and 0.52 eV respectively. For all systems (both coevaporated and flash evaporated) the SCL activation energy was 0.52 eV. The good straight line regions obtained giving a constant activation energy indicate that a relatively weak temperature dependent contribution arises from the product of phonon limited mobility and the effective density of states as suggested by Pande and Roberts [186]. According to Roberts and Schmidlin [185,187], existence of different activation energies for ohmic and SCL conduction is both a necessary and sufficient condition for ohmic conduction to be non-extrinsic. Also, from the nature of the characteristics it can be observed that the crossover voltage, V_x, from ohms law to square law region is temperature dependent. (Figure 8.22). The activation energy of the crossover voltage, 0.07 eV is almost equal to the difference in the activation energies for ohmic and SCL regions, which confirms that the Sb_2S_3 films are non-extrinsic in nature.

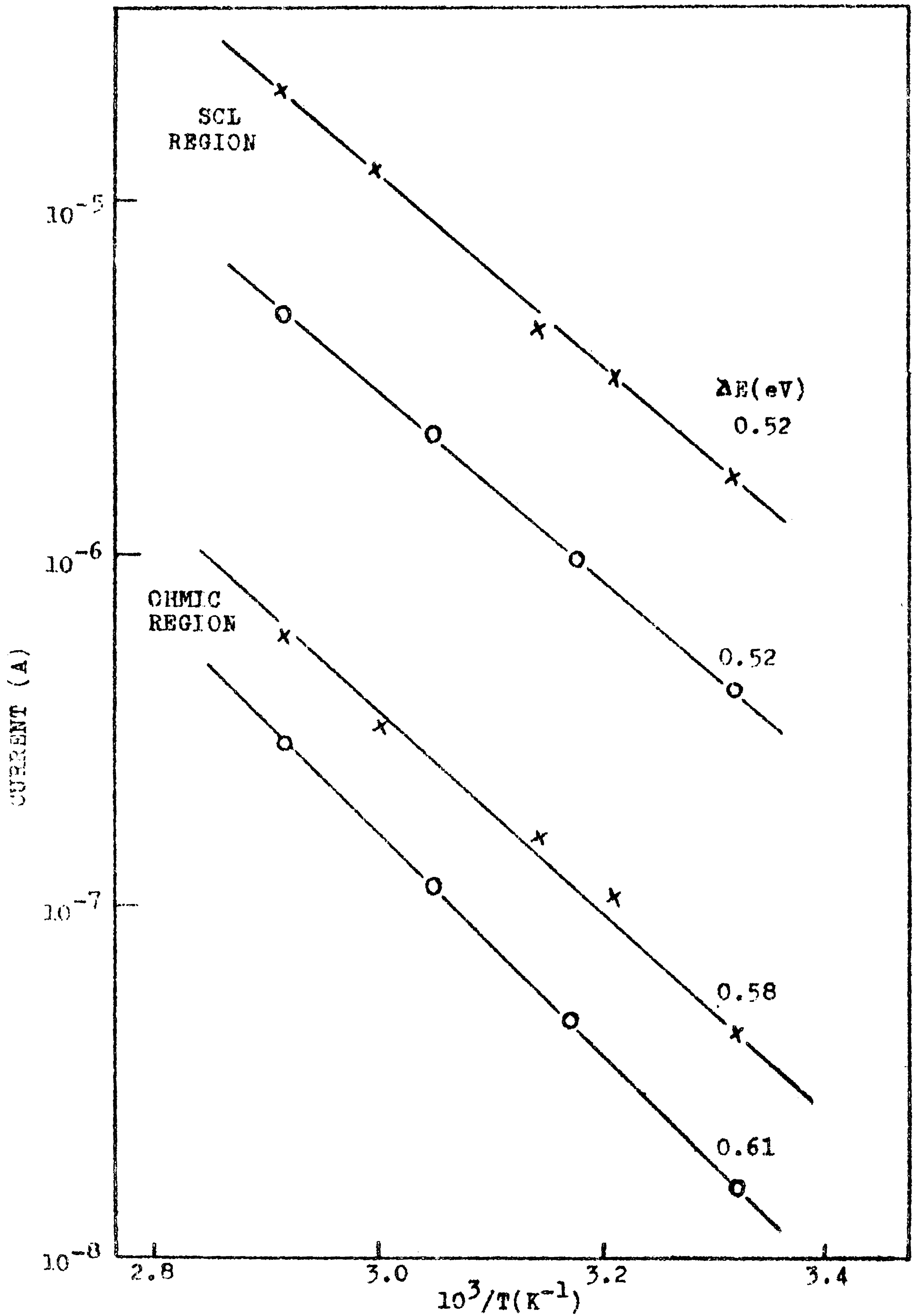

Figure 8.21. Log I versus 1/T plot for Sb_2S_3 films at $V = 4 \times 10^{-2}$V (ohmic region) and $V = 4 \times 10^{-1}$V (SCL region). O – coevaporated (film thickness 5400Å), X – flash evaporated (film thickness 2175Å).

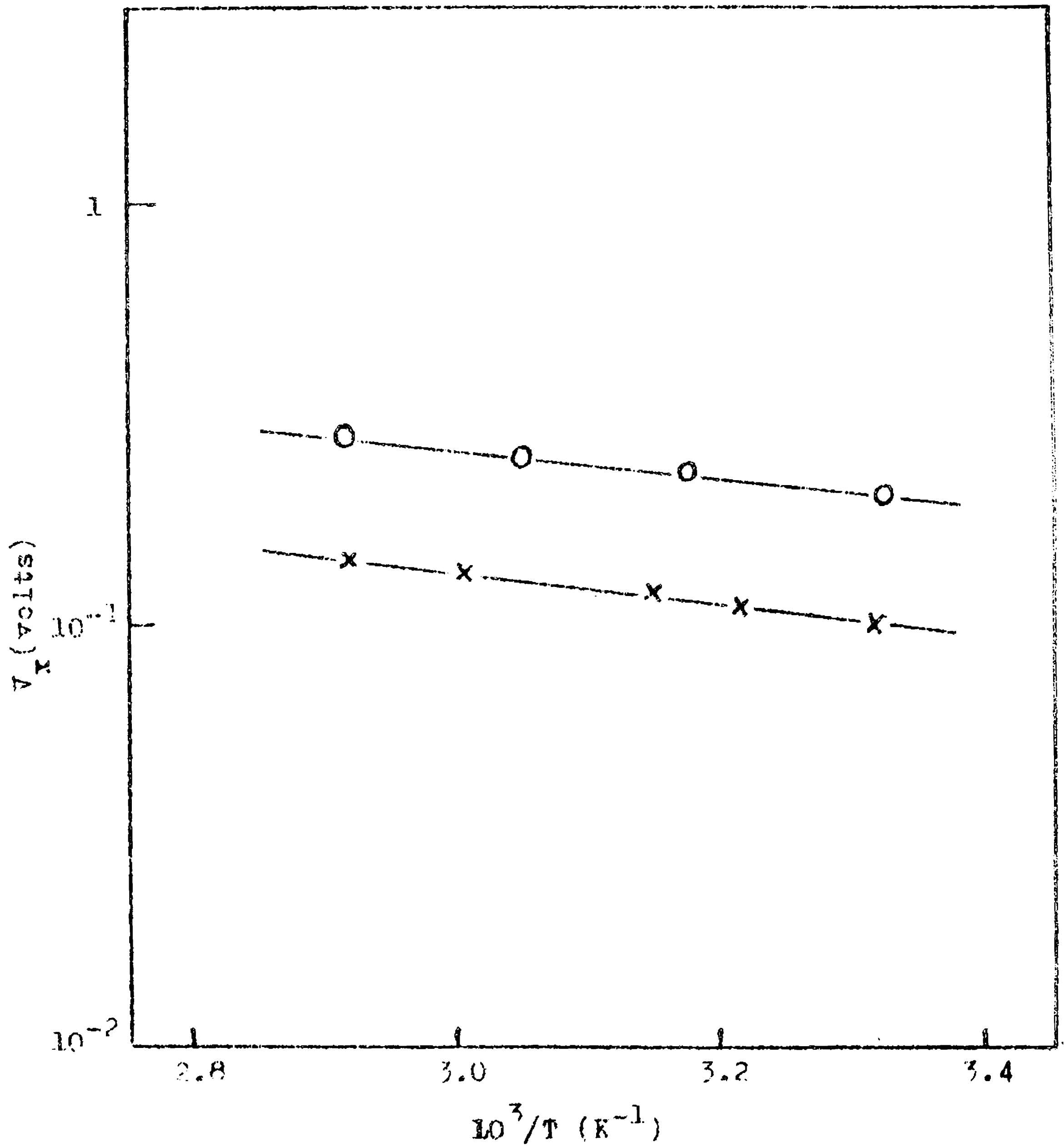

Figure 8.22. Variation of the cross-over voltage V_x with temperature for the film systems. O – coevaporated, X – flash evaporated. $\Delta E = 0.07$ eV.

The non-extrinsic nature can explain the dominant electron and hole levels in a material. In the case of p-type Sb_2S_3 films, the density of the conduction carrier p_v and the ratio of free to total carriers θ_p are

$$p_v = N_v \left(\frac{N_m}{N_q}\right)^{\frac{1}{2}} \exp - \frac{(E_q - E_v) + \frac{1}{2}(E_m - E_q)}{kT} \qquad (8.8)$$

and

$$\theta_p = \frac{N_v}{N_q} \exp - \left(\frac{E_q - E_v}{kT}\right) \qquad (8.9)$$

where the suffices v, m and q refer to the valence band, dominant electron level and dominant hole level respectively. In terms of the dominant levels, the non-extrinsic situation for a p-type material is as follows. If the excess acceptor concentration in a p-type material is small in comparison with the concentration of electrons excited from the dominant hole level, E_q, to the dominant electron level, E_m, then the Fermi energy is located between the two dominant levels in such a way as to make the concentration of holes at E_q equal to the concentration of electrons at E_m.

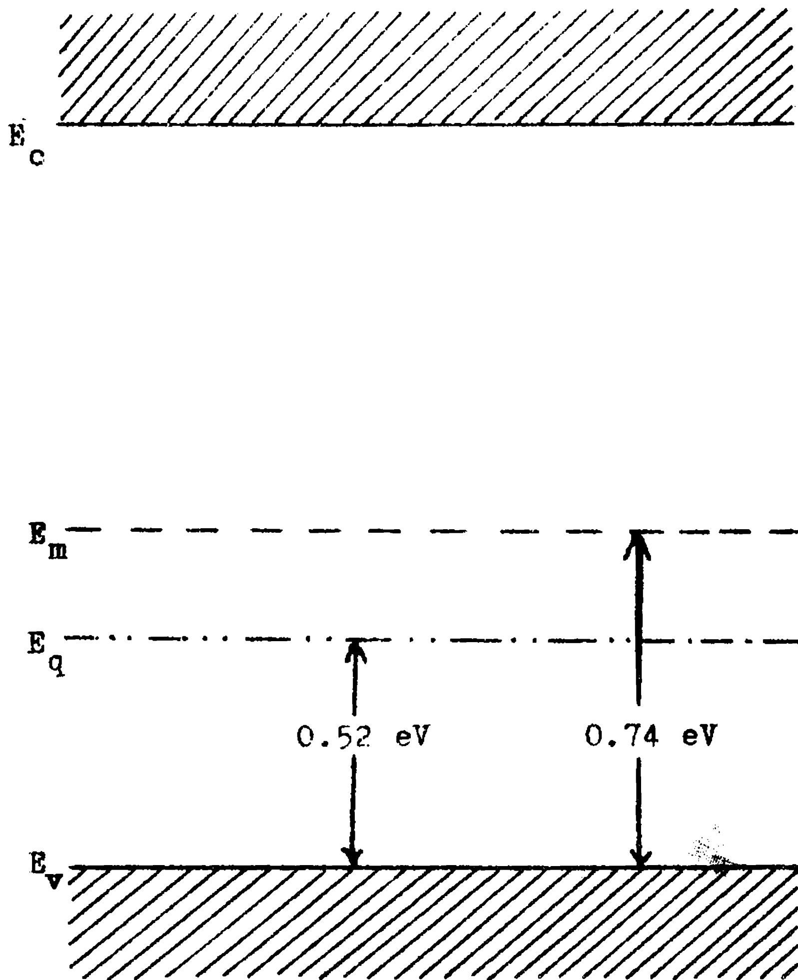

Figure 8.23. Schematic energy level diagram for p-type Sb_2S_3.

8.3.3. Energy Band Diagram for Sb_2S_3

The activation energy values 0.52 eV deducted from the SCL region of log I versus 1/T curves corresponds to the dominant hole level. This means that there exists a hole level E_q, at a distance 0.52 eV from the top of the valence band such that $E_q - E_v = 0.52$ eV. This result is in agreement with that of Brodovii et al [338], who reported a localised level for p-type Sb_2S_3 crystals at 0.54 eV above the valence band. The depth of the trap level $E_t = 0.74$ eV indicate another dominant level which can be the dominant electron level E_m. This dominant electron level is in agreement with the activation energy $\Delta E = 0.75$ eV obtained from the temperature dependence of conductivity. Using these two levels E_m and E_q an energy band diagram for the p-type Sb_2S_3 is proposed as in figure 8.23. This energy level scheme indicates the presence of a trap at 0.74 eV for the ohmic conduction in the case of p-type Sb_2S_3. It may be possible to explain the existence of widely separated trap levels in any system by the dominant level analysis.

8.4. Dielectric Studies

The dielectric studies were carried out

for both coevaporated and flash evaporated antimony trisulphide films. The dependence of capacitance on frequency and temperature for films prepared by both these methods was found to be of similar nature.

8.4.1. Frequency Dependence

At lower temperature (303K) the capacitance of the $Sb-Sb_2S_3-Sb$ structure was found to have little dependence on frequency. At the lower frequency, the capacitance was higher and as frequency increased a gradual decrease in capacitance was observed. As the temperature of the system increased, the change in capacitance with frequency also increased. Figure 8.24 and 8.25 show the capacitance versus frequency curves at different temperatures for both coevaporated and flash evaporated films respectively.

Knowing the capacitance, C, the thickness, d, and the effective area A of the structure, the dielectric constant was calculated using the formula

$$\varepsilon = \frac{4\pi C d}{A} \qquad (8.9)$$

The dielectric constant was calculated for films at different temperatures and frequencies. Figures 8.26 and 8.27 are the dielectric constant versus frequency

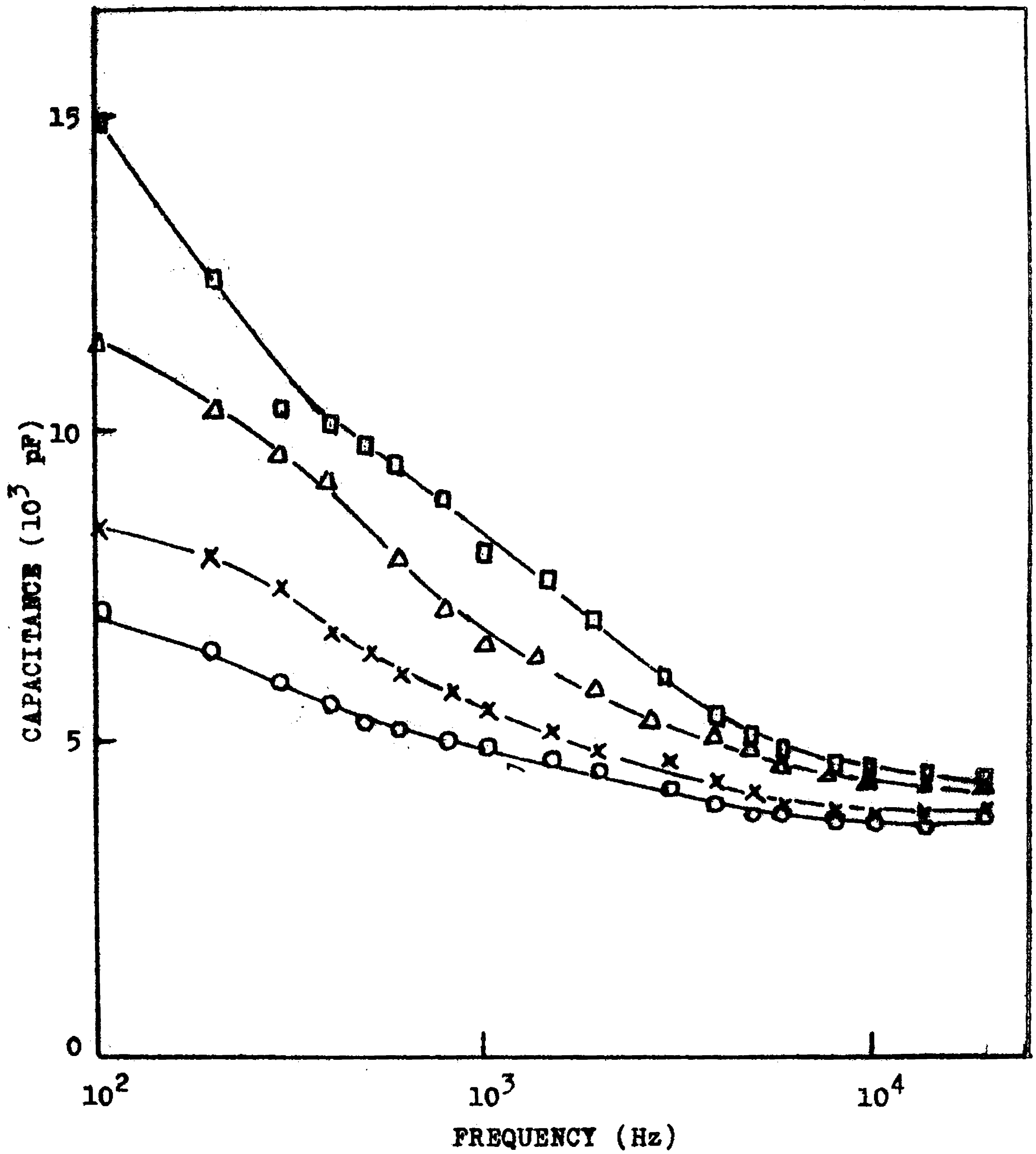

Figure 8.24. Frequency dependence of capacitance for coevaporated Sb_2S_3 films, at different temperatures. O - 303K, X - 318K, Δ - 333K, □ - 348K. Film thickness 1180 Å.

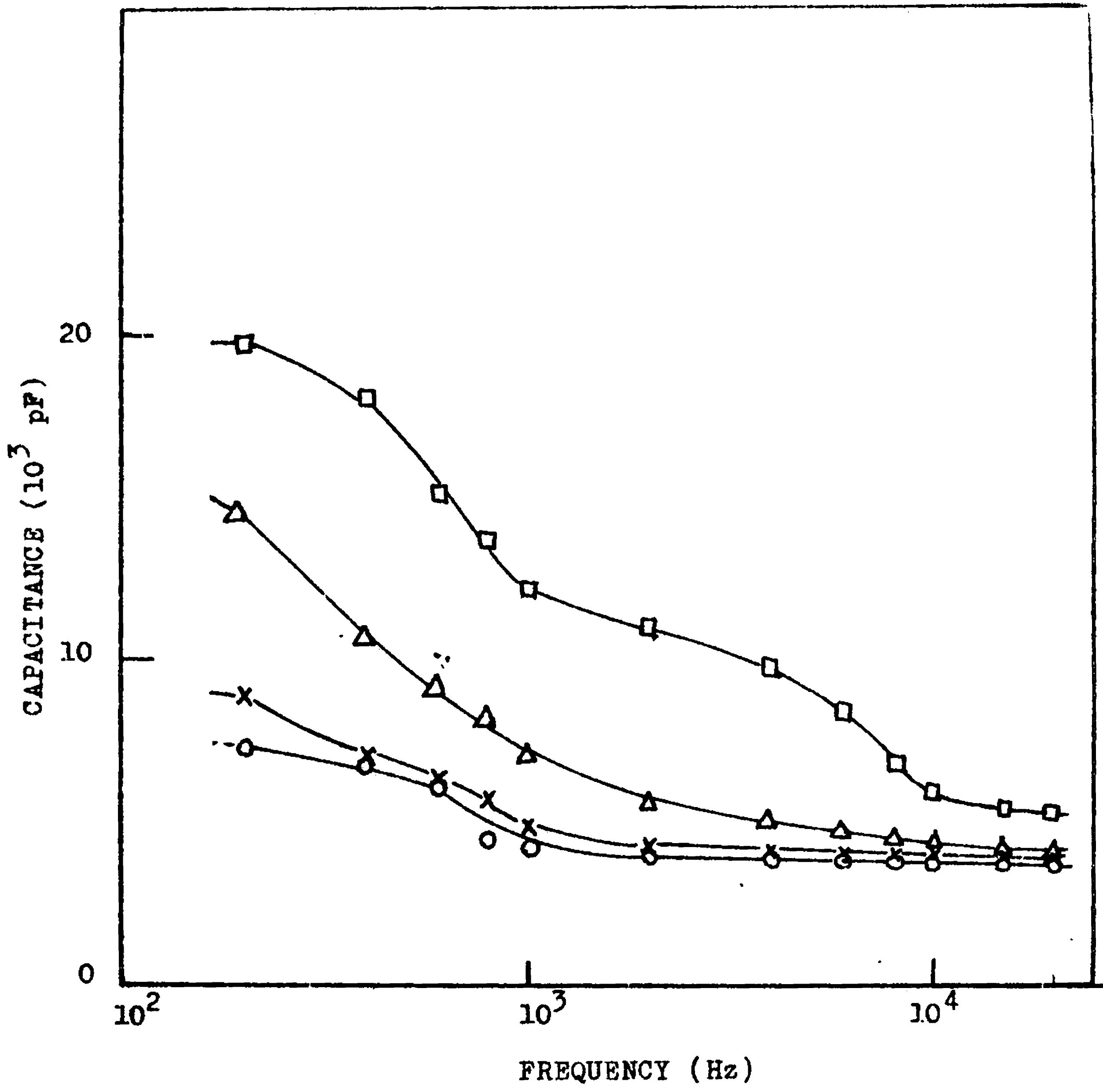

Figure 8.25. Frequency dependence of capacitance for flash evaporated film, at different temperatures. O - 302K, X - 311K, ▲ - 321K, □ - 333K. Film thickness 2175 Å.

curves at different temperatures for film structures shown in figures 8.24 and 8.25.

The dielectric constant calculated for films of different thicknesses was found to be almost same giving an average value 14.5 for coevaporated and 15.5 for flash evaporated films. The values of dielectric constant for films of different thicknesses is tabulated in Table 8.6.

The dielectric constant of antimony trisulphide crystals perpendicular and parallel to the c-axis are reported to be widely different in the values [339]. At microwave frequencies the dielectric constant of Sb_2S_3 is found to be varying from 150 to to 200 [30,340]. However, the dielectric constant is reported to be 15 in all other directions except that parallel to the c-axis. For antimony trisulphide films Patel and George [335] obtained almost the same value of dielectric constant (14.5). In the present investigation, the dielectric constant varying from 14.2 to 14.8 obtained for coevaporated films (Table 8.6) is in good confirmity with the earlier reported results. A slightly higher value of the dielectric constant, around 15.5, is obtained for flash evaporated films.

TABLE 8.6

Dielectric constant for films of different thicknesses

	Film thickness d Å	Dielectric constant ε
Coevaporated	1180	14.19
	1490	14.67
	1810	14.5
	2720	14.75
	3310	14.78
Flash evaporated	1240	15.3
	1600	16.0
	1730	15.8
	1960	15.6
	2175	16.52

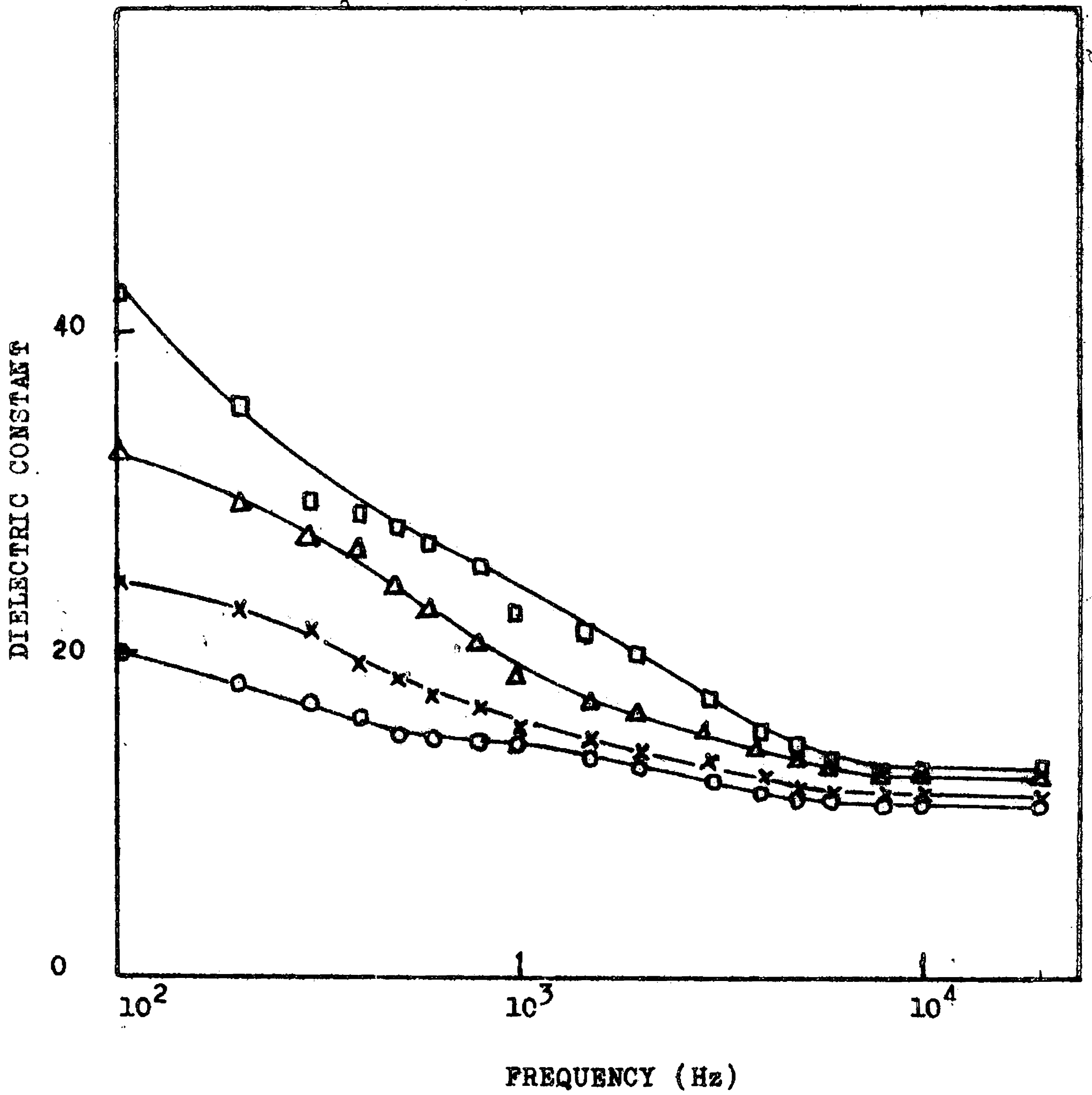

Figure 8.26. Frequency dependence of dielectric constant for coevaporated film at different temperatures. O - 303K, X - 318K, ▲ - 333K, □ - 348K.

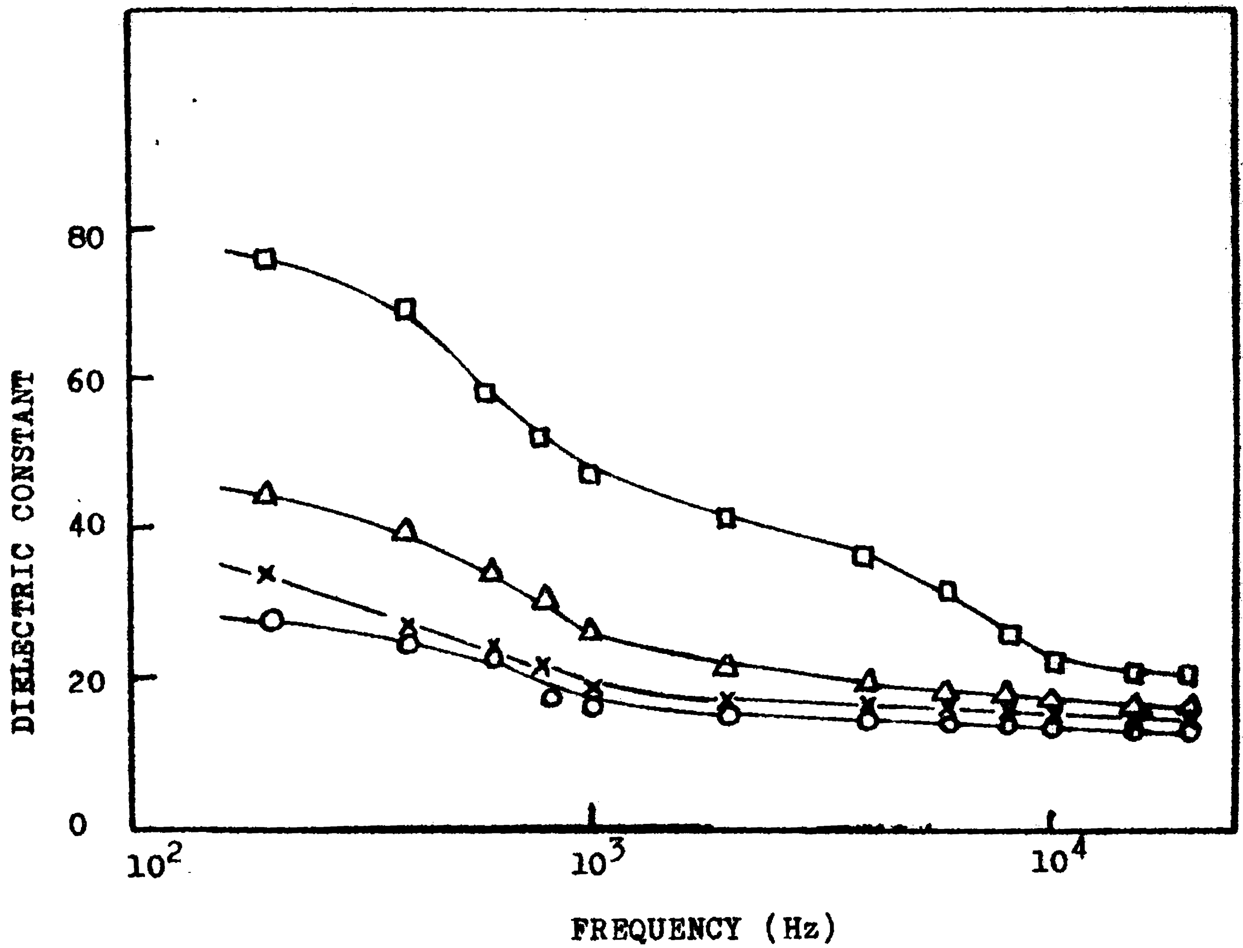

Figure 8.27. Frequency dependence of dielectric constant for flash evaporated film at different temperatures. O - 302K, X — 311K, Δ - 321K, □ - 333K.

This may be due to variation in the nature of the films prepared by both the methods. However, not much variation in ε with thickness has been observed in each case. At higher frequencies the capacitance of the system remained almost invariant.

8.4.2. Temperature Dependence

The temperature dependence of capacitance at different frequencies are shown in figures 8.28 and 8.29 for coevaporated and flash evaporated films respectively. In both cases, not much variation in the capacitance was observed upto a temperature about 313K. For higher temperature the increase in capacitance was almost rapid at 1 k c/s frequency. The temperature coefficient of capacitance (TCC) was calculated from these graphs using equation (4.4). The TCC value for coevaporated film (thickness 1180 Å) 133 ppm $^{\circ}C^{-1}$ and for flash evaporated film (thickness 2175 Å) is 614 ppm $^{\circ}C^{-1}$. The values are comparable with the results for other dielectric films like LaF_3 [342].

The variation of tan δ with temperature at 1 kc/s frequency did not show any peak. The loss tangent was found to increase with temperature

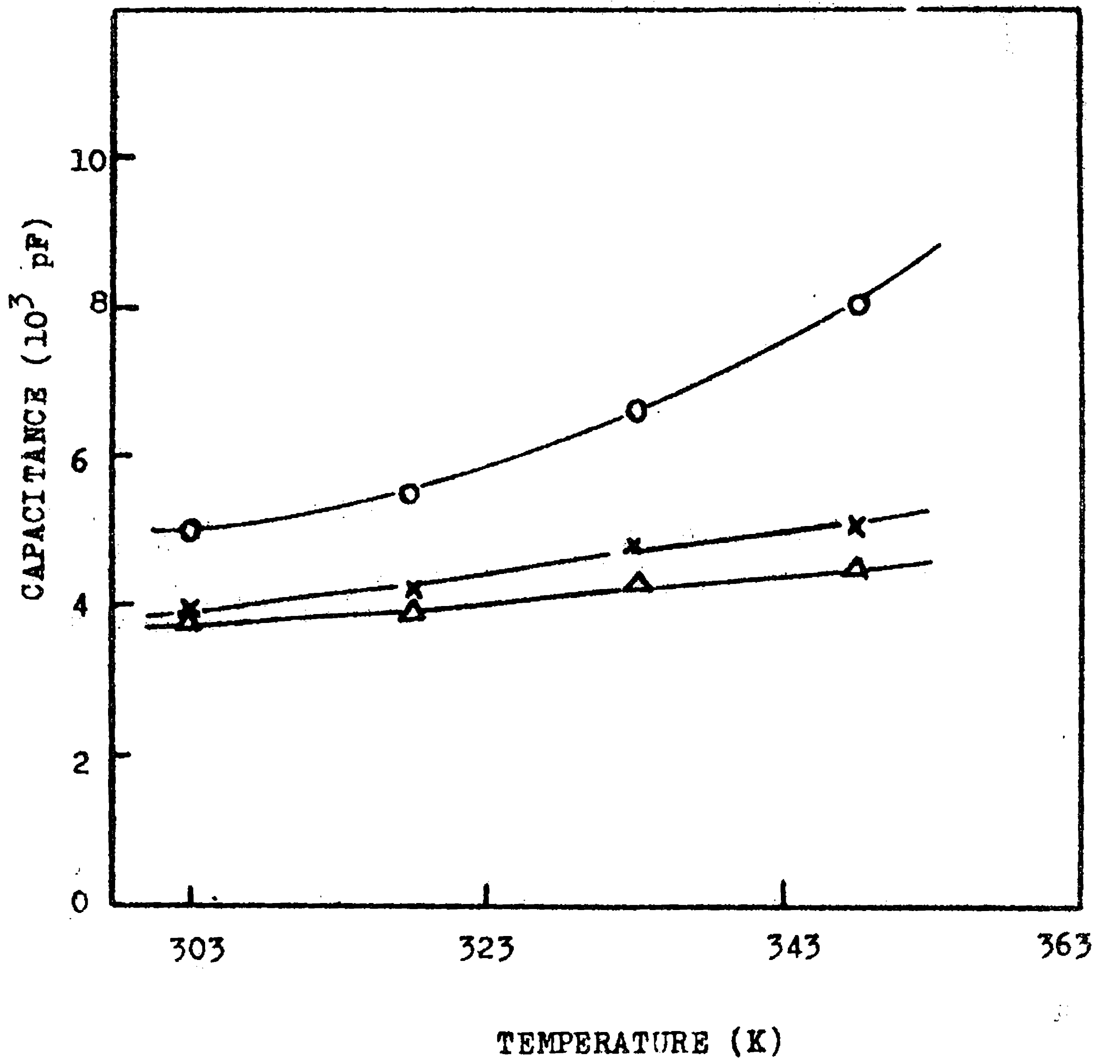

Figure 8.28. Temperature dependence of capacitance at different frequencies for coevaporated film. O – 1 KHz, X – 5 KHz, Δ – 10 KHz. Film thickness 1180 Å.

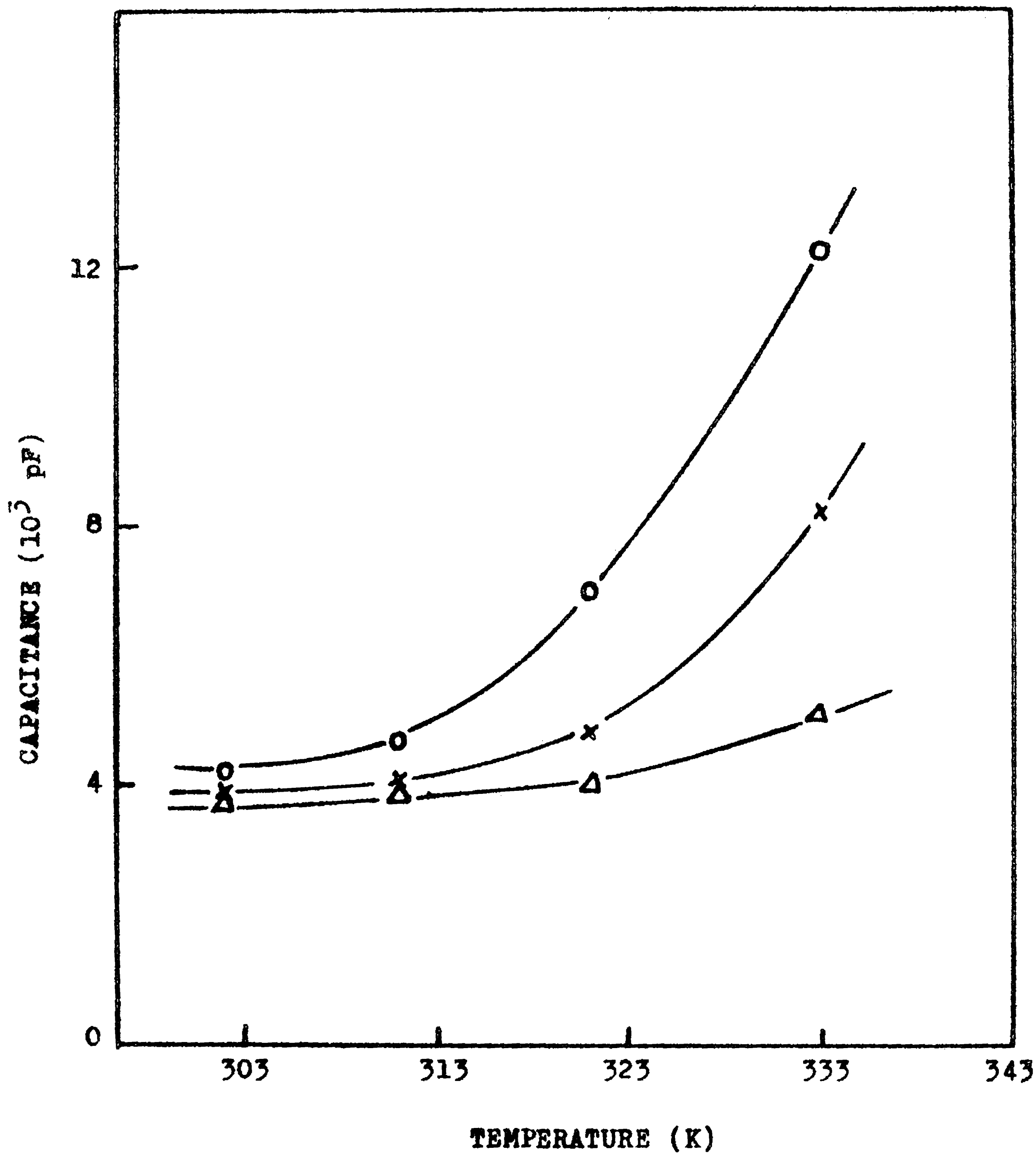

Figure 8.29. Temperature dependence of capacitance at different frequencies for flash evaporated film. O – 1 KHz, X – 6 KHz, Δ – 20 KHz, Film thickness 2175 Å.

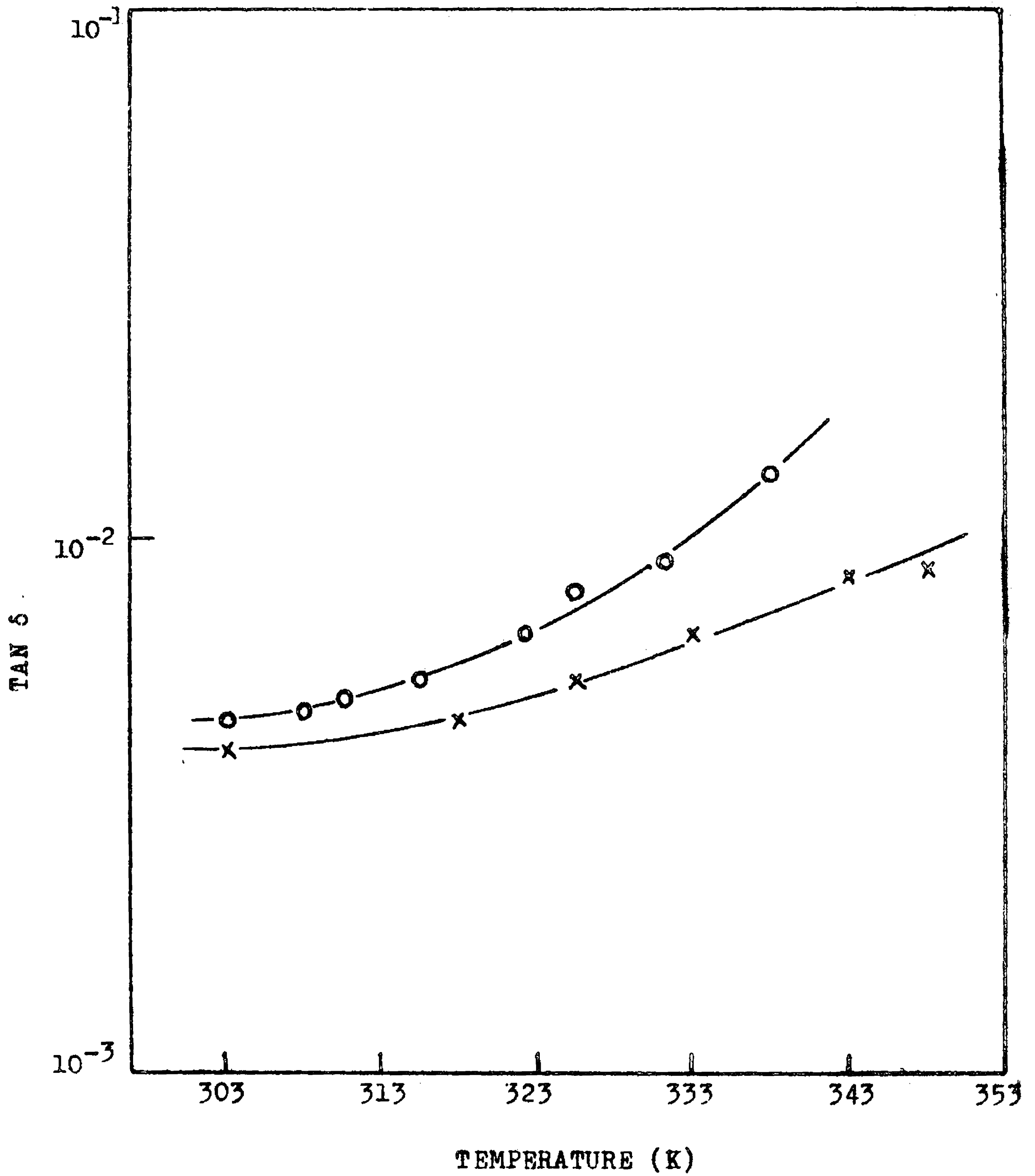

Figure 8.30. Tan δ versus temperature at 1 KHz.
X – coevaporated (film thickness 1180 Å)
O – flash evaporated (film thickness 3310 Å).

(figure 8.30). The temperature dependence of tan δ showing no loss peak reveals that there is dielectric relaxation effect in the system.

The almost frequency independent nature of the capacitance and the low loss factors observed suggest that the antimony trisulphide films with its high dielectric constant is a suitable material to be used for thin film capacitors. However, in preparing capacitors with Sb_2S_3 film structures, the nature of the contact made by the metal to the semiconductor is important, since the diffusion of the metal electrode can cause adverse effect on the performance of the systems.

8.5. Thin Film Transistor

The source-drain characteristics of the thin film transistor using polymer film as the insulator for different gate voltages is shown in figure 8.31. The observed characteristics is similar to the drain family of a field effect transistor. In the case of the observed drain family the gate field was not applied so as to get a pinch off. The TFT's were used as the field effect diodes by shorting the gate and the drain and the characteristics

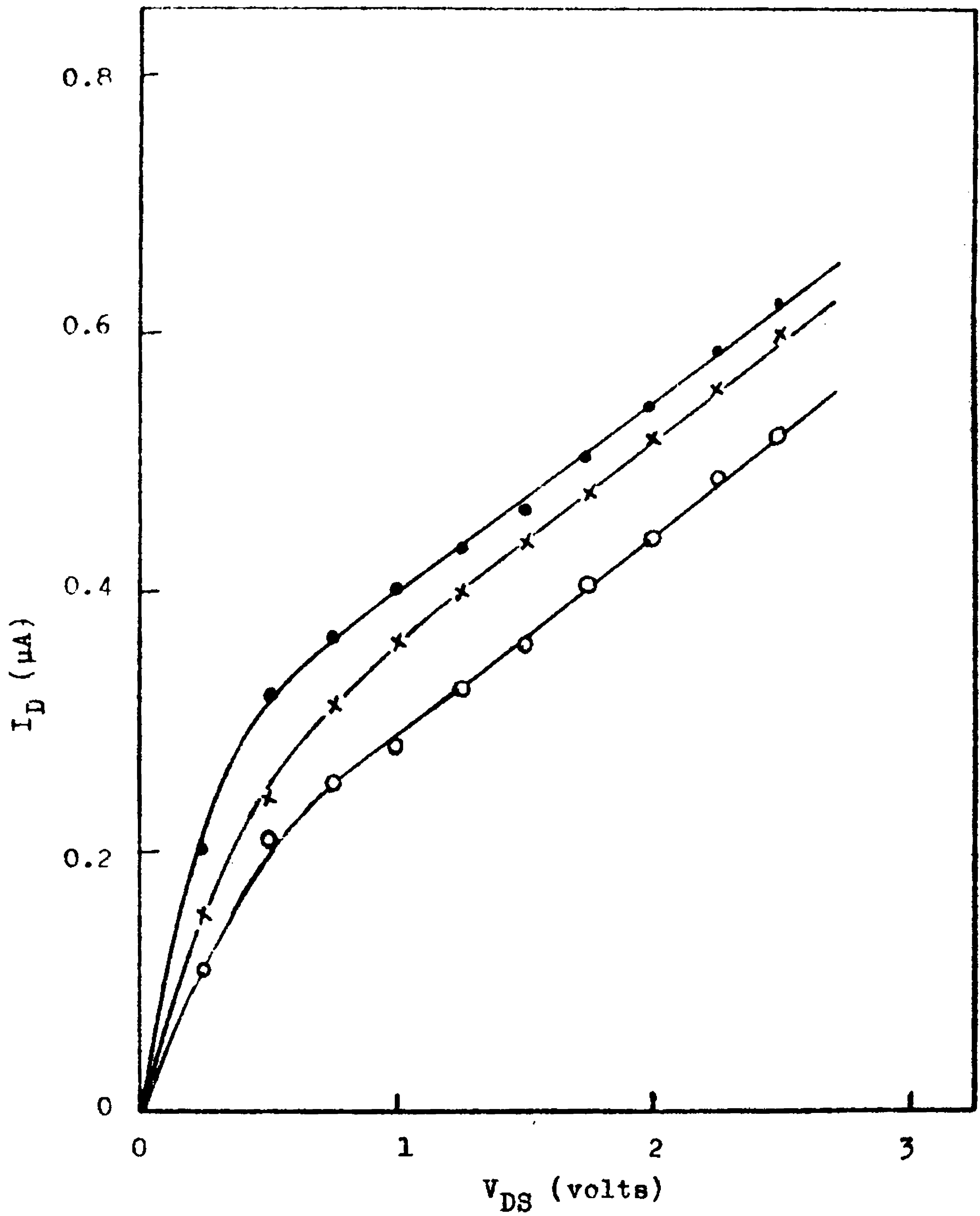

Figure 8.31. Drain characteristics of the Thin Film Transistor at different gate potentials. ◐ – V_g = 0.5 V, X – V_g = 0 V, ● – V_g = –0.5 V.

of such a field effect diode for different gate voltages is shown in figure 8.32. These curves show a dependence of the current on gate voltage, similar to that described by Weimer [343].

The source-drain separation is a very important factor determining the performance of a TFT. This problem has been solved by a suitable mask capable of producing a uniform 15 μm wide conduction channel between the source and the drain. However, since many grain boundaries in the semiconductor layer intersect the conducting channel they may cause an interruption to the mean free path of the carriers [344]. Also, the source and the drain should make low resistive contacts to the semiconductor.[345]. Since antimony makes ohmic contact to Sb_2S_3, antimony films were used for source and drain electrodes and found effective.

Even though several trials were made using reactively oxidised aluminium oxide films as gate insulator, none was found successful. The factors such as the porosity of the oxide film and the limitations of monitoring the thickness may be the reasons for the failure of these systems. Also, while using the polymer para-toluene as the insulator,

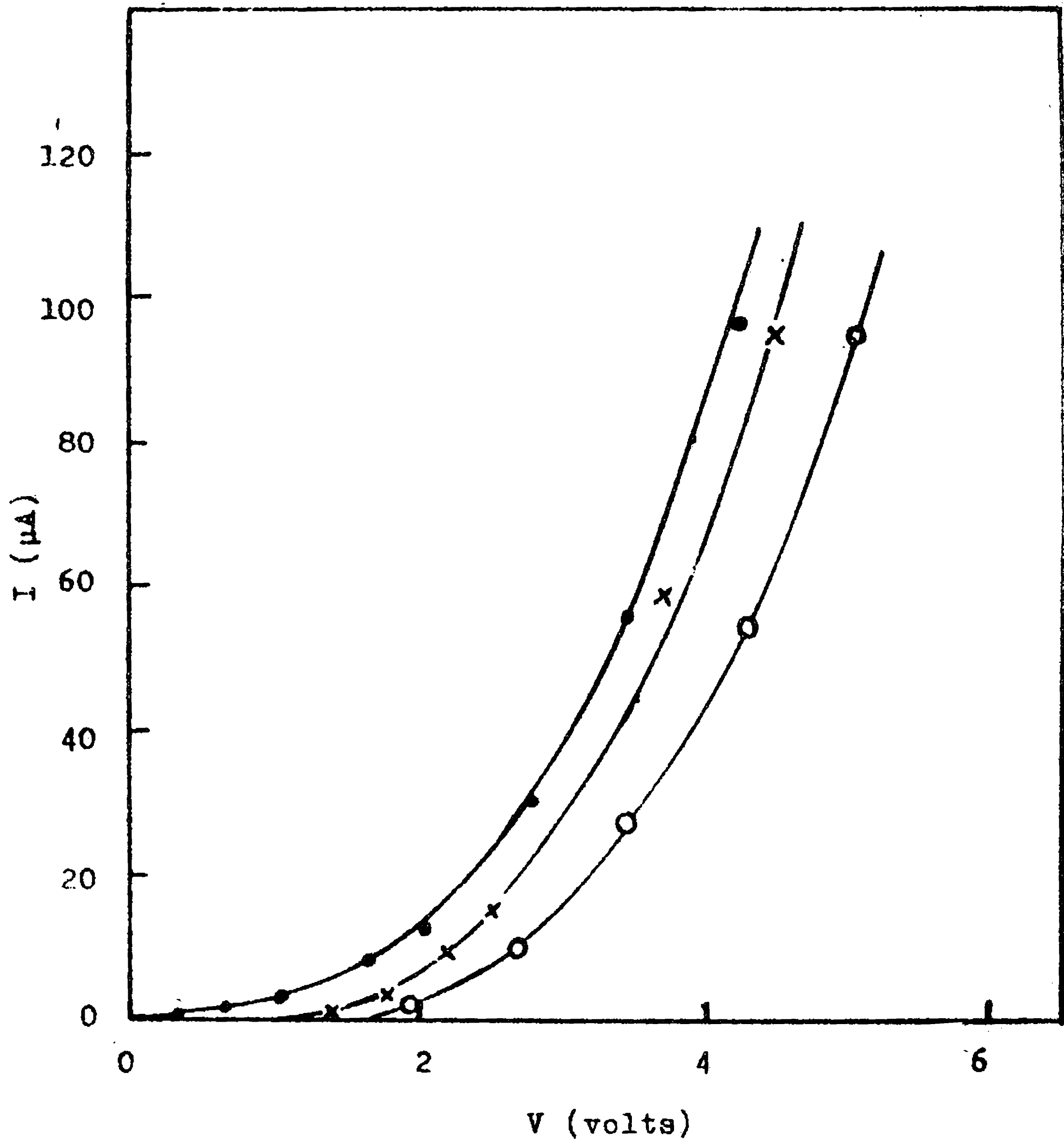

Figure 8.32. Diode characteristics of the TFT (gate tied to the drain) for different gate potential, ● - V_g = 0.5 V, × V_g = 0 V, o-V_g = -0.5 V.

the controlling of the insulator layer thickness was found to be important for the efficient device performance. Polymer films have been reported as insulator layers for CdSe [346] and p-type Te [347] transistors.

The performances of the TFT devices will be dominated by slow trapping states which caused decay of the source to drain current [348]. In the case of compound semiconductor TFT's the potential barriers at the grain boundaries affect the characteristics as the gate field changes [349,350]. According to Anderson [351] there is an optimum crystallite size for each semiconductor material which produce best barrier modulation characteristics. This crystallite size can be reached by control of film thickness and annealing treatment. However the band bending at the semiconductor-insulator interface is the main factor determining the source-drain current in a TFT [350,352] and this dominates the effect due to the grain boundaries in the semiconductor. To compensate the effect of poor modulation due to interfaces, Brody et al [353] and Fisher [354] used double gate structures.

Several compound semiconductors used for the fabrication of TFT's evolved excellent results. The compound semiconductor films of InAs prepared by the three temperature method have been found effective to produce high gain transistors [355]. Further, several IV-VI compounds such as PbS [356] and PbTe [357] have been used to produce TFT's. However, no attempt has been reported using V-VI compounds. From the present investigations on Sb_2S_3 TFT, it can be seen that a proper insulator layer combination of suitable thickness can produce transistors using antimony trisulphide as the semiconductor.

CONCLUSION

Antimony trisulphide films were prepared by the three temperature method, keeping the substrate at different temperatures ranging from 303K to 423K. The films prepared were found to be p-type. From the electrical conductivity measurements of these films at different temperatures, it was observed that the films prepared at substrate temperature, T_s, ranging from 333K to 368K possessed stoichiometric uniformity. An optimum substrate temperature, T_{os} = 345K, was selected from this range of T_s values for the preparation of the films. This T_{os} value is in agreement with the optimum substrate temperature suggested by Vincett et al for compound semiconductor films. The films thus prepared had a thermal activation energy 0.75 eV.

In the analysis of the current-voltage characteristics of the Sb-Sb_2S_3-metal systems, the electrical behaviour of different metal contacts of metals—antimony, indium, tin, aluminium, silver and bismuth—having work functions less than that of Sb_2S_3, was found to be different. Antimony,

indium and tin provided ohmic contacts with antimony trisulphide and a space charge limited conduction was observed in these systems. Aluminium made a rectifying contact to Sb_2S_3 and the conduction mechanism was found to be of the Poole-Frenkel type. The experimentally determined values of Poole-Frenkel factor (β_{PF} = 1.79 x 10^{-4} eV $V^{-\frac{1}{2}}cm^{\frac{1}{2}}$) were in agreement with the theoretically calculated value (β = 1.99 x 10^{-4}eV $V^{-\frac{1}{2}}$ $cm^{\frac{1}{2}}$). Bismuth made an ohmic injecting type contact and the Sb-Sb_2S_3-Bi system showed a current controlled negative resistance behaviour which was explained on the basis of Lampert's double injection model. Silver contacts to Sb_2S_3 showed very poor stability even at low fields.

Electrical conduction measurements were made at different temperatures on antimony trisulphide films prepared by the three-temperature method and by flash evaporation, these films being sandwiched between antimony electrodes. The flash evaporated films were also found to be p-type. The trap density and the trap energy level in the systems were calculated using the observed trap filled limit voltage and the crossover voltage from ohms law to square law region and this gave a trap depth of 0.74 eV from the top of the valence

band. From the temperature dependence of ohmic and SCL conduction, in both coevaporated and flash evaporated films, the dominant electron and hole levels were evaluated using the Roberts-Schmidlin approach. The activation energy values gave a localised level at 0.52 eV above the valence band which corresponded to the dominant hole level. From the dominant levels obtained, an energy level diagram for p-type Sb_2S_3 was deduced.

The capacitance of the MSM structures measured at different frequencies and temperatures, showed no relaxation effects. Fairly constant value for the dielectric constant was obtained for both coevaporated and flash evaporated films of varying thicknesses.

The thin film transistor fabricated using Sb_2S_3 as the semiconductor and a polymer film as insulator showed drain family characteristics similar to that of field effect transistors. The insulator layer thickness, the semiconductor-insulator combination and the source-drain separation were found to be critical factors for optimising the characteristics of the transistor.

REFERENCES

1. P.K. Weimer, H. Borkan, G. Sadasiv, L. Meray-Horvath and F.V. Shallcross, Proc. IEEE, 52, 1479 (1964).
2. P.K. Weimer, G. Sadasiv, L. Meray-Horvath and W.S. Homa, Proc. IEEE, 54, 354 (1966).
3. P.K. Weimer, G. Sadasiv, J.E. Meyer Jr., L. Meray-Horvath and W.S. Pike, Proc. IEEE, 55, 1591 (1967).
4. N.K. Annamalai, Proceedings of 12th IEEE Photovoltaic Conference, (1976), p.547.
5. F. Pfisterer, G. Bilger, H.W. Schock and W.H. Bloss, Proceedings of International Solar Energy Conference, 1977, New Delhi, Jan. 16-21 (1978).
6. H.W. Schock, G. Bilger, W.H. Bloss, G.H. Hewig and F. Pfisterer, Vacuum, 27, 281 (1977).
7. A.A. Mostovskii, L.G. Timofeeva and O.A. Timofeev, Sov. Phys.-Solid State, 6, 389 (1964).
8. L. Harris and B.M. Siegel, J. Appl. Phys., 19, 739 (1948).
9. G.A. Kurov and Z.G. Pinsker, Sov. Phys.-Tech. Phys., 3, 26 (1958).
10. M.V. Kot and G.P. Sorokin, Sov. Phys.-Tech. Phys., 3, 1528 (1959).

11. K.G. Gunther in "Compound Semiconductors," Vol.1, R.K. Willardson and H.L. Goering (eds.), (Reinhold, New York, 1962), p.313.

12. J. Bardeen, Phys. Rev., 71, 717 (1947).

13. R.V. Smith, Phys. Rev., 97, 1525 (1955).

14. J.R. Knight, D. Effer and P.R. Evans, Solid State Electron., 8, 178 (1965).

15. D.V. Eddolls, Phys. Stat. Solidi, 17, 67 (1966).

16. K.L. Lawley, J. Electrochem. Soc., 113, 240 (1966).

17. K.G. Gunther and H. Freller, Z. Naturforsch, 16a, 279 (1961).

18. C. Juhasz and J.C. Anderson, Physics Letters, 12, 163 (1964).

19. R.F. Potter and H.H. Wieder, Solid State Electron., 7, 253 (1964).

20. R.H. Bube, J. Appl. Phys., 33, 1733 (1962).

21. J. deKlerk and E.F. Kelley, Rev. Sci. Instr., 36, 506 (1965).

22. S. Jatar, A.C. Rastogi and V.G. Bhide, Pramana, 10, 477 (1978).

23. N.G. Dhere, N.R. Parikh and A. Ferreira, Thin Solid Films, 44, 83 (1977).

24. J.C. Anderson, Vacuum, 27, 263 (1977).

25. M. Jamai and P.S. Rudman, in "Amorphous and Liquid Semiconductors," J.Stuke and W. Brenig (eds.), (Taylor and Francis, London, 1974), p.425.

26. M. Jamai, A. Afif, I. Reiss and P.S. Rudman, in "Amorphous and Liquid Semiconductors," W.E. Spear (ed.), (Centre for Industrial Consultancy and Laison, University of Edinburgh, Edinburgh, 1977) p.575.

27. M. Jamai and P.S. Rudman, Phys. Stat. Solidi (a), 42, 729 (1977).

28. C. Bowlt, Proc. Phys. Soc. London, 80, 810 (1962).

29. S.V. Forgue, R.R. Goodrich and A.D. Cope, RCA Rev., 12, 335 (1951).

30. J. Grigas, J. Meshkauskas and A. Orliukas, Phys. Stat. Solidi (a), 37, K39 (1976).

31. M.S. Ablova, A.A. Andreev, T.T. Dedegkaev, B.T. Melkh, A.B. Pentsov, N.S. Shendel and L.N. Shumilova, Sov. Phys.-Semicond., 10, 629 (1976).

32. B. Roy, B.R. Chakraborty, R. Bhattacharya and A.K. Dutta, Solid State Commun., 25, 937 (1978).

33. J. Kucirek, Czech. J. Phys., B, 18, 795 (1968).

34. R. Ramanujam and Ramakrishna Rao-Vetury, Indian J. Pure and Appl. Phys., 10, 356 (1972).

35. E. Montrimas and A. Pasera, Thin Solid Films, 34, 65 (1976).

36. M.J. Chockalingam, K. Nagaraja Rao, N. Rangarajan and C.V. Suryanarayana, J. Phys. D: Appl. Phys., 3, 1641 (1970).

37. F.J. Blatt, "Physics of Electronic Conduction in Solids", (McGraw Hill, New York, 1968).

38. A.J. Dekker, "Solid State Physics" (Macmillan, London, 1958).

39. C. Kittel, "Introduction to Solid State Physics" (John Wiley, New York, 1971).

40. W. Shockley, "Electrons and Holes in Semiconductors", (D. Van Nostrand, New York, 1950).

41. R.F. Brebrick and W.W. Scanlon, Phys. Rev., 96, 598 (1954).

42. H.Y. Fan, Solid State Physics, 1, 283 (1955).

43. J. Bardeen and W. Shockley, Phys. Rev., 80, 72 (1950).

44. G. Wannier, Phys. Rev., 52, 191 (1937).

45. H.M. James, Phys. Rev., 76, 1602 (1949).

46. H.M. James, Phys. Rev., 76, 1611 (1949).

47. J.C. Slater, Phys. Rev., 76, 1592 (1949).

48. B.R. Nag, "Theory of Electrical Transport in Semiconductors", (Pergamon Press, Oxford, 1972) p.55.

49. A. Many, Y. Goldstein and N.B. Grover, "Semiconductor Surfaces", (North-Holland, Amsterdam, 1971) p.61.

50. F. Seitz, Phys. Rev., 73, 549 (1948).

51. E. Conwell and V.F. Weisskopf, Phys. Rev., 77, 388 (1950).

52. G.L. Pearson and J. Bardeen, Phys. Rev., 75, 865 (1949).

53. C. Erginsoy, Phys. Rev., 79, 1013 (1950).

54. P.P. Debye and E.M. Conwell, Phys. Rev., 93, 693 (1954).

55. N.F. Mott and E.A. Davis, "Electronic Processes in Non-Crystalline Materials", (Clarendon Press, Oxford, 1971) p.197.

56. W.W. Scanlon, Phys. Rev., 92, 1573 (1953).

57. H. Frohlich and N.F. Mott, Proc. Roy. Soc., A 171, 496 (1939).

58. H. Frohlich, Proc. Roy. Soc., A160, 280 (1937).

59. D.J. Howarth and E.H. Sondheimer, Proc. Roy. Soc., A219, 53 (1953).

60. R.L. Petritz and W.W. Scanlon, Phys. Rev., 97, 1620 (1955).

61. R.A. Smith, Physica, 20, 910 (1954).

62. J.N. Zemel in "The Use of Thin Films in Physical Investigations", J.C. Anderson (ed.), (Academic Press, London, 1966) p.319.

63. R.L. Ramey and W.D. McLennan, J. Appl. Phys., 38, 3491 (1967).

64. M.H. Francombe and J.E. Johnson in "Physics of Thin Films", Vol.5, G. Hass and R.E. Thun (eds.), (Academic Press, New York, 1969) p.143.

65. K.L. Chopra, "Thin Film Phenomena" (McGraw Hill, New York, 1969) Ch.7.

66. K. Fuchs, Proc. Camb. Philos. Soc., 34, 100 (1938).

67. A.H. Clark, Phys. Rev., 154, 750 (1967).

68. R.M. Hill in "Physics of Nonmetallic Thin Films" C.H.S. Dupuy and A. Cachard (eds.), (Plenum Press, New York, 1976) p.189.

69. V.B. Sandomirskii, Sov. Phys. JETP, 16, 1630 (1963).

70. B.A. Tavger and V. Ya. Demikhovskii, Sov. Phys. Solid State, 5, 469 (1963).

71. B.A. Tavger and V. Ya. Demikhovskii, Sov. Phys. JETP, 21, 494 (1965).

72. J.E. Davey, R.G. Turner, T. Pankey and M.D. Montgomery, Solid State Electron., 6, 205 (1963).

73. P.J. Price, IBM J. Res. Develop., 4, 152 (1960).

74. F.S. Ham and D.C. Mattis, IBM J. Res. Develop., 4, 143 (1960).

75. F. Seitz, Phys. Rev., 76, 1376 (1949).

76. H. Frohlich and F. Seitz, Phys. Rev., 79, 526 (1950).

77. W. Shockley, Bell System Tech. J., 30, 990 (1951).

78. E.M. Conwell, "High Field Transport in Semiconductors", Solid State Physics, Supplement 9, (Academic Press, New York, 1967).

79. R.W. Smith, Phys. Rev. Letters, 9, 87 (1962).

80. A.R. Hutson, J.H. McFee and D.L. White, Phys. Rev. Letters, 7, 237 (1961).
81. N. Sclar and E. Burstein, Phys. Chem. Solids, 2, 1 (1957).
82. E.J. Ryder, I.M. Ross and D.A. Kleinmann, Phys. Rev., 95, 1342 (1954).
83. S.H. Koenig and G.R. Gunther-Mohr, Phys. Chem. Solids, 2, 268 (1957).
84. W. Kaiser and G.H. Wheatly, Phys. Rev. Letters, 3, 334 (1959).
85. M.C. Steele, Bull. Am. Phys. Soc., [2] 3, 112 (1958).
86. M. Glicksman and M.C. Steele, Phys. Rev., 110, 1204 (1958).
87. A.C. Prior, J. Electron. Control, 4, 165 (1958).
88. W. Schottky, Physik. Z., 15, 872 (1914).
89. J.G. Simmons, in "Handbook of Thin Film Technology", L.I. Maissel and R. Glang (eds.), (McGraw Hill, New York, 1970) Ch.14.
90. J.J. O'Dwyer, "The Theory of Electrical Conduction and Breakdown in Solid Dielectrics" (Clarendon Press, Oxford, 1973) p.105.
91. J.G. Simmons, Phys. Rev. Letters, 15, 967 (1965).
92. C.R. Crowell, Solid State Electron., 8, 395 (1965).

93. C.A. Mead in "Basic Problems in Thin Film Physics", R. Niedermayer and H. Mayer (eds.), (Vandenhoeck and Ruprecht, Goettingen, 1966) p.674.

94. S.R. Pollack, J. Appl. Phys., 34, 877 (1963).

95. W.E. Flannery and S.R. Pollack, J. Appl. Phys., 37, 4417 (1967).

96. P.T. Landsberg, Proc. Roy. Soc., A206, 463 (1951).

97. P.R. Emtage and J.J. O'Dwyer, Phys. Rev. Letters, 16, 356 (1966).

98. H.H. Poole, Philos. Mag., 32, 112 (1916).

99. H.H. Poole, Philos. Mag., 34, 195 (1917).

100. J. Frenkel, Tech. Phys., 5, 685 (1938).

101. J. Frenkel, Phys. Rev., 54, 647 (1938).

102. C.A. Mead, Phys. Rev., 128, 2088 (1962).

103. A.K. Jonscher, Thin Solid Films, 1, 213 (1967).

104. J.L. Hartke, J. Appl. Phys., 39, 487 (1968).

105. R.M. Hill, Philos. Mag., 23, 59 (1971).

106. T.E. Hartman, J.C. Blair and R. Bauer, J. Appl. Phys., 37, 2468 (1966).

107. A.K. Jonscher and A.A. Ansari, Philos. Mag., 23, 205 (1971).

108. J.G. Simmons, Phys. Rev., 166, 912 (1968).

109. W. Fuhs in "Physics of Structurally Disordered Solids", S.S. Mitra (ed.),(Plenum Press, New York, 1974) p.411.

110. P. Nagles in "Amorphous Semiconductors", M.H. Brodsky (ed.), Topics of Applied Physics, Vol.36, (Springer-Verlag, Berlin, 1979) p.113.

111. H. Fritsche in "Electronic and Structural Properties of Amorphous Semiconductors", P.G. LeComber and J. Mort (eds.), (Academic Press, London, 1973) p.55.

112. P.W. Anderson, Phys. Rev., 109, 1492 (1958).

113. M.H. Cohen, H. Fritzsche and S.R. Ovshinsky, Phys. Rev. Letters, 22, 1065 (1969).

114. E.A. Davis and N.F. Mott, Philos. Mag., 22, 903 (1970).

115. N.F. Mott, Philos. Mag., 24, 911 (1971).

116. M.H. Cohen, J. Non Cryst. Solids, 4, 391 (1970).

117. A.W. Owen and W.E. Spear, Phys. Chem. Glasses, 17, 174 (1976).

118. W. Beyer and J. Stuke, Proc. of 5th Inter. Conf. on Amorphous and Liquid Semiconductors, Garmisch Partenkirchen, (1973) p.251.

119. N.F. Mott, Philos. Mag., 19, 835 (1969).

120. P.G. LeComber, A. Madan and W.E. Spear, J. Non Cryst. Solids, 11, 219 (1972).

121. D. Emin in "Electronic and Structural Properties of Amorphous Semiconductors", P.G.LeComber and J. Mort (eds.), (Academic Press, London, 1973), p.261.

122. D. Emin, C.H. Seager and R.K. Quinn, Phys. Rev. Letters, **28**, 813 (1972).

123. K.L. Chopra and S.K. Bahl, Thin Solid Films, **12**, 211 (1972).

124. C.H. Seager and R.K. Quinn, J. Non Cryst. Solids, **17**, 386 (1975).

125. C.H. Seager, D. Emin and R.K. Quinn, Phys. Rev., **B8**, 4746 (1973).

126. E.H. Nicollian and A.K. Sinha in "Thin Films-Interdiffusion and Reactions", J.M. Poate, K.N. Tu and J.W. Mayer (eds.), (Wiley Interscience, New York, 1978) Ch.13.

127. R.H. Cox and H. Strack, Solid State Electron., **10**, 1213 (1967).

128. Y.K. Fang, C.Y. Chang and Y.K. Su, Int. J. Electron., **47**, 577 (1979).

129. A.K. Sinha and J.M. Poate in "Thin Films-Interdiffusion and Reactions", J.M. Poate, K.N. Tu and J.W. Mayer (eds.), (Wiley Interscience, New York, 1978) Ch.11.

130. T. Sebestyen, H. Hartnagel and L.H. Herron, Electron. Letters, **10**, 372 (1974).

131. N. Braslau, J.B. Gunn and J.L. Staples, Solid State Electron., **10**, 381 (1967).

132. J.S. Harris, Y. Nannichi, G.L. Pearson and G.F. Day, J. Appl. Phys., 40, 4575 (1969).

133. H. Temkin, R.J. McCoy, V.G. Keramidas and W.A. Bonner, Appl. Phys. Letters, 36, 444 (1980).

134. A.K. Sinha, T.E. Smith and H.J. Levinstein, IEEE Trans. Electron. Devices, ED22, 218 (1975).

135. J.O. McCaldin and T.C. McGill in "Thin Films-Interdiffusion and Reactions", J.M. Poate, K.N. Tu and J.W. Mayer (eds.), (Wiley Interscience, New York, 1978) Ch.4.

136. D.L. Lile and D.A. Collins, Appl. Phys. Letters, 28, 554 (1976).

137. D.L. Lile, A.R. Clawson and D.A. Collins, Appl. Phys. Letters, 29, 207 (1976).

138. J.M. Andrews and J.C. Phillips, Phys. Rev. Letters, 35, 56 (1975).

139. J.M. Poate and K.N. Tu, Physics Today, 33, No.(5), 34 (1980).

140. S. Guha, B.M. Arora and V.P. Salvi, Solid State Electron., 20, 431 (1977).

141. A.K. Sinha and J.M. Poate, Appl. Phys. Letters, 23, 666 (1973).

142. G. Margaritondo, J.E. Rowe and S.B. Christman, Phys. Rev., B14, 5396 (1976).

143. J.E. Rowe, G. Margaritondo and S.B. Christman, Phys. Rev., B15, 2195 (1977).

144. L.J. Brillson, J. Vac. Sci. Technol., 15, 1378 (1978).

145. L.J. Brillson, Phys. Rev. Letters, 40, 260 (1978).

146. L.J. Brillson, R. Z. Bacharah, R.S. Bauer and J. McMenamin, Phys. Rev. Letters, 42, 397 (1979).

147. G. Ottaviani, K.N. Tu and J.W. Mayer, Phys. Rev. Letters, 44, 284 (1980).

148. I. Lindau, P.W. Chye, C.M. Garner, P. Pianetta and W.E. Spicer, J. Vac. Sci. Technol., 15, 1332 (1978).

149. P.W. Chye, I. Lindau, P. Pianetta, C.M. Gardner and W.E. Spicer, Phys. Rev., B17, 2682 (1978).

150. P.W. Chye, I. Lindau, P. Pianetta, C.M. Gardner, C.Y. Su and W.E. Spicer, Phys. Rev., B18, 5545 (1978).

151. L.J. Brillson, J. Vac. Sci. Technol., 16, 1137 (1979).

152. W.E. Spicer, I. Lindau, P.W. Chye, P. Skeath and C.Y. Su, J. Vac. Sci. Technol., 16, 1422 (1979).

153. L.J. Brillson, R.S. Bauer, R.Z. Bacharach and G. Hansson, Appl. Phys. Letters, 36, 326 (1980).

154. N.F. Mott and R.W. Gurney, "Electronic Processes in Ionic Crystals" (Clarendon Press, Oxford, 1940) p.168.

155. A. Rose, RCA Rev., **12**, 362 (1951).

156. A. Rose, Phys. Rev., **97**, 1538 (1955).

157. M.A. Lampert, Rep. Progr. Phys., **27**, 329 (1964).

158. M.A. Lampert, Phys. Rev., **103**, 1648 (1956).

159. M.A. Lampert and R.B. Schilling, in "Semiconductors and Semi-metals", Vol.6, R.K. Willardson and A. Beer (eds.), (Academic Press, New York, 1970) Ch.1.

160. M.A. Lampert and P. Mark, "Current Injection in Solids", (Academic Press, New York, 1970).

161. M.A. Lampert, J. Appl. Phys., **29**, 1082 (1958).

162. R.H. Parmenter and W. Ruppel, J. Appl. Phys., **30**, 1548 (1959).

163. M.A. Lampert, RCA Rev., **20**, 682 (1959).

164. M.A. Lampert and A. Rose, Phys. Rev., **121**, 26 (1961).

165. M.A. Lampert, Phys. Rev., **125**, 126 (1962).

166. W. Ruppel and R.W. Smith, RCA Rev., **20**, 702 (1959).

167. G.T. Wright, Nature, **182**, 1296 (1958).

168. G.T. Wright, Nature, **185**, 360 (1960).

169. J. Dresner and F.V. Shallcross, Solid State Electron., **5**, 205 (1962).

170. H. Borkan and P.K. Weimer, RCA Rev., **24**, 153 (1963).

171. R. Zuleeg, Solid State Electron., **6**, 193 (1963).

172. F.V. Shallcross, Proc. Inst. Radio Engrs., **51**, 851 (1963).

173. A.G. Fischer, Solid State Electron., **2**, 232 (1961).

174. W. Helfrich in "Physics and Chemistry of Organic Solid State", Vol.3, (Wiley, New York, 1968).

175. M.H. Pilkuhn, Phys. Stat. Solidi, **25**, 9 (1968).

176. M.A. Lampert, A. Rose and R.W. Smith, J. Appl. Chem. Solids, **8**, 484 (1959).

177. D.R. Lamb, "Electrical Conduction Mechanisms in Thin Insulating Films", (Methuen and Co., London, 1967) Ch.4.

178. L.M. Rosenberg and M.A. Lampert, J. Appl. Phys., **41**, 508 (1970).

179. R.B. Schilling and M.A. Lampert, J. Appl. Phys., **41**, 1791 (1970).

180. R. Hirota, S. Tosima and M.A. Lampert, J. Phys. Soc. Japan, **18**, 535 (1963).

181. A. Waxman and M.A. Lampert, Phys. Rev., **B1**, 2735 (1970).

182. V.I. Stafeev, Sov. Phys. Solid State, **1**, 763 (1959).

183. G.G. Roberts in "Transfer and Storage of Energy by Molecules", Vol.4, The Solid State, G.M. Burnett, A.M. North and J.N. Sherwood (eds.), (Wiley-Interscience, London, 1974) p.153.

184. G.G. Roberts in "Electronic and Structural Properties of Amorphous Semiconductors", P.G. LeComber and J. Mort (eds.), (Academic Press, London, 1973) p.409.

185. G.G. Roberts and F.W. Schmidlin, Phys. Rev., 180, 785 (1969).

186. F.W. Schmidlin and G.G. Roberts, Phys. Rev. Letters, 20, 1173 (1968).

187. F.W. Schmidlin and G.G. Roberts, Phys. Rev., B9, 1578 (1974).

188. K.P. Pande and G.G. Roberts, IEEE Trans. Nucl. Sci., NS24, 2017 (1977).

189. K.O. Lee and T.T. Gan, Phys. Stat. Solidi (a), 43, 565 (1977).

190. A.K. Jonscher, Thin Solid Films, 50, 187 (1978).

191. W. Kohn, Phys. Rev., 110, 857 (1958).

192. K.L. Chopra, J. Appl. Phys., 36, 655 (1965).

193. K.L. Chopra, "Thin Film Phenomena",(McGraw Hill, New York, 1969) Ch.8.

194. C. Weaver, Advan. Phys., 11, 85 (1962).

195. C. Weaver, Vacuum, **15**, 171 (1965).

196. C. Weaver in "The Use of Thin Films in Physical Investigations", J.C. Anderson (ed.), (Academic Press, London, 1966) p.283.

197. P.J. Harrop and J.N. Wanklyn, J. Electrochem. Soc., **111**, 1133 (1964).

198. P.J. Harrop and D.S. Campbell in "Handbook of Thin Film Technology", L.I. Maissel and R. Glang (eds.), (McGraw Hill, New York, 1970) Ch.16.

199. A.K. Jonscher, Nature, **267**, 673 (1977).

200. M.A. Careem and A.K. Jonscher, Philos. Mag., **35**, 1489 (1977).

201. M.A. Careem, A.K. Jonscher and F. Taiedy, Philos. Mag., **35**, 1503 (1977).

202. P. Debye, 'Polar Molecules", (Dover Publ., New York, 1929).

203. K.S. Cole and R.H. Cole, J. Chem. Phys., **9**, 341 (1941).

204. A.K. Jonscher, Phys. Stat. Solidi (b), **83**, 585 (1977).

205. S.J. Fonash, in "Physics of Nonmetallic Thin Films", C.H.S. Dupuy and A. Cachard (eds.), (Plenum Press, New York, 1976) p.225.

206. S.J. Fonash, J.A. Roger, J. Pivot and A.Cachard, J. Appl. Phys., 45, 1225 (1974).

207. J.G. Simmons and G.W. Taylor, Phys. Rev., B6, 4804 (1972).

208. J. R. Macdonald, J. Chem. Phys., 58, 4982 (1973).

209. J.R. Macdonald, J. Appl. Phys., 45, 73 (1974).

210. H. Chang and G. Jaffe, J. Chem. Phys., 20, 1071 (1952).

211. J.R. Macdonald, J. Chem. Phys., 40, 3735 (1964).

212. S.J. Fonash, J.A. Roger and C.H.S. Dupuy, J. Appl. Phys., 45, 2907 (1974).

213. J.G. Simmons, G.S. Nadkarni and M.C. Lancaster, J. Appl. Phys., 41, 538 (1970).

214. J. Maserjian, J. Vac. Sci. Technol., 6, 843 (1969).

215. M. Perlman and S. Unger, J. Appl. Phys., 45, 2384 (1974).

216. M. Baird, Rev. Mod. Phys., 40, 219 (1968).

217. J.G. Simmons and G.S. Nadkarni, Phys. Rev., B6, 4815 (1972).

218. C. Bucci, R. Fieschi and G. Guidi, Phys. Rev., 148, 816 (1966).

219. M. Gevers, Philips Res. Rept., 1, 279 (1946).

220. A. Herzping, Z. Angew. Phys., 5, 369 (1966).

221. A.J. Bosman and R.E. Havinga, Phys. Rev., 129, 1593 (1963).

222. A.G. Cockbain and P.J. Harrop, Brit. J. Appl. Phys., **18**, 1109 (1968).

223. P.P. Budenstein and P.J. Hayes, J. Vac. Sci. Technol., **6**, 602 (1969).

224. L. Holland, "Vacuum Deposition of Thin Films", (Chapman and Hall, London, 1956).

225. K.L. Chopra, " Thin Film Phenomena", (McGraw Hill, New York, 1969) Ch.1.

226. R.W. Berry, P.M. Hall and M.T. Harris, "Thin Film Technology", (Van Nonstrand, New York, 1968).

227. D.S. Campbell in "The Use of Thin Films in Physical Investigations", J.C. Anderson (ed.), (Academic Press, London, 1966) p.11.

228. D.S. Campbell in "Physics of Nonmetallic Thin Films", C.H.S. Dupuy and A. Cachard (eds.), (Plenum Press, New York, 1976) p.9.

229. B.N. Chapman and J.C. Anderson (eds.), "Science and Technology of Surface Coatings" , (Academic Press, London, 1974).

230. W.M. Feist, S.R. Steele and D.W. Readey in "Physics of Thin Films", Vol.5, G. Hass and R.F. Thun (eds.), (Academic Press, New York, 1969) p.237.

231. J.C. Viguie in "Science and Technology of Surface Coatings", B.N. Chapman and J.C. Anderson (eds.), (Academic Press, London, 1974) p.149.

232. J.E. Mee, J.L. Archer, R.H. Meade and T.N. Hamilton, Appl. Phys. Letters, 10, 289 (1967).

233. B.A. Joyce in "The Use of Thin Films in Physical Investigations", J.C. Anderson (ed.), (Academic Press, London, 1966) p.87.

234. S.R. Bhola and A. Mayer, RCA Rev., 24, 511 (1963).

235. B.A. Joyce and R.R. Bradley, J. Electrochem. Soc., 110, 1235 (1963).

236. K.R. Lawless, J. Vac. Sci. Technol., 2, 1 (1965).

237. D.S. Campbell in 'Handbook of Thin Film Technology', L.I. Maissel and R. Glang (eds.), (McGraw Hill, New York, 1970) p.5-9.

238. R.J. Heritage and M.T. Walker, J. Electron. Control, 7, 542 (1960).

239. J.C. Hendy, N.D. Richards and A.W. Simpson, J. Mater. Sci., 1, 127 (1966).

240. M. Schlesinger, in "Science and Technology of Surface Coatings", B.N. Chapman and J.C. Anderson (eds.), (Academic Press, London, 1974) p.176.

241. J.F. D'Amico, M.A. DeAngelo, J.F. Henrikson, J.T. Kenney and D.J. Sharp, J. Electrochem. Soc., **118**, 1695 (1971).

242. L. Young, "Anodic Oxide Films", (Academic Press, New York, 1961).

243. C.J. Dell'Oca, D.L. Pulfey and L. Young, in "Physics of Thin Films", Vol.6, M.H. Francombe and R.W. Hoffman (eds.), (Academic Press, New York, 1971) p.1.

244. V.K. Srivastava, in "Physics of Thin Films", Vol.7, G. Hass, M.H. Francombe and R.W. Hoffman (eds.), (Academic Press, New York, 1973) p.311.

245. N.R. Pavaskar, C.A. Menezes and A.P.B. Sinha, J. Electrochem. Soc., **124**, 743 (1977).

246. L.I. Maissel and P. Shaible, J. Appl. Phys., **36**, 237 (1965).

247. G.S. Anderson, W.N. Mayer and G.K. Wehner, J. Appl. Phys., **33**, 2991 (1962).

248. M. Knudsen, Ann. Physik., **47**, 697 (1915).

249. I. Langmuir, Phys. Rev., **2**, 329 (1913).

250. I. Langmuir, Physik. Z., **14**, 1283 (1913).

251. K.H. Behrndt in "Techniques of Metals Research", Vol.1, R.F. Bunshah (ed.), (Interscience Publishers, New York, 1968) p.1225.

252. R. Glang in "Handbook of Thin Film Technology", L.I. Maissel and R. Glang (eds.), (McGraw Hill, New York, 1970) p.1-36.

253. T.N. Rhodin and D. Walton, "Metal Surfaces", (American Society for Metals, Metals Park, Ohio, 1963) p.259.

254. J.P. Hirth and G.M. Pound, Progr. Mater. Sci., 11, 41 (1963).

255. K.G. Gunther in "The Use of Thin Films in Physical Investigations", J.C. Anderson (ed.), (Academic Press, London, 1966) p.213.

256. H.H. Wieder, "Intermetallic Semiconducting Films", (Pergamon Press, Oxford, 1970) Ch.1.

257. R.F. Bis, A.S. Rodolakis and J.N. Zemel, Rev. Sci. Instr., 36, 1626 (1965).

258. F.A. Pizzarello, J. Appl. Phys., 35, 2730 (1964).

259. J.E. Davey and T. Pankey, J. Appl. Phys., 35, 2203 (1964).

260. L. Harris and R.M. Siegel, J. Appl. Phys., 19, 739 (1948).

261. W.R. Beam and T. Takahashi, Rev. Sci. Instr., 35, 1623 (1964).

262. J.L. Richards in "The Use of Thin Films in Physical Investigations", J.C. Anderson (ed.), (Academic Press, London, 1966) p.71.

263. E.K. Muller, B.J. Nicholson and G.L'E. Turner, J. Electrochem. Soc., 110, 969 (1963).

264. N.S. Platakis and H.C. Gatos, J. Electrochem. Soc., 123, 1410 (1976).

265. N.S. Platakis and H.C. Gatos, US Patent No.4080926, Mar. 28, 1978.

266. R.F. Bunshah in "Science and Technology of Surface Coatings", B.N. Chapman and J.C. Anderson (eds.), (Academic Press, London, 1974) p.361.

267. A.Y. Cho and J.R. Arthur, Progr. Solid State Chem., 10, 157 (1975).

268. B.A. Joyce, Surf. Sci., 86, 92 (1979).

269. L.L. Chang and L. Esaki, Progr. Cryst. Growth, 2, 3 (1979).

270. D.W. Pashley, M.J. Stowell, M.H. Jacobs and T.J. Law, Philos. Mag., 10, 127 (1964).

271. C.A. Neugebauer, in "Handbook of Thin Film Technology", L.I. Maissel and R.Glang (eds.), (McGraw Hill, New York, 1970) Ch.8.

272. I. Langmuir, Phys. Rev., 8, 149 (1916).

273. J. Frenkel, Z. Physik, 26, 117 (1924).

274. K.L. Chopra, "Thin Film Phenomena", (McGraw Hill, New York, 1969) Ch.4.

275. N. Semenoff, Z. Phys. Chem., B7, 741 (1930).

276. B. Lewis, Thin Solid Films, 50, 233 (1978).

277. M. Volmer and A. Weber, Z. Phys. Chem., 119, 277 (1925).

278. R. Becker and W. Doering, Ann. Physik, 24, 719 (1935).

279. J.P. Hirth and G.M. Pound, in "Condensation and Evaporation", Progress in Material Science, B. Chalmer (ed.) Vol.11, (MacMillan, New York, 1963) p.41.

280. T.N. Rhodin in "The Use of Thin Films in Physical Investigations", J.C.Anderson (ed.), (Academic Press, London, 1966) p.187.

281. D. Walton, J. Chem. Phys., 37, 2182 (1962).

282. D. Walton, Philos. Mag., 7, 1671 (1962).

283. T. Rhodin and D. Walton, in "Single Crystal Films'', M.H. Francombe and H. Sato (eds.), (Pergamon Press, New York, 1964) p.31.

284. D. Walton, T. Rhodin and R.W. Rollins, J. Chem. Phys., 38, 2698 (1963).

285. B. Lewis, Thin Solid Films, 1, 85 (1967).

286. B. Lewis, Thin Solid Films, 7, 179 (1971).

287. R. Niedermayer in "Physics of Nonmetallic Thin Films", C.H.S. Dupuy and A. Cachard (eds.), (Plenum Press, New York, 1976) p.49.

288. V. Halpern, J. Appl. Phys., **40**, 4627 (1969).

289. J.W. Mathews, Philos. Mag., **12**, 1143 (1965).

290. K.L. Chopra and I.H. Khan, Surf. Sci., **6**, 33 (1967).

291. H. Raether in "Physics of Nonmetallic Thin Films", C.H.S. Dupuy and A. Cachard (eds.), (Plenum Press, New York, 1976) p.123.

292. P. Archibald and E. Parent, Solid State Technol., **19**, 32 (1976).

293. L. Holland, Brit. J. Appl. Phys., **9**, 410 (1958).

294. T. Putner, Brit. J. Appl. Phys., **10**, 332 (1959).

295. H.E. Bennet and J.M. Bennet, in "Physics of Thin Films", Vol.4, G. Hass and R.E. Thun (eds.), (Academic Press, New York, 1967) p.1.

296. R. Brown in "Handbook of Thin Film Technology", L.I. Maissel and R. Glang (eds.), (McGraw Hill, New York, 1970) p.6.1.

297. A.A. Agasiev, A. Kh. Zeinally, V.M. Salmanov, V.I. Tagirov and K.Yu. Karakurkchi, Sov. Phys. Semicond., **9**, 777 (1975).

298. D.S. Campbell and B. Hendry, Brit. J. Appl. Phys., 16, 1719 (1965).

299. R.B. Adler, A.C. Smith and R.L. Longini, "Introduction to Semiconductor Physics", (John Wiley, New York, 1964) p.197.

300. D.S. Campbell in "Physics of Nonmetallic Thin Films", C.H.S. Dupuy and A. Cachard (eds.), (Plenum Press, New York, 1976) p.165.

301. S. Tolansky, "Multiple beam Interferometry of Surfaces and Films", (Oxford University Press, London, 1948).

302. S. Tolansky, "Surface Microtopography", (Interscience, New York, 1960).

303. P.K. Weimer, Proc. IRE, 50, 1462 (1962).

304. F.V. Shallcross, Proc. IEEE, 51, 851 (1963).

305. P.K. Weimer, Proc. IEEE, 52, 608 (1964).

306. W.B. Pennebaker, Solid State Electron., 5, 509 (1965).

307. C.A.T. Salama and L. Young, Proc. IEEE, 53, 2156 (1965).

308. J.F. Skalski, Proc. IEEE, 53, 1792 (1965).

309. P.K. Weimer, in "Physics of Thin Films", Vol.2, G. Hass and R.E. Thun (eds.), (Academic Press, New York, 1964) p.147.

310. N. Onodera, H. Suga and S. Seki, J. Non Cryst. Solids, 1, 331 (1969).

311. Z.M. Hanafi and F.M. Ismail, Z. Phys. Chem., 244, 219 (1970).

312. T. Budinas, P. Mackus, T. Smilga and J.Viscakas, Phys. Stat. Solidi, 31, 375 (1969).

313. P.S. Vincett, W.A. Barlow and G.G. Roberts, J. Appl. Phys., 48, 3800 (1977).

314. P.S. Vincett, W.A. Barlow and G.G. Roberts, Nature, 255, 542 (1975).

315. K. Okamoto and Y. Ugai, Electronics Commun. Jpn., 56C, 97 (1973).

316. L.S. Palatnik and V.K. Sorokin, Sov. Phys. Solid State, 8, 2233 (1967).

317. S. Ibuki and S. Yoshimatsu, J. Phys. Soc. Japan, 10, 549 (1955).

318. A.A. Andreev, V.A. Alekseev, E.A. Lebedev, M. Mamadaliev, B.T. Melekh, A.R. Regel and Yu.F. Ryshkov, Sov. Phys. Semicond., 6, 570 (1972).

319. R. Suryanarayana, Thin Solid Films, 50, 349 (1978).

320. T. Fleisch and Abermann, Thin Solid Films, 42, 255 (1977).

321. J.S. Best, J.D. McCaldin, T.C. McGill, C.A. Mead and J.B. Mooney, Appl. Phys. Letters, 29, 433 (1976).

322. R.R. Varma, M.H. Patterson and R.H. Williams, J. Phys. D: Appl. Phys., 12, L71 (1979).

323. V.I. Makendonskii and A.K. Pustovoit, Sov. Phys. Solid State, 4, 1490 (1963).

324. J.P. Mitchell and D.G. Demure, Thin Solid Films, 16, 285 (1973).

325. Joy George, B.C. Joy and M.K. Radhakrishnan, Thin Solid Films, 68, 289 (1980).

326. H. Goebel, K. Dettmer and F.R. Kessler, Phys. Stat. Solidi (a), 16, 61 (1973).

327. D.R. Goyal, O.S. Panwar, K.K. Srivastava, K.N. Lakshminarayan, A. Kumar and D.R. Ravikar, Indian J. Pure and Appl. Phys., 15, 10 (1977).

328. M. Hafiz, B. Mgbenu, P.A. Tove, H. Norde and S. Petersson, Vacuum, 27, 193 (1977).

329. B. Seiri and R. Chabicovsky, Vacuum, 27, 299 (1977).

330. S. Gogoi and K. Barua, Japan J. Appl. Phys., 18, 2233 (1979).

331. H. Krause and R. Grunler, Phys. Stat. Solidi (a), 42, 149 (1977).

332. K.L. Chopra, "Thin Film Phenomena", (McGraw Hill, New York, 1969) p.506.

333. S.P.S. Arya and H.P. Singh, Thin Solid Films, **62**, 353 (1979).

334. Y. Onuma and K. Miyata, Japan J. Appl. Phys., **18**, 2179 (1979).

335. S.M. Patel and Varghese George, Indian J. Phys., **52A**, 77 (1978).

336. R.H. Bube, J. Appl. Phys., **31**, 315 (1960).

337. I.A. Karpovich and M.V. Shilova, Sov. Phys. Solid State, **5**, 2612 (1964).

338. V.A. Brodovoi, G.P. Peka and A.N. Smolyar, Sov. Phys. Semicond., **13**, 207 (1979).

339. I.P. Grigas and A.S. Karpus, Sov. Phys. Solid State, **9**, 2265 (1968).

340. I.P. Grigas and A.S. Karpus, Sov. Phys. Solid State, **8**, 1558 (1966).

341. I.P. Grigas, V.P. Kunigelis, A.S. Orlyukas and V.I. Samulionis, Sov. Phys. Solid State, **14**, 796 (1972).

342. T. Mahalingam, M. Radhakrishnan and C.Balasubramanian, Thin Solid Films, **59**, 221 (1979).

343. P.K. Weimer, in 'Handbook of Thin Film Technology'', L.I. Maissel and R. Glang (eds.), (McGraw Hill, New York, 1970) p.20-7.

344. J.C. Anderson, Thin Solid Films, **36**, 299 (1976).

345. J.T. Wallmark and H. Johnson (eds.),
"Field Effect Transistors",
Printice Hall, (1966).

346. A. De Vos, Solid State Electron., 18, 895 (1975).

347. A. De Vos and B. Hindryckx, IEE Proc.,
127, Pt.1, 42 (1980).

348. J.C. Anderson, Thin Solid Films, 50, 25 (1978).

349. J.C. Anderson, Thin Solid Films, 37, 127 (1976).

350. J.C. Anderson, Thin Solid Films, 36, 151 (1976).

351. J.C. Anderson, Proc. Int. Conf. on Thin and Thick
Film Technol., Augsburg, Germany (1977).

352. A. Van Calster and A. De Vos, Proc. European
Hybrid Micro Electronics Conference,
Ghent-Belgium (1979) p.197.

353. T.P. Brody, F.C. Luo, Z.P. Szepesi and D.H.Davies,
IEEE Trans.Electron Devices, 22,739(1975).

354. A.G. Fisher, Microelectronics, 7, 5 (1976).

355. T. Brody and H. Kunig, Appl. Phys. Letters,
9, 259 (1966).

356. W. Pennebaker, Solid State Electron., 8, 509 (1966).

357. D. Lile and J.C. Anderson, Solid State Electron.,
12, 735 (1969).

ACKNOWLEDGEMENTS

My greatest personal debt is to Dr.Joy George, Professor in Industrial Physics, whose profound interest and able and invaluable guidance were my inspiration throughout the period of research. May I express my sincere thanks to him.

I wish to record my sincere thanks to Dr.K. Sathianandan, Head of the Department, for providing excellent laboratory and library facilities and for his interest in the work.

I am thankful to Dr.V. Unnikrishnan Nayar, Reader, Department of Physics, University of Kerala, who assisted and guided me during the early stages of my work.

I am extremely grateful to all the members of the Faculty, Library and Laboratory personnel and non-teaching staff of the Department for their full co-operation throughout.

May I record my acknowledgement to all my fellow researchers in the Department for the co-operation and friendship extended over the years. I am especially thankful to Shri P.K. Sarangadharan, Fr. E.C. Joy,

- G 3608 -

Shri S.K. Premachandran, Shri K.S. Joseph, Shri A.V. Alex, Shri T.I. Palson and Shri B. Pradeep for the help rendered by them at various stages of my work.

I wish to thank the University of Cochin and the University Grants Commission, for awarding junior research fellowships, and the Council of Scientific and Industrial Research, for awarding a senior research fellowship during the course of my work.